Fe-2028-12
Dist. Category UC-90d

KINETICS AND MECHANISM OF DESULFURIZATION AND DENITROGENATION OF COAL-DERIVED LIQUIDS

Tenth Quarterly Report for Period

September 21, 1977, to December 20, 1977

Prepared by:

Bruce C. Gates, James R. Katzer
Jon H. Olson, Harold Kwart, and Alvin B. Stiles

Departments of Chemical Engineering and Chemistry
University of Delaware
Newark, Delaware 19711

Date Published

January 20, 1978

Prepared for

Fossil Energy
Energy Research and Development Administration
Washington, D.C.

Under Contract No. E(49-18)-2028

DISCLAIMER

Available from:

National Technical Information Service (NTIS)
U.S. Department of Commerce
5285 Port Royal Road
Springfield, Virginia 22161

Price: Printed copy: 7.25
Microfiche: $3.00

TABLE OF CONTENTS

LIST OF TABLES

LIST OF FIGURES

FIGURE Page

FIGURE Page

FIGURE Page

I. ABSTRACT

Three high-pressure flow microreactors and two batch autoclave reactors have been used to study the reaction networks and kinetics of (1) catalytic hydrodesulfurization of dibenzothiophene and methyl-substituted dibenzothiophenes and (2) catalytic hydrodenitrogenation of quinoline, methyl-substituted quinolines, acridine and carbazole. The catalysts were commercial, sulfided $CoO-MoO_3/\gamma-Al_2O_3$, $NiO-MoO_3/\gamma-Al_2O_3$, and $NiO-WO_3/\gamma-Al_2O_3$.

At the typical conditions of 300°C and 104 atm, dibenzothiophene reacts to give H_2S and biphenyl in high yield, but there is some hydrogenation preceding desulfurization. Methyl-substituted dibenzothiophenes react similarly, and each reaction is first-order in the sulfur-containing compound. Two methyl groups near the sulfur atom (in the 4 and 6 positions) reduce the reactivity tenfold, whereas methyl groups in positions further removed from the sulfur atom increase reactivity about twofold. The results are consistent with steric and inductive effects influencing adsorption. The data indicate competitive adsorption among the sulfur-containing compounds.

In quinoline hydrodenitrogenation, both rings are saturated before the C-N bond is broken. Similarly, in acridine conversion a large amount of hydrogenation precedes nitrogen removal. Breaking of the carbon-nitrogen bond is evidently one of the slower reactions in the network. The Ni-Mo catalyst is about twice as active as the Co-Mo catalyst for ring hydrogenation, and the two catalysts are about equally active for breaking the carbon-nitrogen bond.

Reactivity of carbazole is slightly lower than that of quinoline but higher than that of acridine. Again, extensive hydrogenation precedes heteroatom removal. The relative activity of nitrogen-containing compounds at 367°C and 136 atm decreases according to: quinoline (2.52), carbazole (2.43), acridine (1.62) and benz[c]acridine (1.54) where the numbers in parentheses are pseudo first-order rate constants in min^{-1}.

Preliminary studies of competing hydroprocessing reactions involving quinoline, indole and naphthlene over $Ni-Mo/\gamma-Al_2O_3$ have shown that the naphthalene hydrogenation rate is markedly reduced by the presence of quinoline; whereas the reactivity of quinoline is virtually unaltered by the presence of naphthalene. Similarly the rate of hydrodenitrogenation of indole is strongly reduced by the presence of quinoline, whereas the rate of hydrodenitrogenation of quinoline is unaffected by the presence of indole.

Aged catalysts taken from the H-Coal® and Synthoil processes contained coke and deposits of mineral matter (primarily FeS, titanium and clays). The H-Coal catalysts were examined, for example, in experiments with dibenzothiophene hydrodesulfurization and quinoline hydrodenitrogenation. The activity of the used catalyst was reduced 20-fold for hydrodesulfurization of dibenzothiophene and fivefold for hydrodenitrogenation of quinoline. Most of the loss of hydrodesulfurization activity was associated with the mineral deposits and not with the coke.

II. OBJECTIVES AND SCOPE

The major objectives of this research are as follows:

i) To develop high-pressure liquid-phase microreactors for operation in pulse and steady-state modes to allow determination of quantitative reaction kinetics and catalytic activities in experiments with small quantities of reactants and catalyst.

ii) To determine reaction networks, reaction kinetics, and relative reactivities for catalytic hydrodesulfurization of multi-ring aromatic sulfur-containing compounds found in coal-derived liquids.

iii) To determine reaction networks, reaction kinetics, and relative reactivities for catalytic hydrodenitrogenation of multi-ring aromatic nitrogen-containing compounds found in coal-derived liquids.

iv) To obtain quantitative data characterizing the chemical and physical properties of aged hydroprocessing catalysts used in coal liquefaction processes and to establish the mechanisms of deactivation of these hydroprocessing catalysts.

v) To develop reaction engineering models for predicting the behavior of coal-to-oil processing and of catalytic hydroprocessing of coal-derived liquids and to suggest methods for improved operation of hydrodesulfurization and hydrodenitrogenation processes.

vi) In summary, to recommend improvements in processes for the catalytic hydroprocessing of coal-derived liquids.

SCOPE

A unique high-pressure, liquid-phase microreactor is being developed for pulse (transient) and steady-state modes of operation for kinetic measurements to achieve objectives ii) through iv). The relative reactivities of the important types of multi-ring aromatic compounds containing sulfur and nitrogen are being measured under industrially important conditions (300-450°C and 500-4000 psi). The reaction networks and kinetics of several of the least-reactive multi-ring aromatic sulfur-containing and nitrogen-containing compounds commonly present in coal-derived liquids will be determined. Catalyst deactivation is an important aspect of the commercial scale upgrading of coal-derived liquids. Accordingly, the chemical and physical properties of commercially aged coal-processing catalysts are being determined to provide an understanding of catalyst deactivation; these efforts can lead to improved catalysts or procedures to minimize the problem. To make the results of this and related research most useful to ERDA, reaction engineering models of coal-to-coal processing in trickle-bed and slurry-bed catalytic reactors including deactivation will be developed to predict conditions for optimum operation of these processes. Based on the integrated result of all of the above work, recommendations will be made to ERDA for improved catalytic hydro-desulfurization and hydrodenitrogenation processing.

III. SUMMARY OF PROGRESS TO DATE

This summary is organized to parallel the task statements of the contract. A milestone chart is provided at the end of this section.

Microreactor Development

Three continuous-flow, liquid-phase, high-pressure microreactors have been built and operated under this contract. The work in this report confirms the success of these microreactors; the data from the batch autoclave runs are effectively identical to data from the flow microreactors. This task has been completed.

Catalytic Hydrodesulfurization

The hydrodesulfurization of dibenzothiophene (DBT) has been examined with a high-pressure microreactor and in batch, stirred-autoclave experiments. The range of data show that the reaction network is slightly more complex than the direct reduction of dibenzothiophene (DBT) to hydrocarbon products; the network is the following at 300°C and 100 atm:

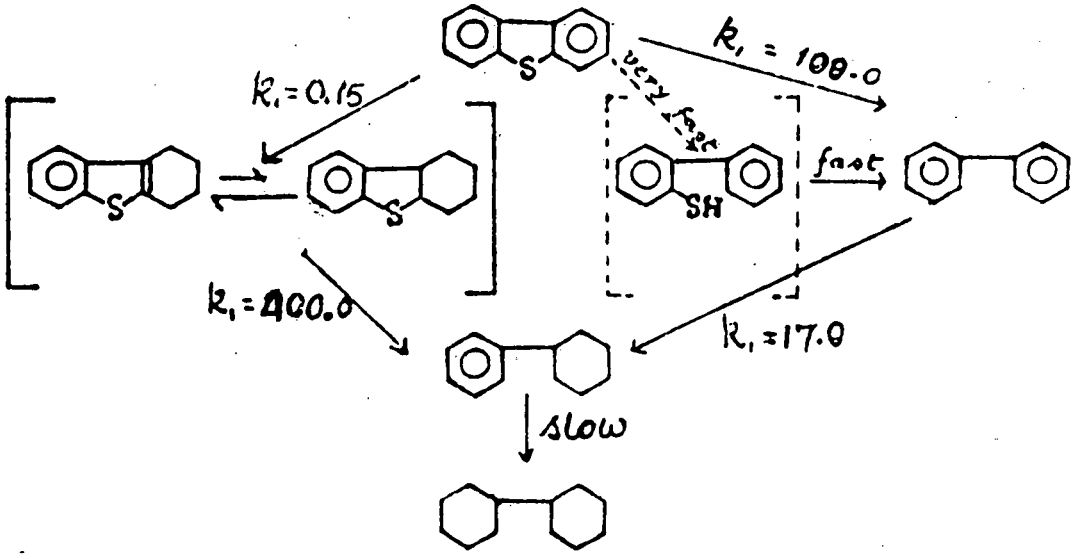

The relative rates of hydrodesulfurization of a variety of the important sulfur-containing compounds in coal-derived liquids have been determined. The compounds include methyl-substituted dibenzothiophenes, which evidently are among the least reactive compounds in hydrodesulfurization. The relative rate constants for the various reactants are the following: BT, very large; DBT, 1; 4-MeDBT, 0.16; 4,6-diMeDBT, 0.10; 3,7-diMeDBT, 1.7; and 2,8-diMeDBT, 2.6. These results are largely explained by steric and inductive effects. Groups located near the 'S' atom restrict its interaction with a surface anion vacancy and lower the reactivity. Inductive effects explain the higher reactivities of the compounds having methyl substituents where they exert no steric influence.

The reactivities of the compounds have been determined with individual sulfur-containing compounds and with pairs of these compounds. The reactivities of these compounds are influenced by competitive adsorption determined by the previously mentioned steric and inductive effects.

More detailed study of the hydrodesulfurization of 4,6-dimethyldibenzothiophene, which is the least reactive sulfur-containing compound found so far, shows that the reaction network is similar to that of dibenzothiophene but that hydrogenation of the aromatic ring is more pronounced than for dibenzothiophene.

Three different catalysts, namely Co-Mo/γ-Al_2O_3, Ni-Mo/γ-Al_2O_3 and Ni-W/Al_2O_3 have been tested for the hydrodesulfurization of dibenzothiophene. The activities of these catalysts have been found to decrease in the order: Ni-Mo > Ni-W $\geq$ Co-Mo.

Catalytic Hydrodenitrogenation

The hydrodenitrogenation of quinoline has been studied to yield a nearly complete identification of the reaction network and partial identification of the rate parameters in this network. The network is as follows:

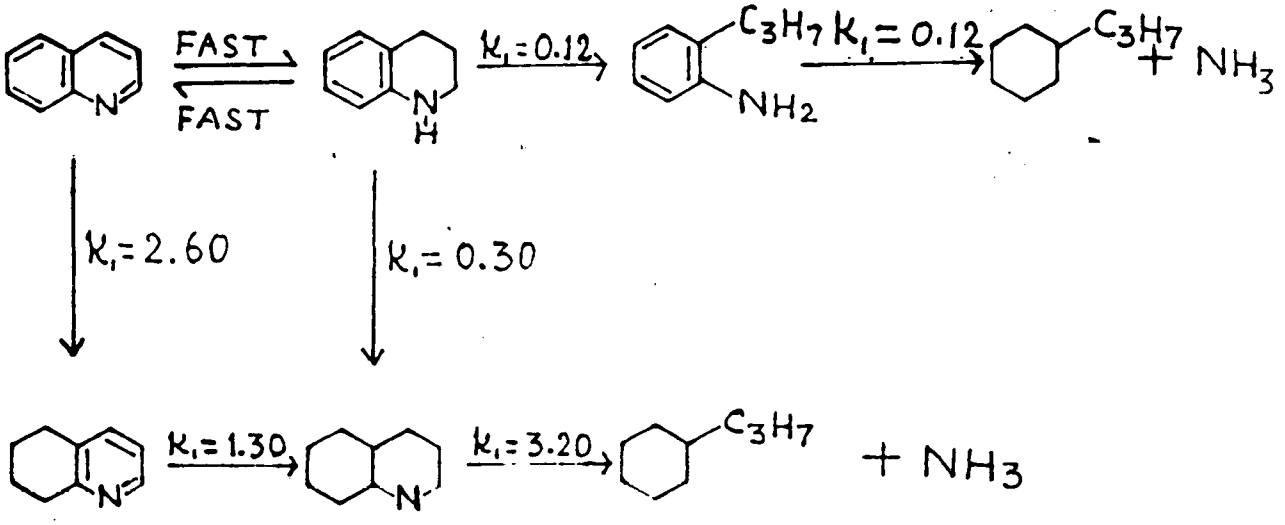

This network shows that usually both the benzene and pyridine rings are saturated before the C-N bond in the (now) piperidine ring is broken. Thus, the hydrodenitrogenation of quinoline requires a large consumption of hydrogen before the nitrogen atom is removed from the hydrocarbon structure. The lack of selectivity encountered in hydrodenitrogenation stands in sharp contrast to the high selectivity in hydrodesulfurization.

The total rate of hydrodenitrogenation shows a maximum with respect to hydrogen partial pressure. This is because the pseudo first-order constant for the C-N bond scission step is reduced by increasing hydrogen pressure and the rate constants for the hydrogenation steps, which increase with hydrogen pressure at lower hydrogen pressures, pass through a maximum and decrease with increasing hydrogen pressure at the high hydrogen pressures.

Also in hydrodenitrogenation of acridine, a large amount of hydrogenation precedes nitrogen removal, and the carbon-nitrogen bond breaking reactions are relatively slow. In the presence of Co-Mo/γ-Al_2O_3 catalyst, heteroaromatic ring hydrogenation is favored, and with a Ni-Mo/γ-Al_2O_3 catalyst, aromatic ring hydrogenation is favored. For both acridine and quinoline, little effect of replacing Co with Ni could be detected in the nitrogen removal reaction, although Ni-Mo/γ-Al_2O_3 is roughly twice as active for hydrogenation as Co-Mo/γ-Al_2O_3.

The hydrodenitrogenation of carbazole has been examined under conditions similar to those used for acridine. Both carbazole disappearance and total nitrogen removal can be represented as first-order reactions. Tetrahydrocarbazole was the major intermediate compound present in the dry column extract. Both cis-hexahydrocarbazole and octahydrocarbazole were identified as minor products. Reactivity of carbazole is slightly less than that of quinoline and acridine is the least reactive. Hydrodenitrogenation of four- and five-ring nitrogen-containing compounds are currently being studied.

Preliminary experiments have been carried out to characterize hydrodenitrogenation of substituted quinolines. The conditions used were similar to those used for quinoline hydrodenitrogenation. 2,6-, 2,7- and 2,8-dimethylquinolines were studied and products identified were analogous to those observed in the quinoline network. The reactivity of these compounds to hydrodenitrogenation is comparable to that of quinoline.

The reaction network for the hydrodenitrogenation of acridine (in White Oil) catalyzed by Ni-Mo/γ-Al_2O_3 catalyst is as given below:

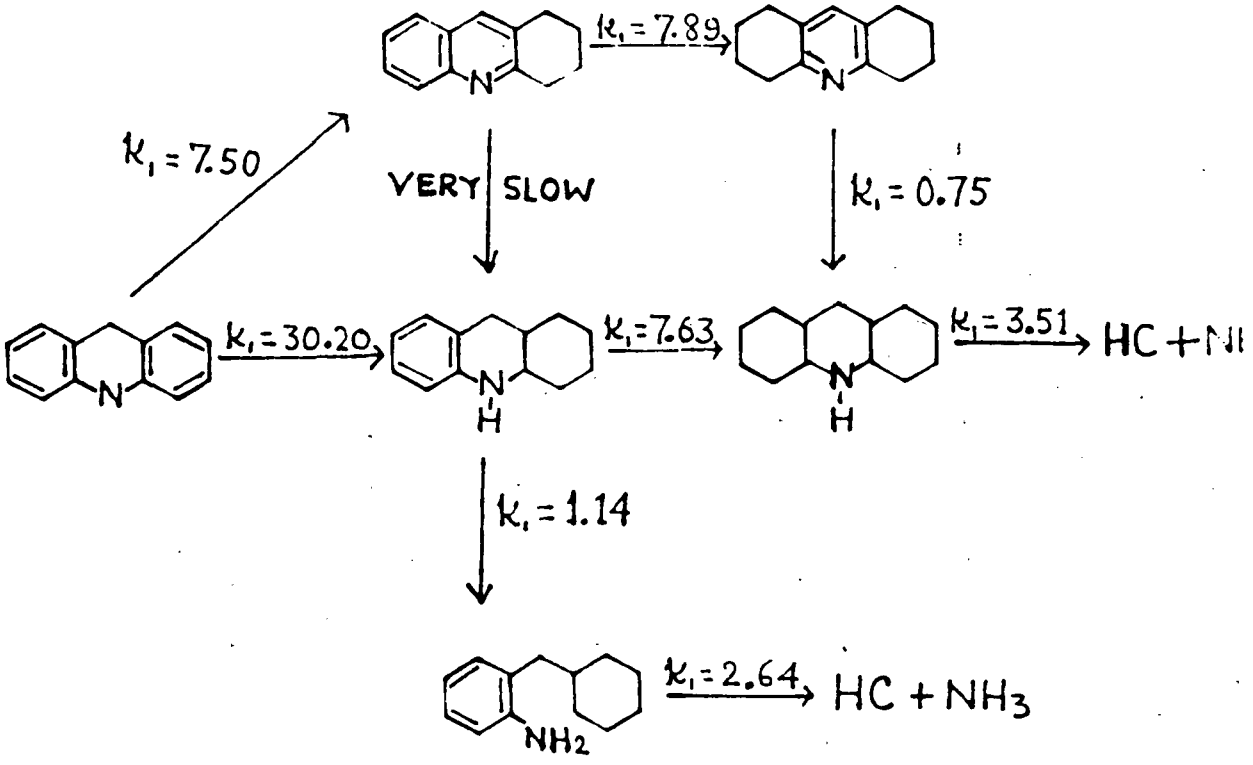

The pseudo first-order rate constants are for 367°C and 136 atm. The pseudo first-order rate constants for hydrodenitrogenation (total nitrogen removal) at 367°C and 136 atm catalyzed by Ni-Mo/γ-Al_2O_3 falls in the following order:

Reactant	Pseudo first-order rate constant for total nitrogen removal, min^{-1}
Quinoline	2.52
Carbazole	2.43
Acridine	1.62
Benz[c]acridine	1.54

Preliminary studies of competing hydroprocessing reactions catalyzed by Ni-Mo/γ-Al_2O_3 and involving quinoline, indole and naphthalene in White Oil show that marked interactions exist. The naphthalene hydrogenation rate is markedly reduced by the presence of quinoline; whereas the reactivity of quinoline is virtually unchanged by the presence of naphthalene. Similarly the rate of hydrodenitrogenation of indole, a non-basic nitrogen-containing compound, is strongly reduced by the presence of quinoline, whereas the rate of hydrodenitrogenation of quinoline, a basic nitrogen-containing compound, is unaffected by the presence of indole. Studies involving combinations of nitrogen- and sulfur-containing compounds and aromatic hydrocarbons are underway.

Catalyst Deactivation

A variety of physical techniques have been used to identify the aging process for catalysts used in synthetic liquid fuel processes. Catalyst samples from three processes have been examined: a proprietary fixed-bed process, Synthoil, and H-Coal^R. The spent fixed-bed catalysts show the formation of an external crust which appears to be formed by columnar grain growth combined with the deposition of coal mineral matter, particularly clays and rutile. This external crust is absent from the H-Coal^R catalyst. The interior of the catalyst is altered by several processes: coking, reactive deposition of mineral matter, passive deposition of mineral matter, and crack enhancement. These four processes are found in catalysts from all three processes. Coking fills the micropore volume of the catalyst. Reactive deposition of mineral matter penetrates about 200 μm from the outer surface into the interior of the catalyst. The concentration profile is approximately exponentially decreasing from the exterior surface. Passive cementing occurs within 50 μm of the surface unless the irregular concentration profiles. Finally, grain growth can occur inside the catalyst near the surface and tends to increase these cracks. When the surface cracks become a significant portion of the pore volume, passive deposition can penetrate further into the interior of the catalyst.

The activity of aged catalyst from the H-Coal^R process has been measured in batch experiments with dibenzothiophene and with quinoline. The activity was reduced 20-fold for hydrodesulfurization of dibenzothiophene and five-fold for hydrodenitrogenation of quinoline. Burning off of carbonaceous deposits increased the activity of the aged catalyst only

three-fold for dibenzothiophene hydrodesulfurization, which implies that irreversibly deposited inorganic matter was responsible for most of the loss of catalytic activity.

Microreactor Engineering

The use of moments as a tool in interpreting pulse data from microreactors has been extended to fairly complex reaction networks. This work is now complete. The complex data from quinoline and acridine reactions have been reduced to rate parameters by extension of nonlinear regression analysis. Reaction engineering concerned with coal hydroprocessing is now underway.

TIME PLAN* AND MILESTONE CHART**

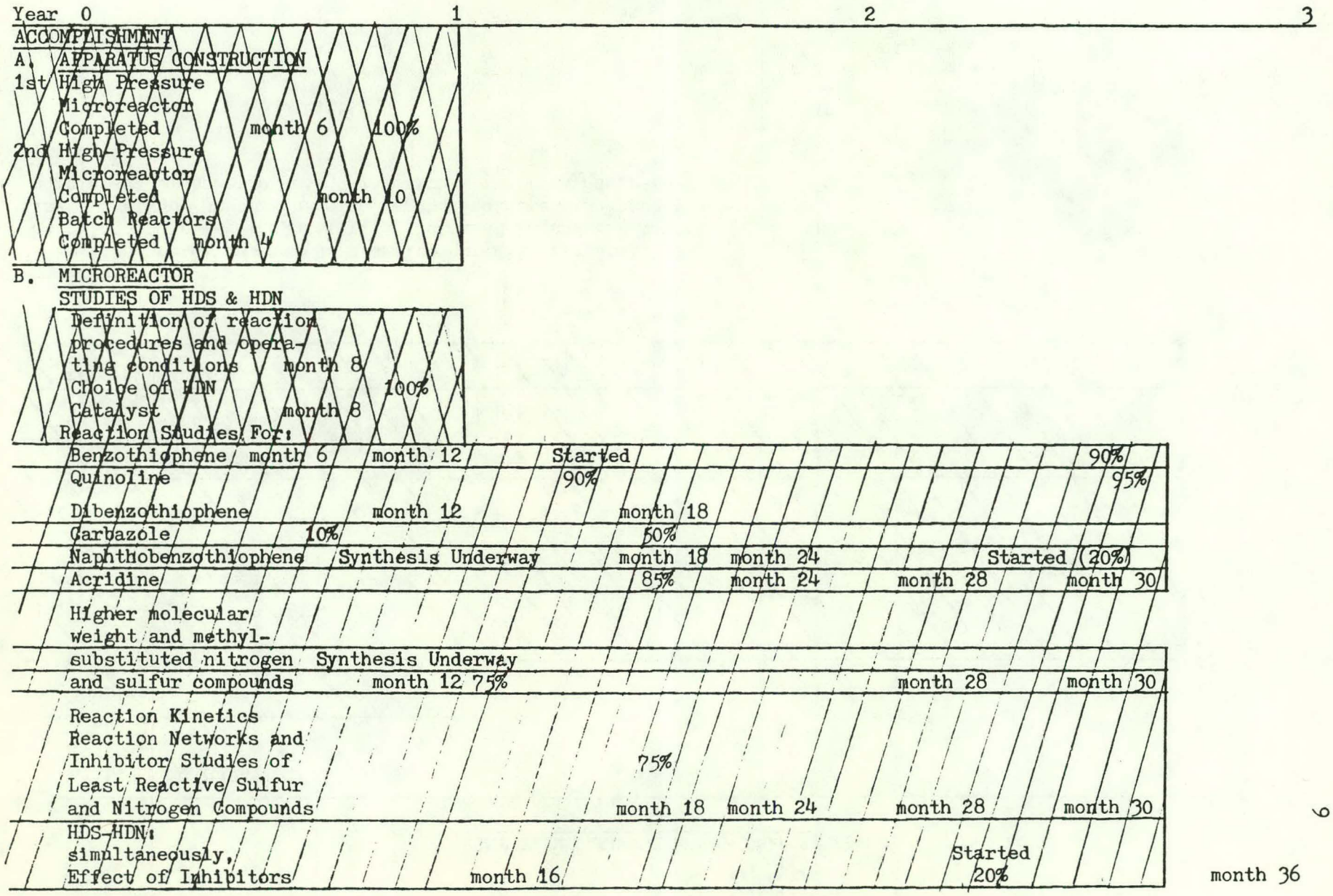

TIME PLAN* AND MILESTONE CHART** (cont)

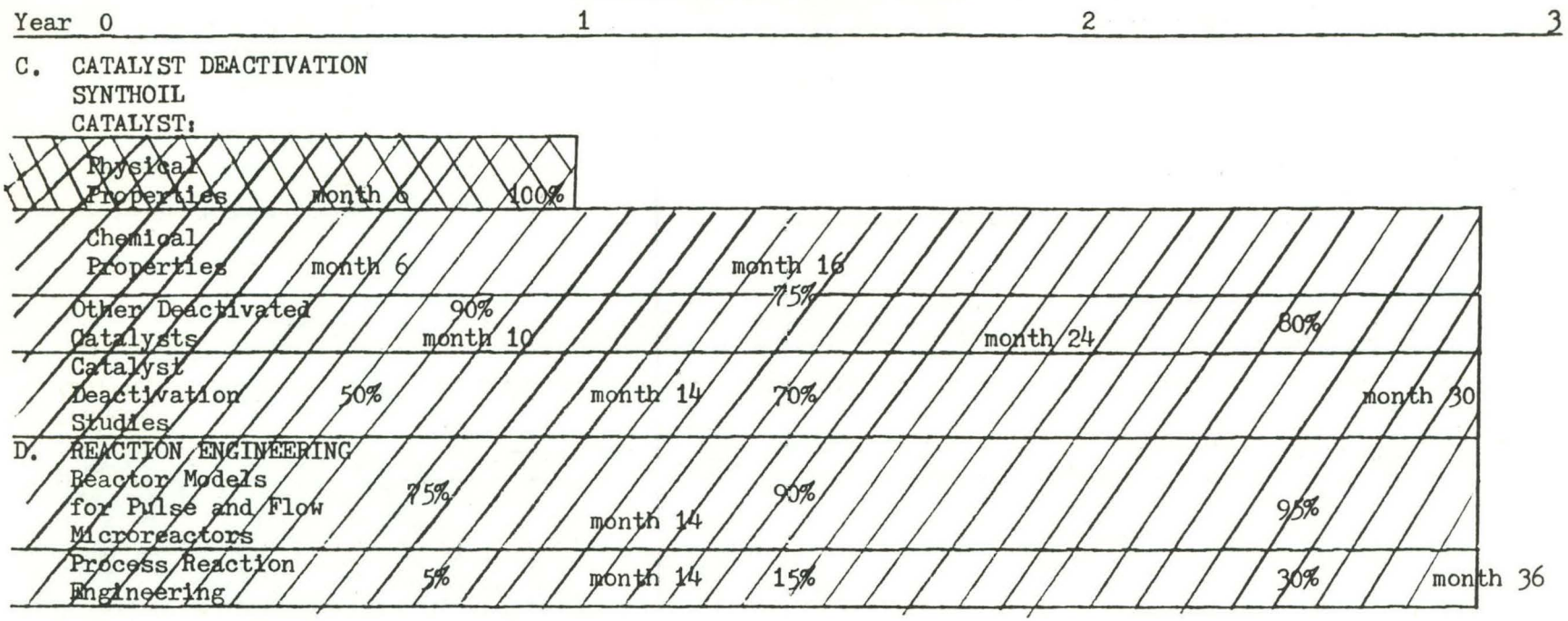

*Time Plan and Milestone Chart as Presented in Proposal.

**Hatching indicates that activity indicated is under active investigation; number in hatch region indicates the percentage completed; crosshatching indicates that the task has been completed.

CUMULATIVE EXPENDITURES*

Item	Quarter									
	First	Second	Third	Fourth	Fifth	Sixth	Seventh	Eighth	Ninth	Tenth
Personnel	$5,807	$20,740	$37,396	$53,418	$91,593	$112,666	$132,669	$146,146	$167,884	$192,658
Travel	28	528	1,152	1,152	1,521	2,458	3,140	3,814	5,119	6,113
Supplies & Expense	4,674	10,007	19,582	25,735	37,291	42,341	51,589	56,488	64,778	70,579
Occupancy & Maintenance	6,110	9,208	10,108	10,634	13,755	13,920	14,396	14,600	16,325	18,010
Equipment	610	17,978	30,704	34,930	50,614	54,013	54,013	52,295	54,977	54,977
Information Processing	--	--	--	97	154	375	1,180	1,868	2,044	2,248
Transfers (Overhead)	--	10,202	20,035	38,710	75,839	93,287	113,830	123,576	117,681	134,895

*Includes encumbrances

IV. DETAILED DESCRIPTION OF TECHNICAL PROGRESS:

A. Hydroprocessing Microreactor Development

All the three flow microreactors are operational in a nearly continuous fashion. The first microreactor is being used to study the reactivities of various sulfur-compounds like dibenzothiophene and its various methyl substituted derivatives and benzonaphthothiophene and its methyl derivatives. In the two previous quarterly reports (viz., 7th and 8th) comparative studies were given on the relative reactivities of these compounds. The degree and position of substitution of the methyl groups on the DBT skeleton has been found to have marked influence on the HDS reactivity. The catalysts so far studied are: Co-Mo/γ-Al_2O_3, Ni-Mo/γ-Al_2O_3 and Ni-W/γ-Al_2O_3 at various stages. The reaction network of DBT has been discussed in detail in the last quarterly (i.e., 9th) report. In this quarterly report, we discuss the network of 4,6-dimethyl DBT. The second microreactor continues to be used occasionally for the hydrodenitrogenation (HDN) reactions.

The third microreactor is in regular use for the full kinetic studies of hydrodesulfurization of dibenzothiophene.

In addition to this, the two batch autoclaves have been extensively used in this quarter.

B. Catalytic Hydrodesulfurization

1. First High-pressure Flow Reactor

a. Dibenzothiophene Kinetics:

It has been indicated in the earlier report (see the 8th quarterly report in this series) that DBT can react in two ways, namely,

(i) with sulfur extrusion preceding hydrogenation of the aromatic ring(s).
(ii) with hydrogenation of aromatic ring(s) preceding the sulfur removal.

The first reaction is predominant at all the conditions. The importance of the second reaction depends on the catalyst composition and the concentration of H_2S in the reactant mixture.

Experiments were performed with different initial wt %s of DBT in the feed by the first flow microreactor. The operating conditions are as indicated below:

- Catalyst: HDS-16A, mass: 25 mg; volume of the reactor bed: 0.325 cm^3; length of bed 4.1 cm; catalyst particle size: 149-178 μm.
- Catalyst pretreatment: catalyst sulfided in situ with 10% H_2S in H_2 (V/V) for two hours at 400°C. Flow rate was 30-50 cm^3/min.
- Liquid flow rate: 1.2 to 7.2 cm^3/hr.
- Saturation pressure applied to liquid feed: 68 atm.
- Reactor temperature: 300 ± 1°C.
- Reactant mixture: DBT in n-hexadecane carrier oil.

Figure 1 shows the reaction network for DBT hydrodesulfurization reported earlier (8th quarterly report). Figure 2 shows the lumped-parameter model used for subsequent kinetic parameter estimation purposes. All the reaction paths are considered to follow pseudo first-order kinetics; the corresponding pseudo first-order rate constants are shown in Figure 2.

Four different initial concentrations of DBT were used. Table 1 briefly summarizes the selectivity pattern for biphenyl (BPh) and cyclohexylbenzene (CHB), and indicates the pseudo first-order rate constants for overall DBT disappearance.

From Table 1 it is seen that for any particular run selectivity for CHB decreased with increasing flow rate, whereas selectivity for BPh

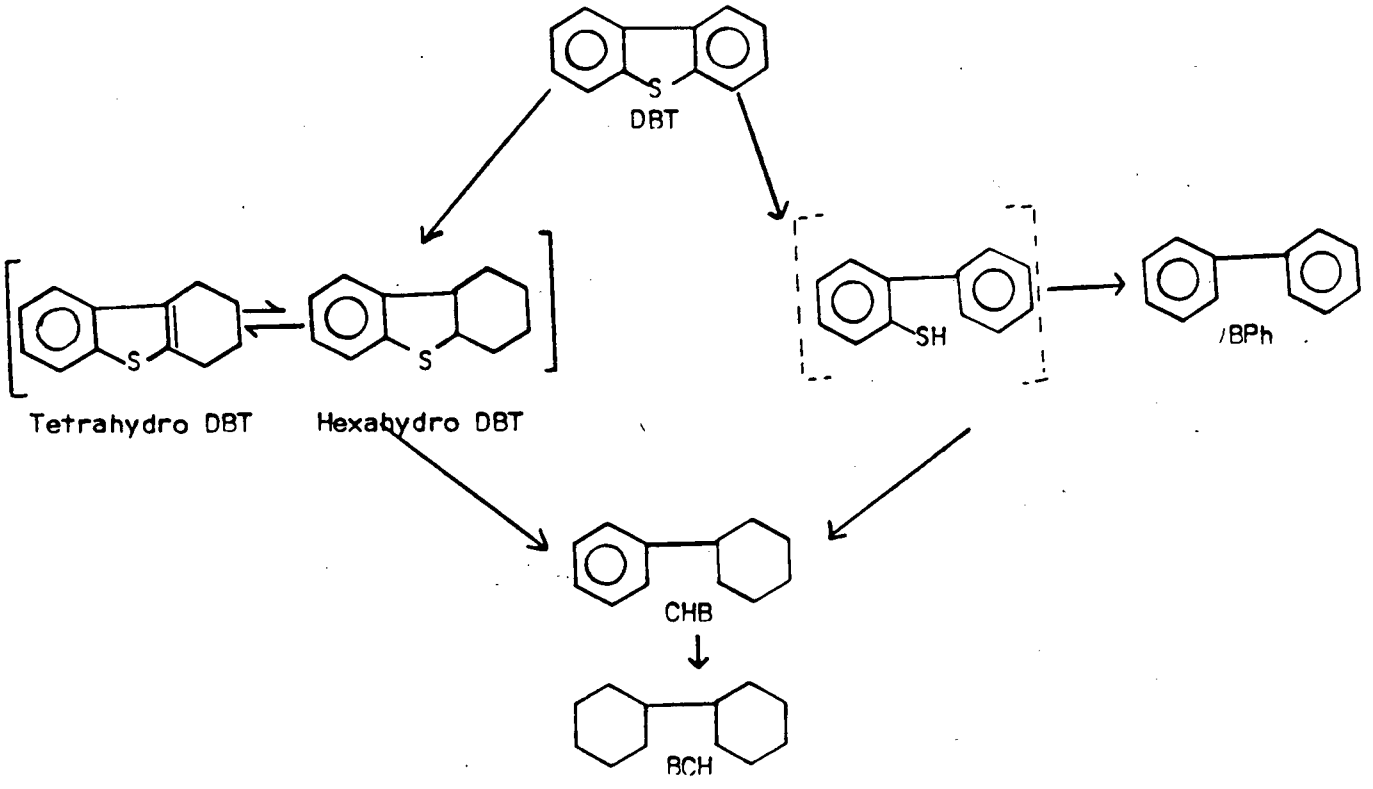

Fig. 1. Reaction network for hydrodesulfurization of dibenzothiophene over Co-Mo/γ-Al_2O_3.

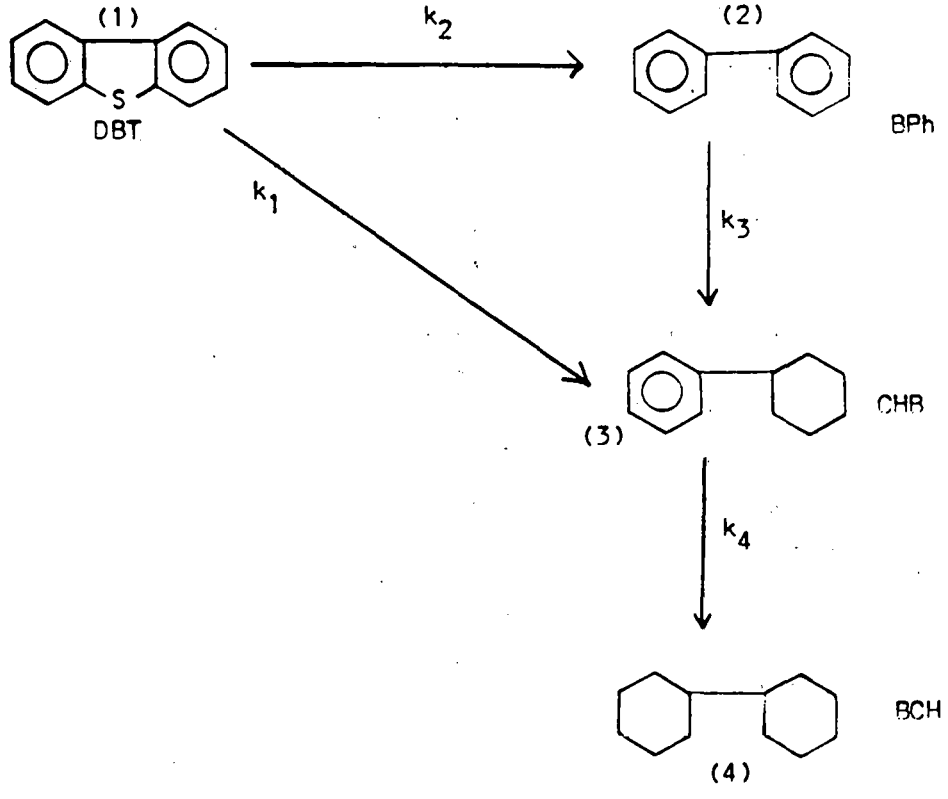

Fig. 2. Lumped-parameter model used to estimate first-order rate constants in hydrodesulfurization of dibenzothiophene over Co-Mo/γ-Al_2O_3.

TABLE 1

Effect of Initial Dibenzothiophene Concentration on Selectivity and Kinetics

RUN	Flow ml/hr	$(LHSV)^{-1}$ gm catalyst hr / cm^3 of feed	% Selectivity BPh	% Selectivity CHB	Pseudo first-order rate constant for overall DBT disappearance k_{obs} $cm^3/gm\ hr$
53	1.2	0.0208	96.8	6.7	
0.0543	2.4	0.0104	86.9	3.8	
wt % DBT	3.6	0.0069	92.6	3.3	256.0
	4.8	0.0052	90.6	2.7	
	6.0	0.0042	88.7	2.1	
54	1.2	0.0208	87.1	6.7	
0.1154	2.4	0.0104	90.4	4.1	
wt % DBT	4.8	0.0052	89.8	2.5	104.0
	6.0	0.0042	87.4	1.9	
	7.2	0.0035	97.6	1.8	
55	1.2	0.0208	84.6	7.7	
0.1637	2.4	0.0104	89.6	4.6	
wt % DBT	3.6	0.0069	91.8	3.6	73.5
	6.0	0.0042	89.8	2.2	
	7.2	0.0035	96.7	1.8	
56	1.2	0.0208	80.0	9.8	
0.2348	2.4	0.0104	87.1	6.1	
wt % DBT	3.6	0.0069	80.4	4.8	69.9
	6.0	0.0042	89.7	3.6	
	7.2	0.0035	87.7	3.1	

fluctuates randomly about mean and could be considered to be constant in any particular run.

Figs. 3 to 6 show the pseudo first-order kinetics of overall DBT conversion for these runs. Fig. 7 shows the pseudo first-order rate constant for hydrodesulfurization of dibenzothiophene versus the initial feed concentration of DBT. It is seen that at higher concentrations of DBT in the feed the curve flattens to give an almost constant pseudo first-order rate constant. The same data are replotted in Fig. 8 as $1/k_{obs}$ versus initial feed concentration (C_o) in order to fit an empirical relation of the form,

$$k_{obs} = \frac{K'}{1 + \alpha C_o}$$

From the least squares line shown in the Fig. 8, K' and α are determined to be:

$$K' = 500 \quad cm^3/gm\ hr$$
$$\alpha = 0.5 \quad gm/micro\ gm\ moles$$

Hence the overall disappearance rate constant for DBT can be represented as

$$K_{obs} = \frac{500}{1 + 0.5\ C_o} \ .$$

The aim of the subsequent development is to determine the individual linear kinetic constants shown in the Fig. 2. Each of the above runs provides concentration of DBT, BPh and CHB for different space times ($LHSV^{-1}$). For any particular run the above concentration versus space time data for each component is fitted with a non-linear least squares curve. The fitted curve has about the same form as the analytical solution for the above mentioned lumped-parameter model. These smoothed non-linear curves are con-

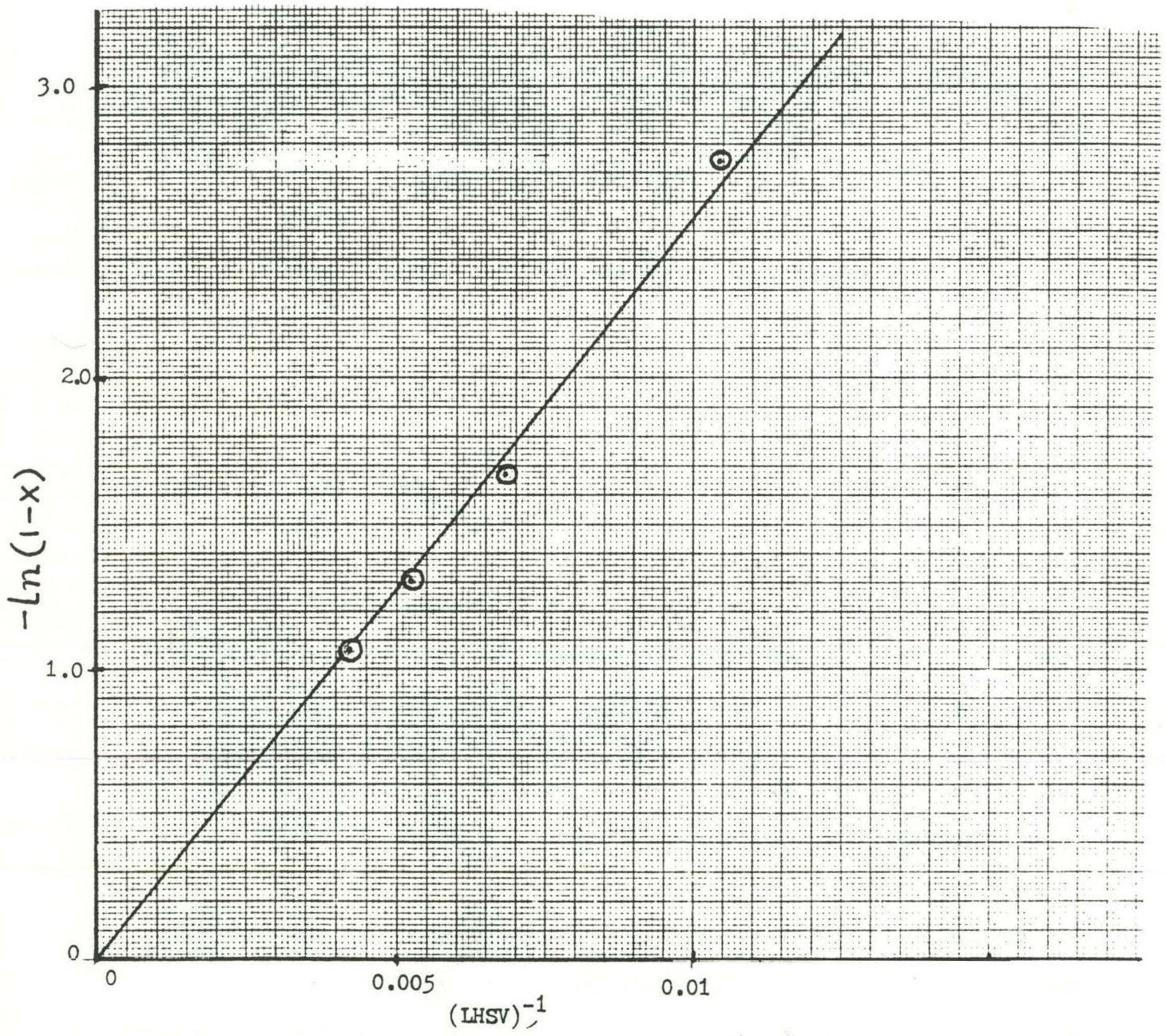

Fig. 3. Hydrodesulfurization of dibenzothiophene over Co-Mo/γ-Al_2O_3: Run 53, 0.0543 wt % DBT.

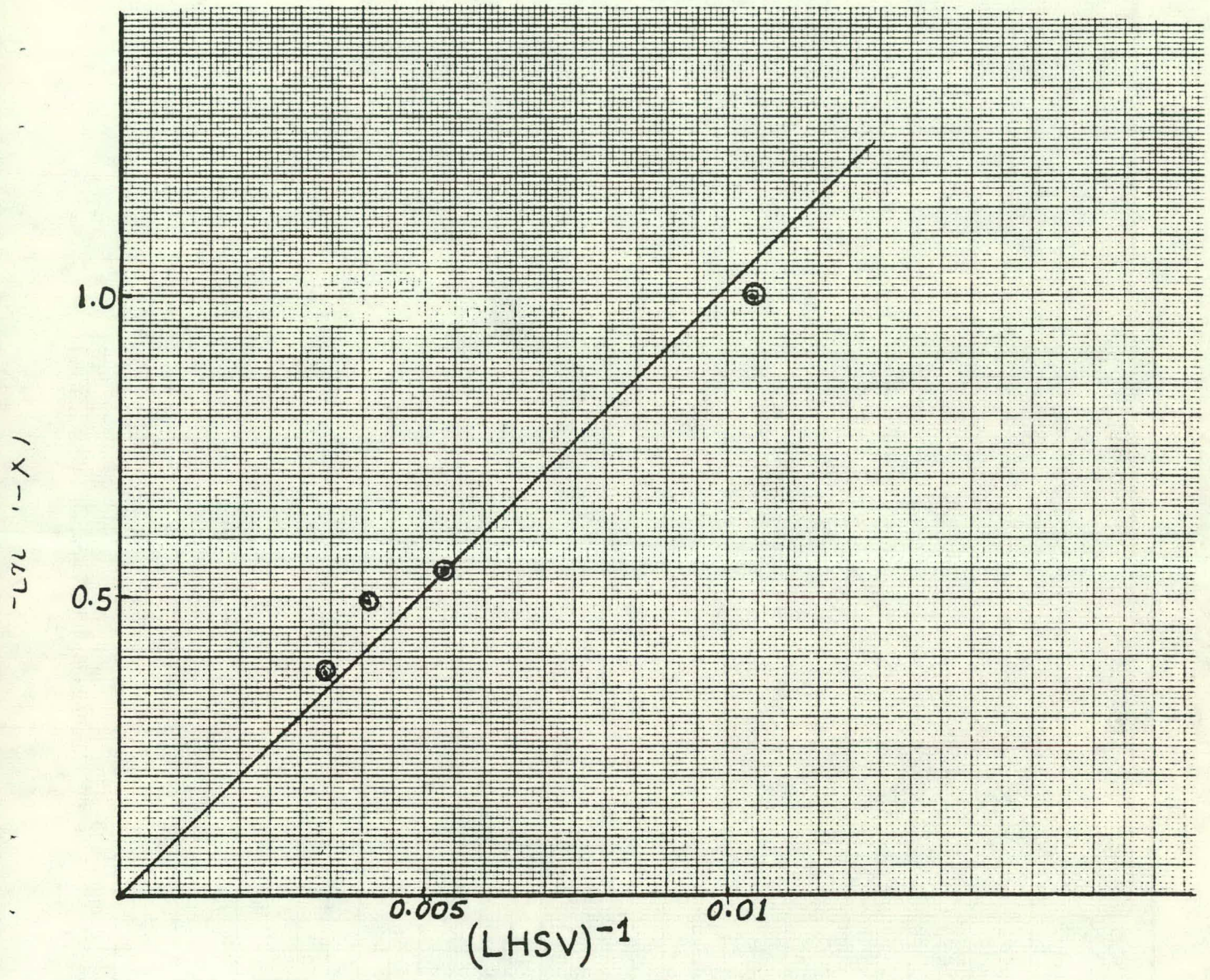

Fig. 4. Hydrodesulfurization of dibenzothiophene over Co-Mo/γ-Al_2O_3: Run 54, 0.1154 wt % DBT.

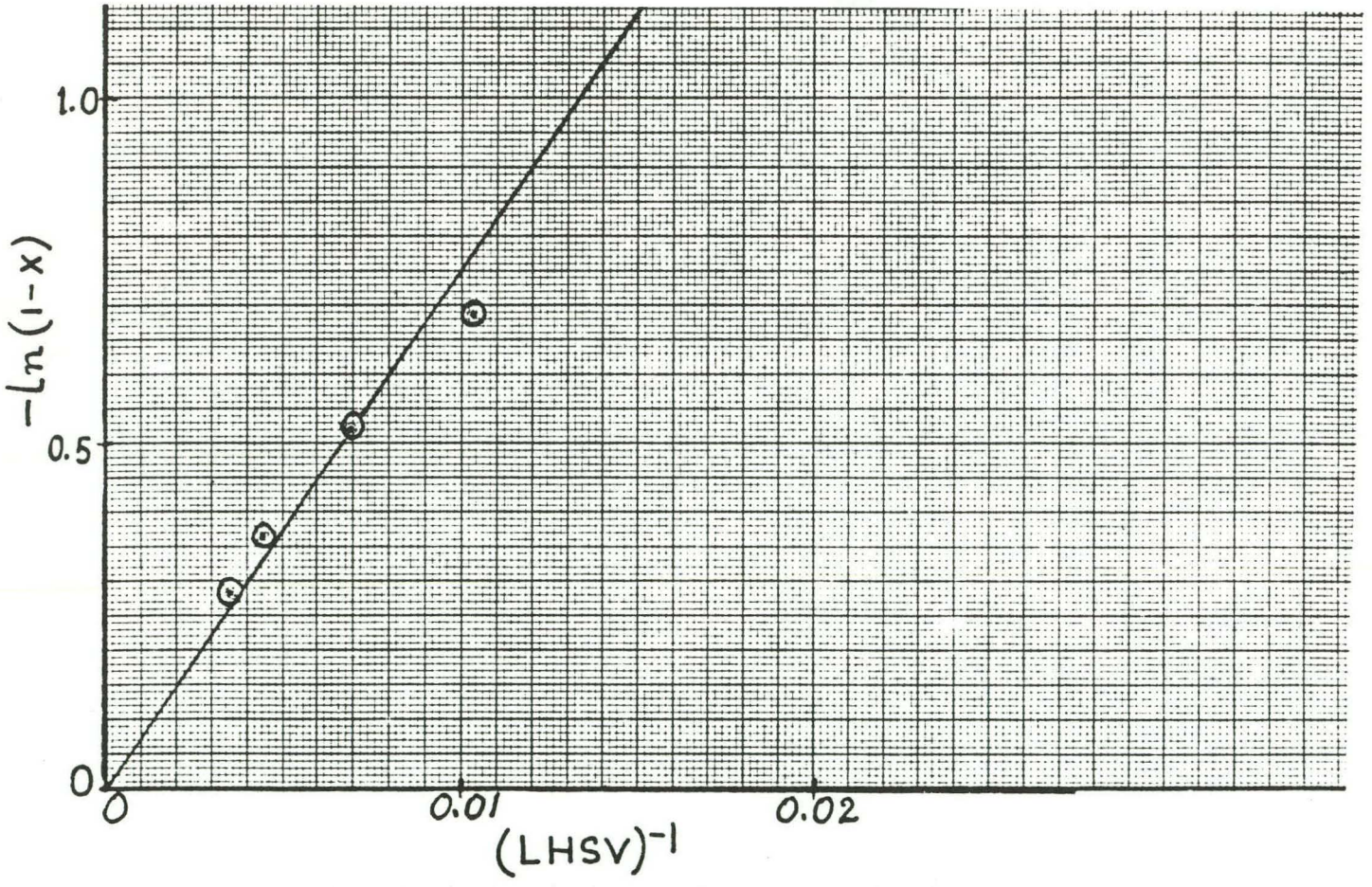

Fig. 5. Hydrodesulfurization of dibenzothiophene over Co-Mo/γ-Al_2O_3: Run 55, 0.1637 wt % DBT.

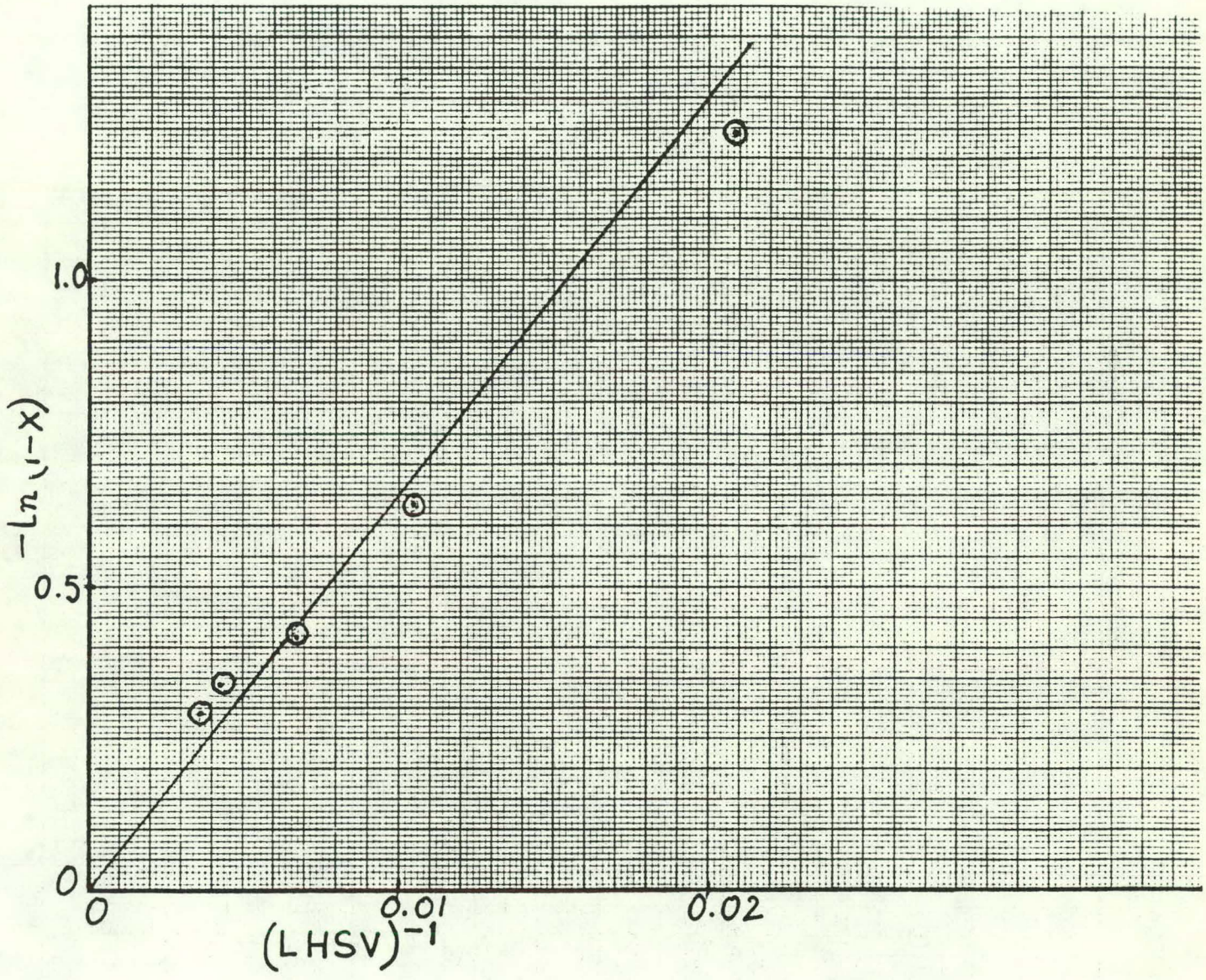

Fig. 6. Hydrodesulfurization of dibenzothiophene over Co-Mo/γ-Al_2O_3: Run 56, 0.2348 wt % DBT.

Co - initial Concentration of Dibenzothiophene in the feed (micro gm moles / gm)

k_{obs} - Overall Dibenzothiophene disappearance rate constant ($Cm^3/gm\ hr$).

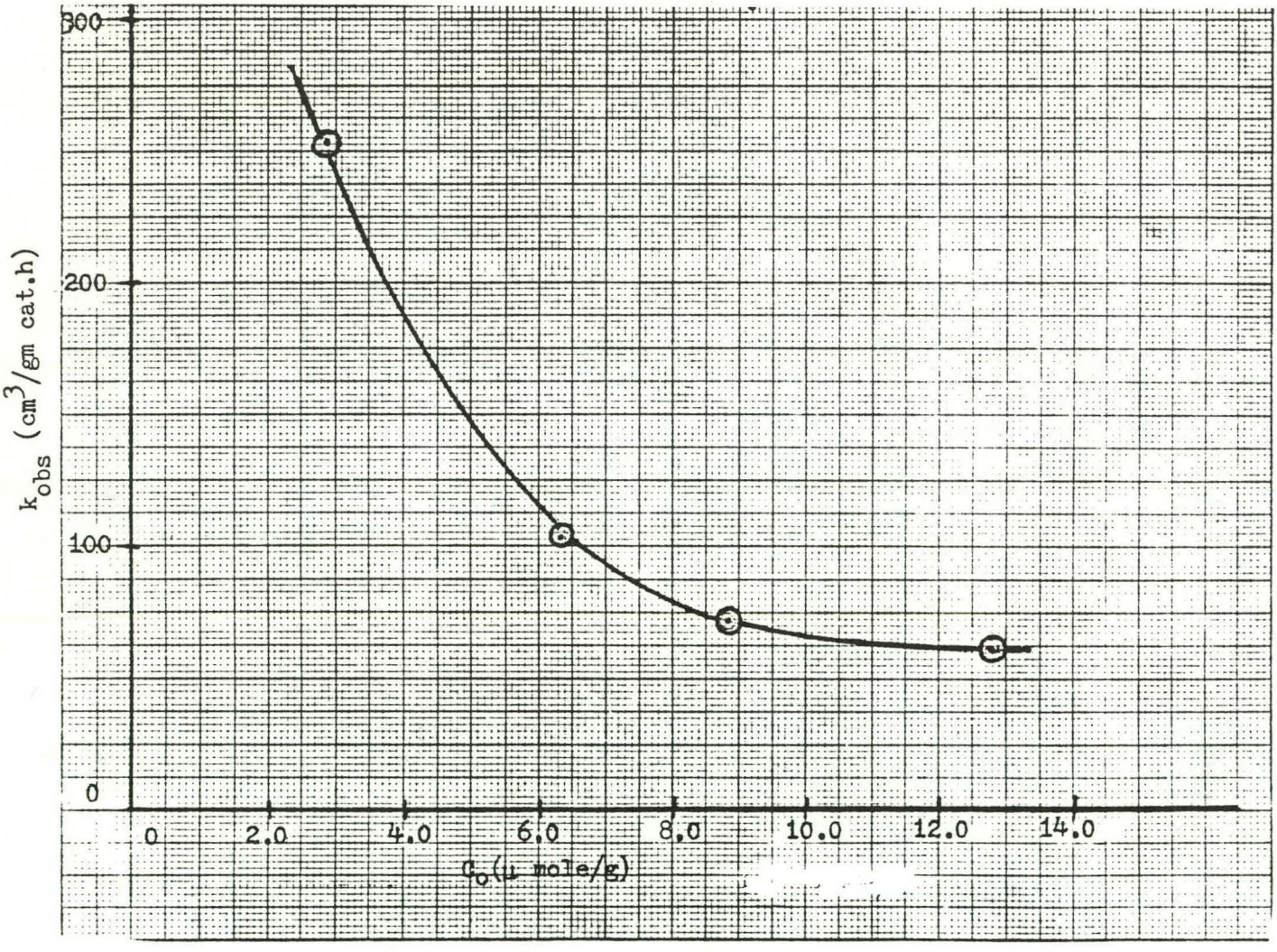

Fig. 7. Effect of initial concentration of dibenzothiophene on the pseudo first-order rate constant for hydrodesulfurization.

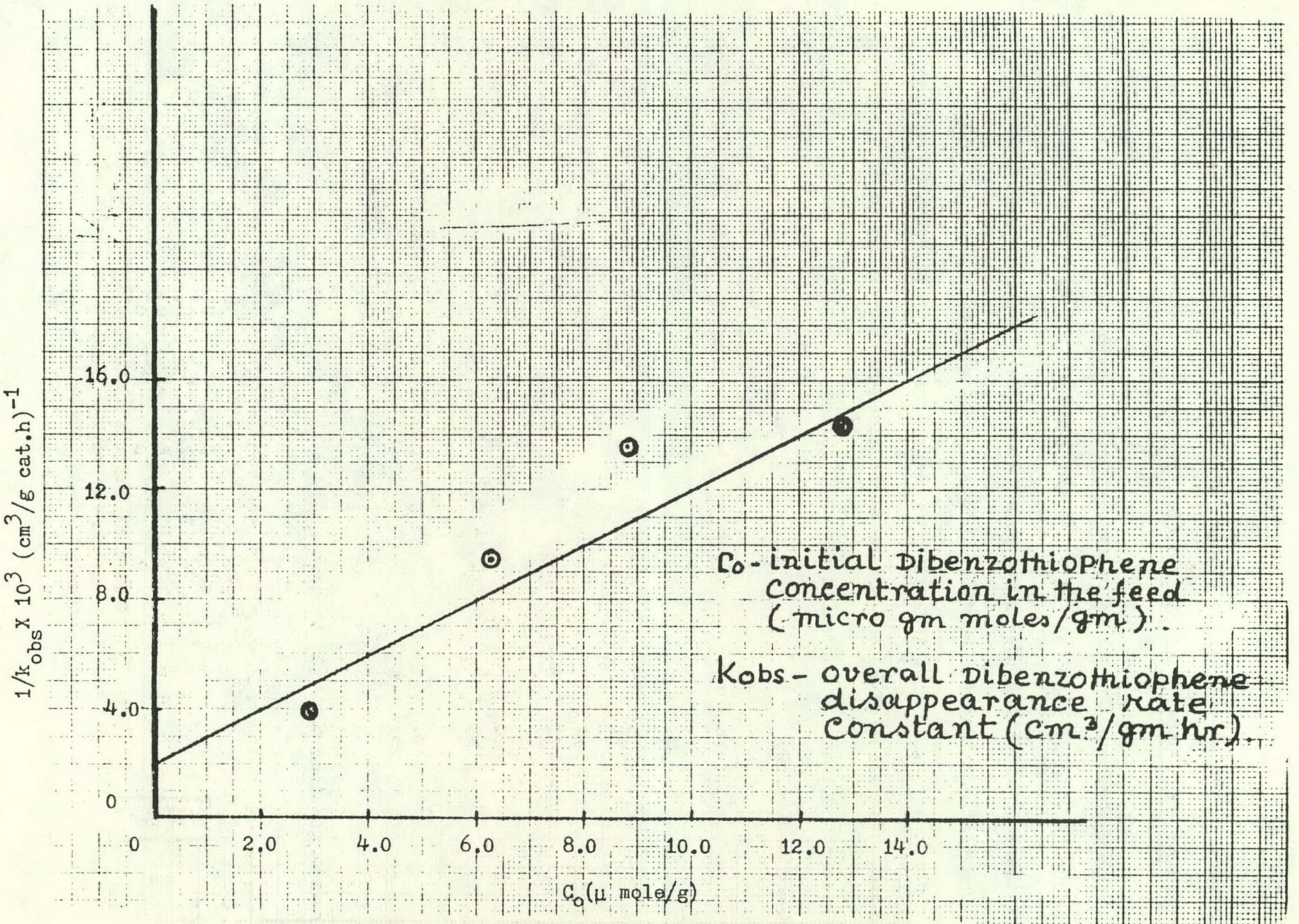

Fig. 8. Effect of initial feed on reciprocal pseudo first-order rate constant; linearized form of the rate equation.

sidered as data to the "Carlton 2" program, which can determine kinetic parameters in the linear system of equations. (Ref: D. M. Himmelblau et al., Ind. Eng. Chem. Fundamentals, 6, 539, 1967).

The check on the values of rate constants (k's) obtained by this procedure is made by plotting the concentration versus space time curves using these k values and the actual experimental data points. Fig. 9 is one such plot obtained for Run 54. Similar plots were also obtained for the other runs. This plot indicates the degree of accuracy of the procedure employed. The value of k_4 can not be ascertained accurately as we do not have quantitative information about BCH. The mathematical analysis is described below:

First consider Fig. 2. Assuming a linear kinetic model, we have,

$$\frac{dC_1}{dt} = -(k_1 + k_2)C_1$$

$$\frac{dC_2}{dt} = k_2C_1 - k_3C_2$$

$$\frac{dC_3}{dt} = k_1C_1 + k_3C_2 - k_4C_3$$

$$\frac{dC_4}{dt} = k_4C_3 \qquad (1)$$

In matrix notation Eqn. (1) becomes,

$$\frac{d\underline{C}}{dt} = \underline{\underline{k}}\,\underline{C} \qquad (2)$$

where $\underline{C} = \begin{bmatrix} C_1 \\ C_2 \\ C_3 \\ C_4 \end{bmatrix}$, $\underline{\underline{k}} = \begin{bmatrix} -(k_1 + k_2) & 0 & 0 & 0 \\ k_2 & -k_3 & 0 & 0 \\ k_1 & k_3 & -k_4 & 0 \\ 0 & 0 & k_4 & 0 \end{bmatrix}$

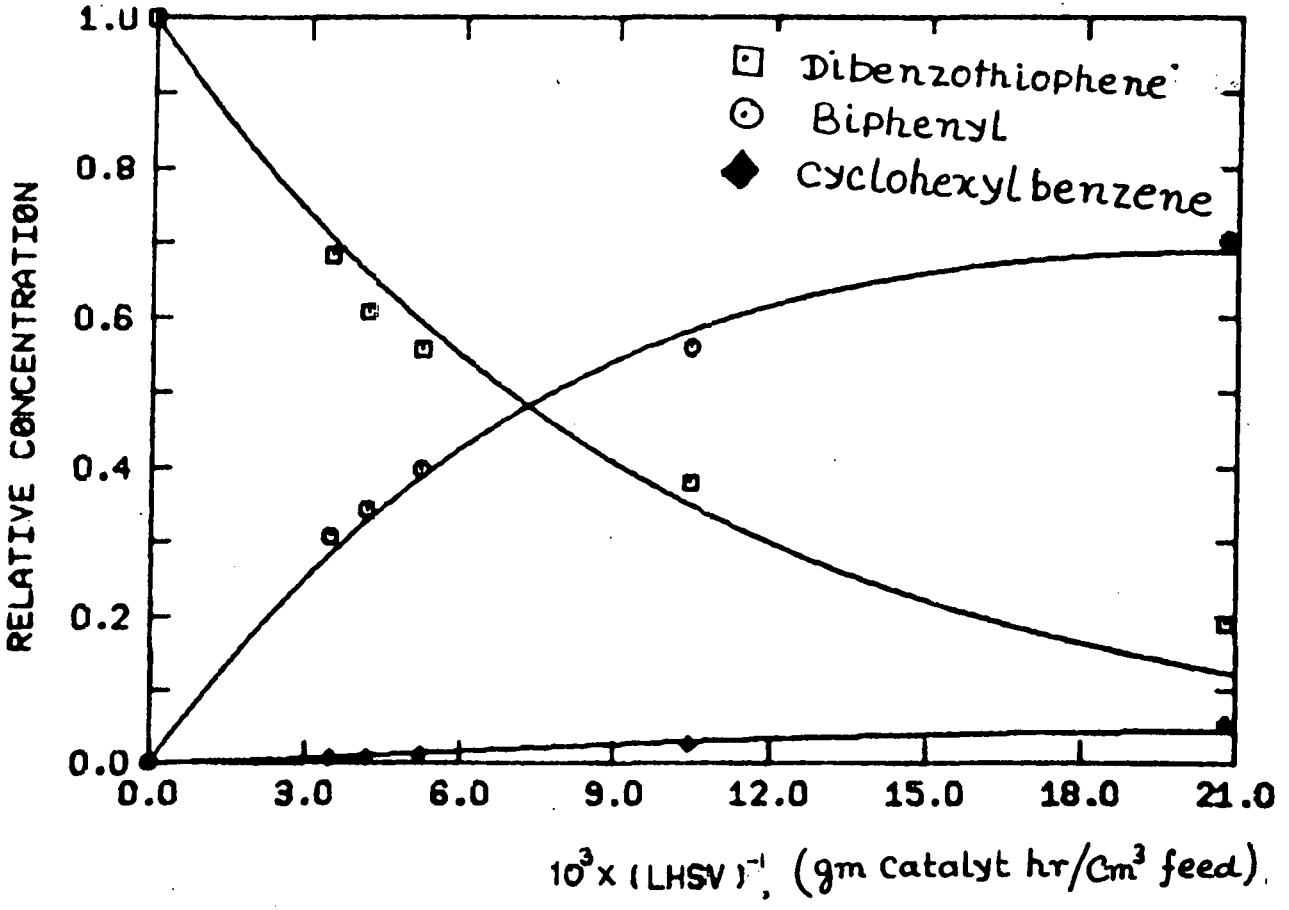

Fig. 9. Comparison of predicted behavior (solid line) using estimated kinetic parameters with the observed behavior (data points) for Run 54.

$\underline{\underline{k}}$ can be written as,

$$\underline{\underline{k}} = \underline{\underline{X}}\,\underline{\underline{\Delta}}\,\underline{\underline{X}}^{-1} \tag{3}$$

$\underline{\underline{X}}$ - Eigen vector matrix of $\underline{\underline{k}}$

$\underline{\underline{\Delta}}$ - Matrix formed from eigen values of $\underline{\underline{k}}$

$$\underline{\underline{\Delta}} = \begin{bmatrix} \lambda_1 & 0 & 0 & 0 \\ 0 & \lambda_2 & 0 & 0 \\ 0 & 0 & \lambda_3 & 0 \\ 0 & 0 & 0 & \lambda_4 \end{bmatrix}, \qquad \underline{\underline{x}} = [\underline{x}_1, \underline{x}_2, \underline{x}_3, \underline{x}_4]$$

x_i's are eigen vectors corresponding to eigen values x_i's.

Now Eqn. (2) becomes,

$$\frac{d\underline{C}}{dt} = \underline{\underline{X}}\,\underline{\underline{\Delta}}\,\underline{\underline{X}}^{-1}\underline{C} \tag{4}$$

let $\underline{\underline{X}}^{-1}\underline{C} = \underline{a}$ (5)

Therefore Eqn. (4) becomes

$$\frac{d\underline{a}}{dt} = \underline{\underline{\Delta}}\,\underline{a} \tag{6}$$

Thus we have uncoupled the original Eqn. (2).

Integrating Eqn. (6) gives

$$\underline{a} = e^{\underline{\underline{\Delta}} t}\,\underline{a}\,(o) \tag{7}$$

where

$$\underline{a}(o) = \begin{bmatrix} a_1(o) \\ a_2(o) \\ a_3(o) \\ a_4(o) \end{bmatrix} = \underline{\underline{x}}^{-1} \begin{bmatrix} C_1(o) \\ C_2(o) \\ C_3(o) \\ C_4(o) \end{bmatrix} \tag{8}$$

and $\underline{C}(o)$ = the known initial concentration vector.

From Eqns. (7) and (5)

$$\underline{C} = \underline{\underline{X}}\, e^{\underline{\underline{\Lambda}}t}\underline{a}(o) \qquad (9)$$

$\underline{a}(o)$ can be determined from the Eqn. (8). Eqn. (9) in more familiar form can be written as,

$$\underline{c} = \underline{x}_1 a_1(o)e^{\lambda_1 t} + \underline{x}_2 a_2(o)e^{\lambda_2 t} + \underline{x}_3 a_3(o)e^{\lambda_3 t} + \underline{x}_4 a_4(o)^{\lambda_4 t} \qquad (10)$$

Using 'Carlton 2' program, $\underline{\underline{k}}$ can be determined as discussed above. Programs were written to determine eigen values and eigen vectors of $\underline{\underline{k}}$. Eqn. (10) is then used to generate the concentration versus space time curves as shown in the Fig. 9.

Table 2 summarizes the rate constants obtained for these runs.

From the Table 2 it is seen that as the wt % DBT in the feed is increased the rate of hydrogenation is increased (both k_1 and k_3 increase), whereas desulfurization rate is decreased (k_2 decreases).

2. Third High-pressure Flow Microreactor

a. Experimental

A series of runs with dibenzothiophene (DBT) and various levels of H_2S in the feed was made in the differential reaction regime (as discussed in the 8th Quarterly Report, p. 28). The purpose of these experiments was to determine the effect of H_2S in low but increasing concentrations on intrinsic catalyst activity at low conversions. Operating conditions were identical to those reported in the 8th Quarterly Report except for the addition of H_2S to the feed. H_2S was added to the n-hexadecane - DBT mixture in the saturator by pressurizing with a known mixture of H_2S in H_2 to the desired pressure. After allowing time for saturation, pure H_2 was introduced to achieve the final desired pressure.

TABLE 2

Pseudo First-Order Rate Constants for Dibenzothiophene Reaction Network

RUN	wt% DBT in feed	k_1[a]	k_2[a]	k_3[a]
53	0.0543	0.515	246.0	5.9
54	0.1154	0.273	94.5	13.6
55	0.1637	0.313	67.8	19.2
56	0.2348	0.695	65.9	23.9

[a]Pseudo first-order rate constants are in $cm^3/gm\text{-}hr$.

Plots of H_2S concentration as a function of H_2S partial pressure, for two different H_2 partial pressures are shown in Fig. 10. Clearly a Henry's law coefficient describes the solubility in the range of 0-8.2 atm abs. H_2S. The values plotted were generated from the N.G.P.A. version of the Chao-Seander equation of state for vapor-liquid equilibrium of industrial mixtures. Extrapolation to low H_2S partial pressures (1.4 atm abs. or less) gives approximate values of Henry's law coefficient. These are given in Table 3 for two H_2 partial pressures at 300°K. A third value for the Henry's Law coefficient at 300°K from Tremper and Prausnitz (1976) agrees well with those estimated above and indicates that the overall effect of H_2 on H_2S solubility in n-hexadecane is minimal.

b. Analytical

For conversions of DBT to biphenyl (BP) and H_2S below 15% a number of problems are encountered. Because the change in DBT concentration is small, large errors can be introduced in calculating conversions. A second difficulty is the appearance of an apparent solvent cracking product peak having the same retention time as that of biphenyl (BP) in the routine glc analysis. When the BP peak is large, the error is small, and reasonable correction can be made. But at low conversions to BP unsatisfactory results are obtained. For this analysis a new column was selected that allowed good separation of BP from saturated products. The column and conditions are: 10% 1,2,3-Tris (2-cyanoethoxy) propane (TCEP) on 100/120 chromosorb P with acid wash (supplied by SUPELCO, Inc.) packed in a 10 ft x 1/8" column, 155°C column temperature and about 30 cm^3/min He flow. Thus calculations of percentage sulfur removal are based on appearance of BP which can be measured within 5%. Even at high levels of sulfur removal BP accounts for as much as 90% of the DBT reacted.

TABLE 3

Effect of H_2 Pressure on Henry's Law Constant for H_2S: 300°K, 20 psia H_2S

P_{H_2} atm abs.	H_{H_2S}
0	25
34	27
68	29

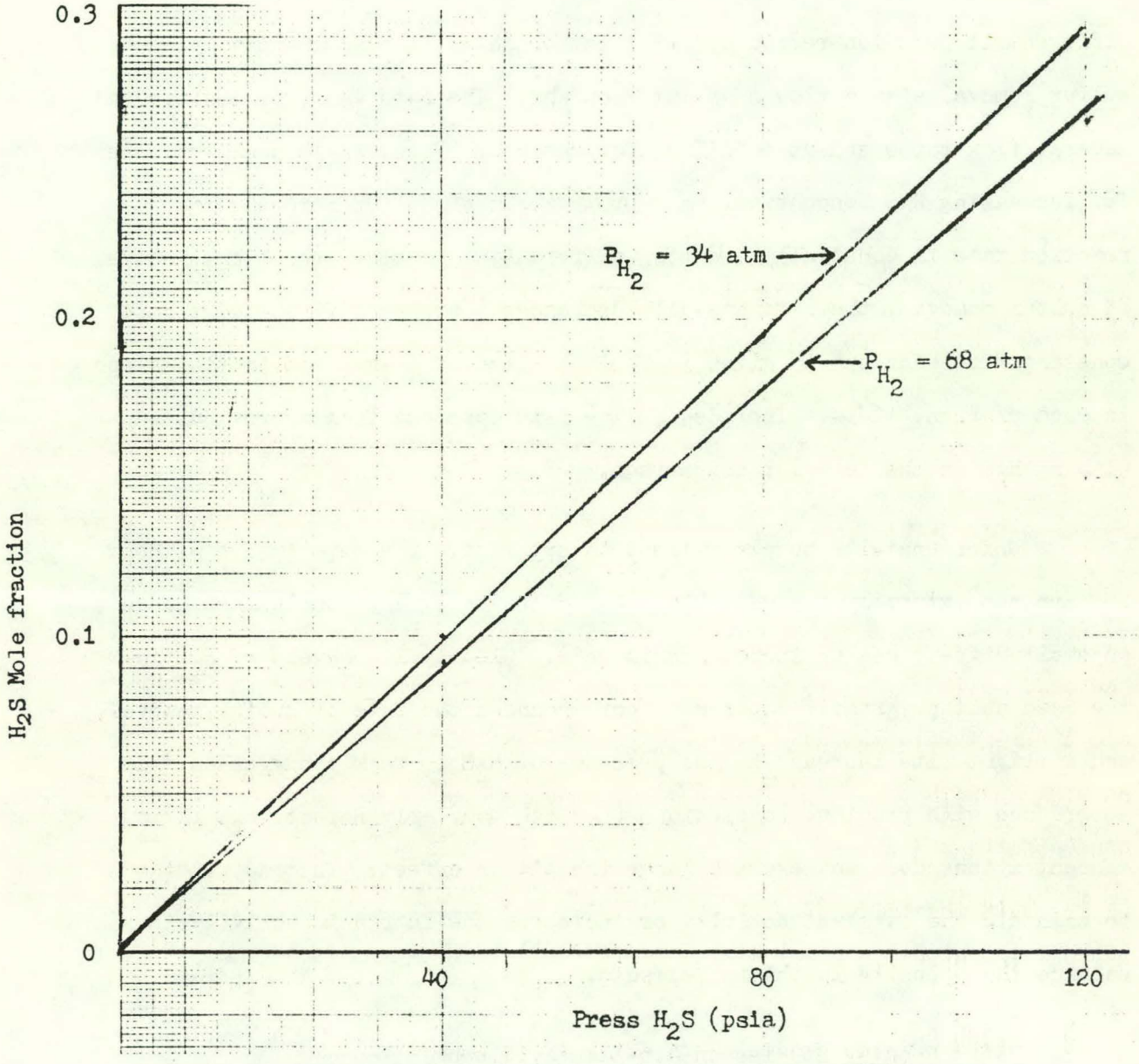

Fig. 10. H_2S mole fraction in the liquid phase as a function of H_2S pressure and H_2 pressure.

c. Results and Discussion

Feed mole fractions of H_2S varied from 0 to 4.2×10^{-4}. In each case the mole fraction of H_2 was 3.6×10^{-2}. Rates were measured in the differential reaction regime by first establishing lined-out activity at 4.5% sulfur removal with a flow of about 7 cm^3/hr. The rate was then measured at several flow rates and up to 15% sulfur removal. Figs. 11-14 show the results for increasing H_2S concentrations. Up to about 8% sulfur removal, the reaction rate is constant indicating differential reactor operation. Above 8% sulfur removal, the rate steadily decreases. A pseudo-first-order rate constant from each run is given in Table 4 calculated from the initial slope in each of Figs. 11-14. Included is the rate constant from a previous run with no H_2S in the feed for comparison.

Unfortunately, no clear trend is apparent. The experiments without H_2S are not extremely reproducible, thus discounting any conclusions based on small differences or increments in rate. Clearly low levels of H_2S in the feed neither greatly suppresses nor enhances the rate of sulfur removal, and a slight rate increase in the presence of H_2S is weakly suggested. In accordance with previous conclusions (see 8th Quarterly Report) H_2S in low concentrations does not exert a large inhibition effect. Instead, it tends to maintain the catalyst activity or increases the intrinsic activity to balance the opposite inhibition effects.

3. Batch Reactor Studies on 4,6-Dimethyldibenzothiophene

Studies with 4,6-diMeDBT

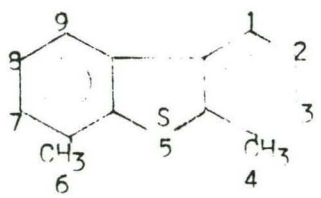

TABLE 4

First-Order Rate Constant for Dibenzothiophene Hydrodesulfurization
300°C, 0.036 mole fraction H_2

Run No.	X_{H_2S}	k, cm^3/h gm of catalyst
3- 9	0.0	15.6
3-17	0.0	24.2
3-18	9.0×10^{-5}	30.0
3-19	1.8×10^{-4}	26.6
3-20	4.2×10^{-4}	27.6

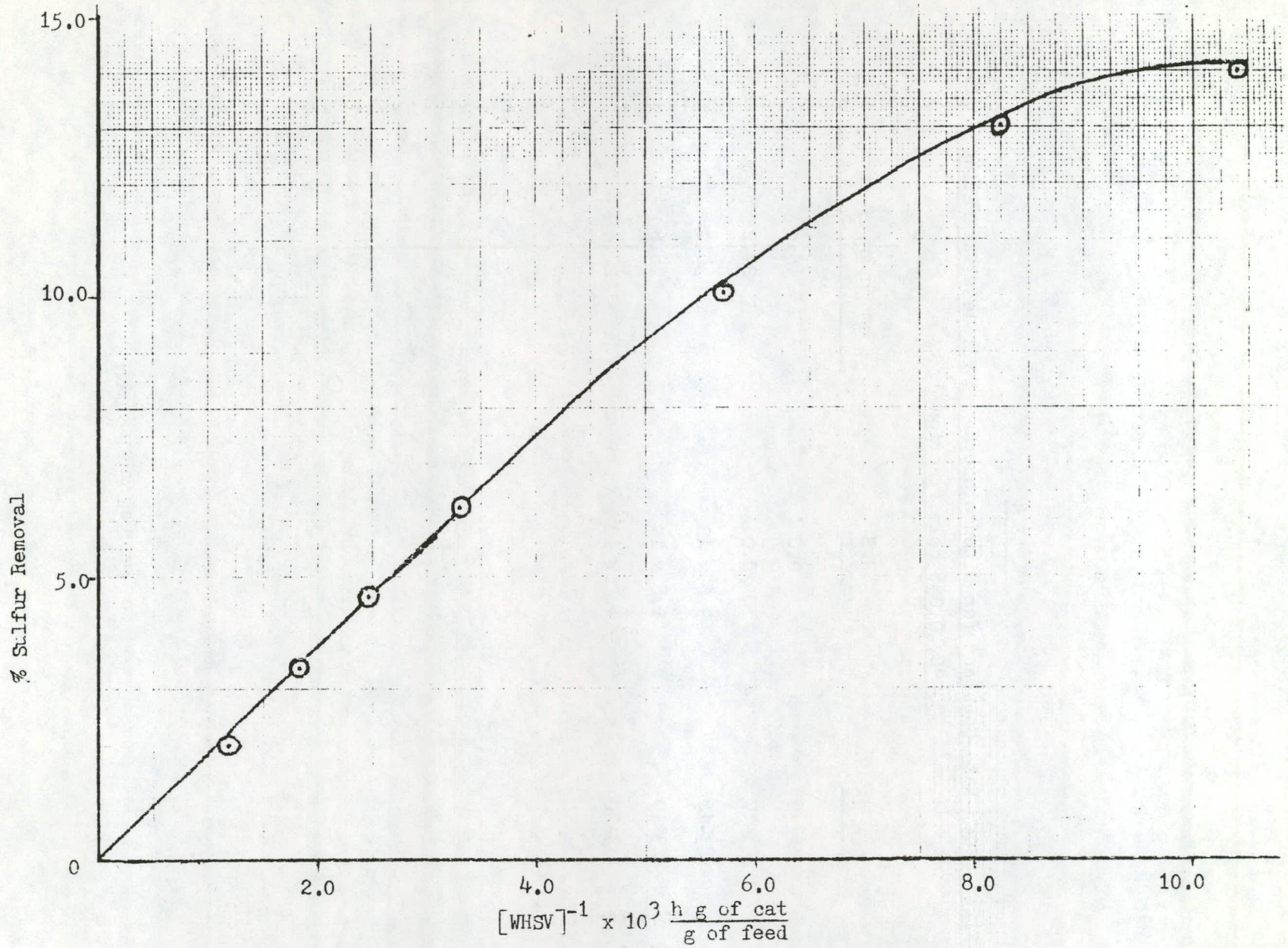

Fig. 11. Effect of contact time on dibenzothiophene conversion over Co-Mo/γ-Al_2O_3 for no H_2S in the feed.

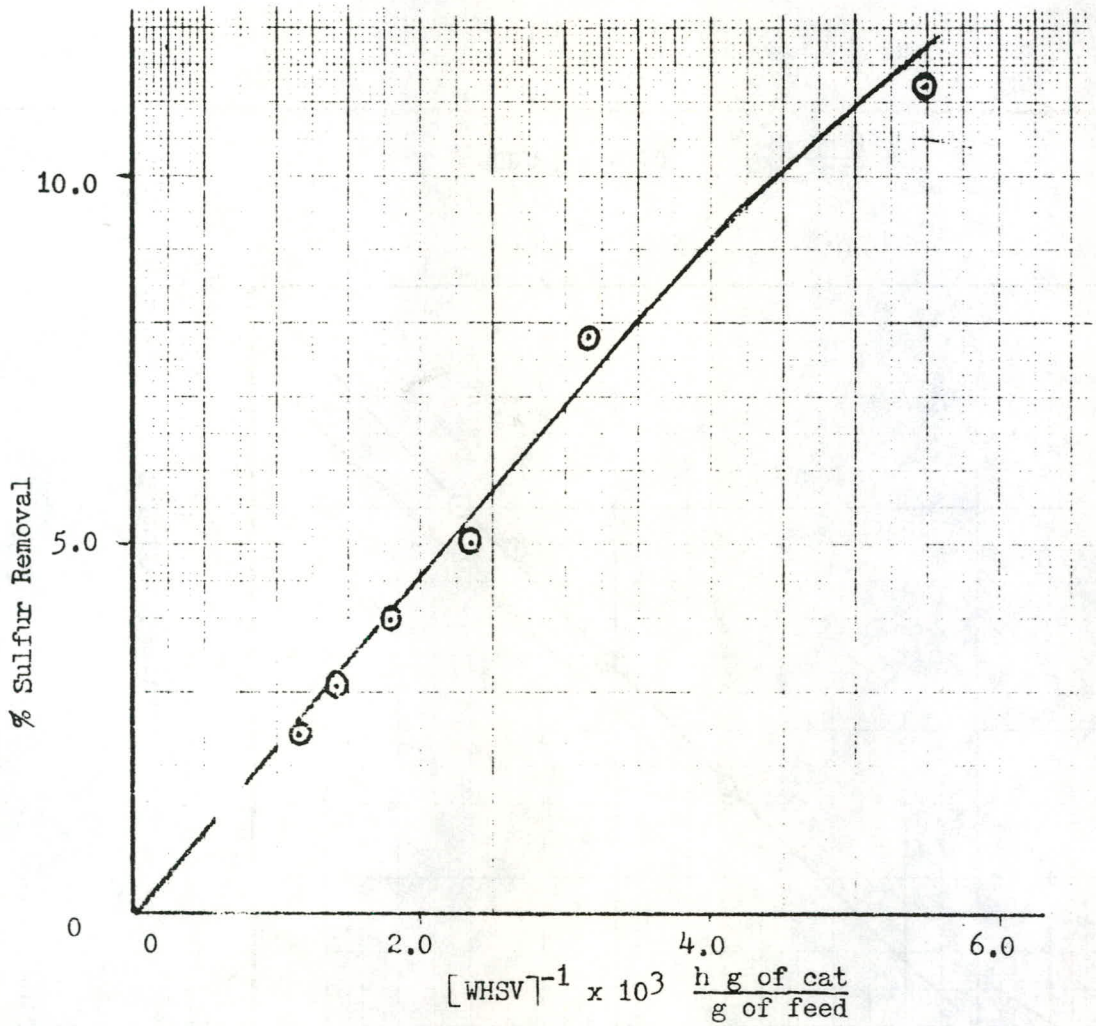

Fig. 12. Effect of contact time on dibenzothiophene conversion over Co-Mo/γ-Al_2O_3 for an H_2S mole fraction of 9.0×10^{-5}.

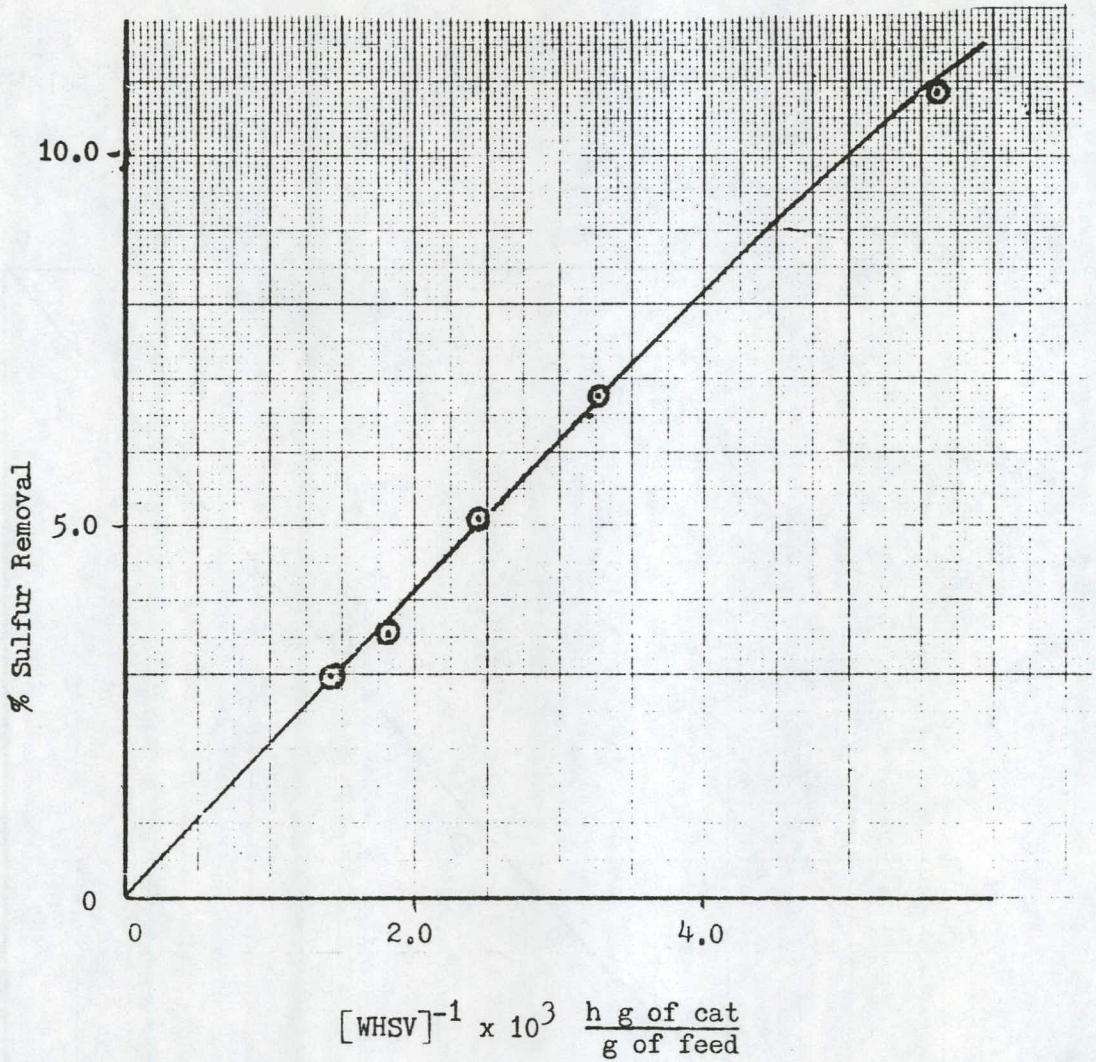

Fig. 13. Effect of contact time on dibenzothiophene conversion over Co-Mo/γ-Al_2O_3 for an H_2S mole fraction of 1.0×10^{-4}.

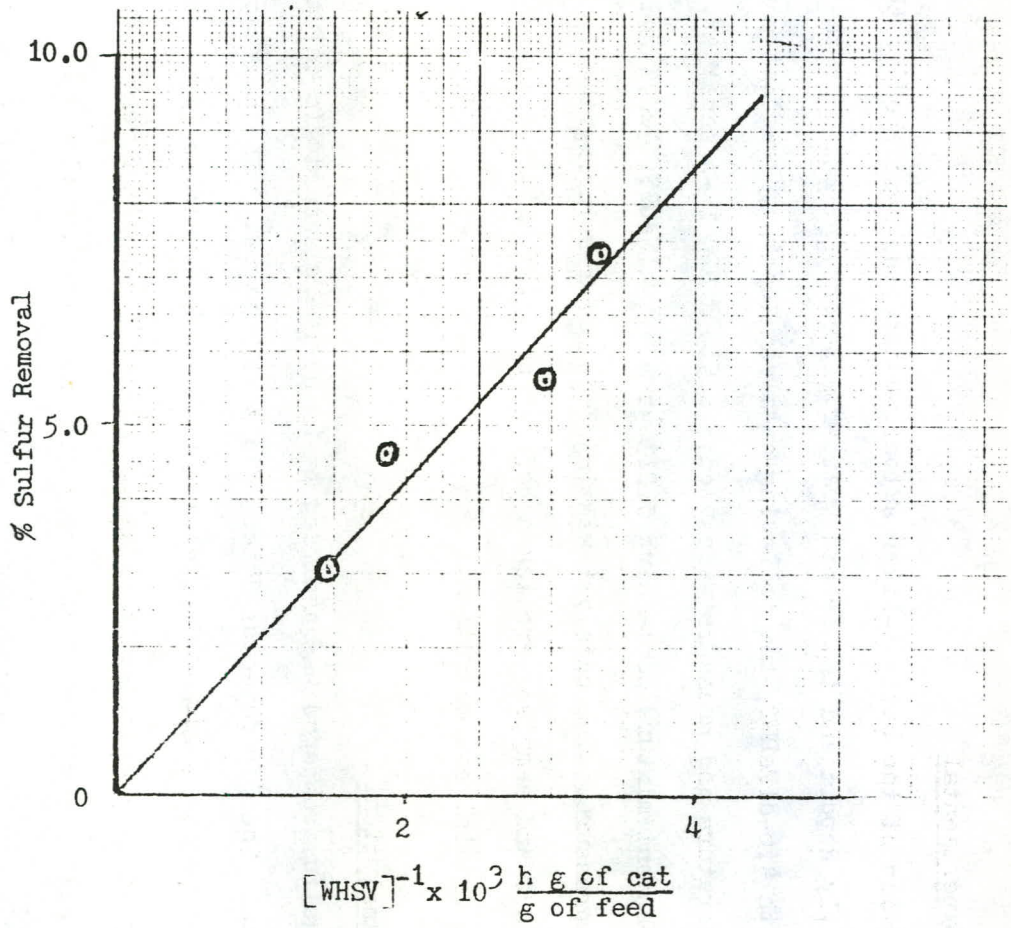

Fig. 14. Effect of contact time on dibenzothiophene conversion over Co-Mo/γ-Al_2O_3 for an H_2S mole fraction of 4.2×10^{-4}.

in the flow microreactor were reported in earlier reports comparing the rate of sulfur removal with other methyl substituted DBT's and DBT itself. The products of 4,6-diMeDBT hydrodesulfurization were not identifiable by glc analysis alone. More recently a batch experiment with 4,6-diMeDBT was carried out using higher reactant concentrations and identification and quantification of products are nearly completed.

a. Experimental

Operation of the batch 1-liter autoclave has been described in the Second Quarterly Report and in the 6th Quarterly Report, p. 22. For the experiment with 4,6-diMeDBT, the following catalyst loading, reactant concentration, temperature and pressure were used: 1.513 g HDS 16-A catalyst, 380 cm^3 of reactant mixture containing 0.211 wt % 4,6-diMeDBT, 300°C and 68 atm total pressure. The catalyst was injected after bringing the reactor to 300°C and samples were taken before and after catalyst injection to verify the initial concentration.

b. Analytical

The sulfur compound was analyzed by using the standard glc column and conditions. The FID detector detected a sulfur impurity in the reactant mixture identified to be 4-MeDBT equal to about 6-7% of total sulfur compound present. 3,3'-diMeBP was identified as one of the products of reaction using the TCEP glc column described under the third high-pressure flow microreactor results in this report. Unknown product peaks were collected using a preparatory chromatography system. A 5 ft x 1/4" OD column packed with 10% SP2100 was used at 200°C and He flow of 40 cm^3/min. The collected products were analyzed using the glc-mass spectrometer system described previously.

c. Results and Discussion

Hydrogenolysis of sulfur in 4,6-diMeDBT fits first-order kinetics well as shown in Fig. 15. The rate constant is found to be $\frac{28\ cm^3}{h\text{-}g\ cat}$. This value cannot be compared directly with earlier values reported from the flow reactor due to differences in H_2 concentrations when saturating at 300°C vs. 25°C and due to the higher sulfur concentration in the batch run. As has been shown with DBT, k is not independent of the initial concentration.

Product identification is not complete, but the major products have been identified. Besides 3,3'-DiMeBP, the glc-mass spectrometer system has identified what appears to be two isomers of

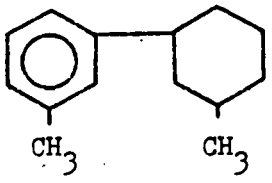

as major products and possibly two isomers of

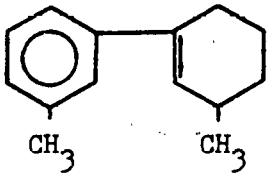

as minor products. The exact isomer in each case is unknown. Evidence is of two kinds. First, Figs. 16 and 17 show the two

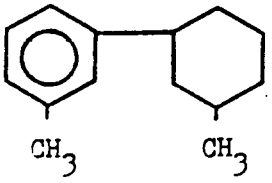

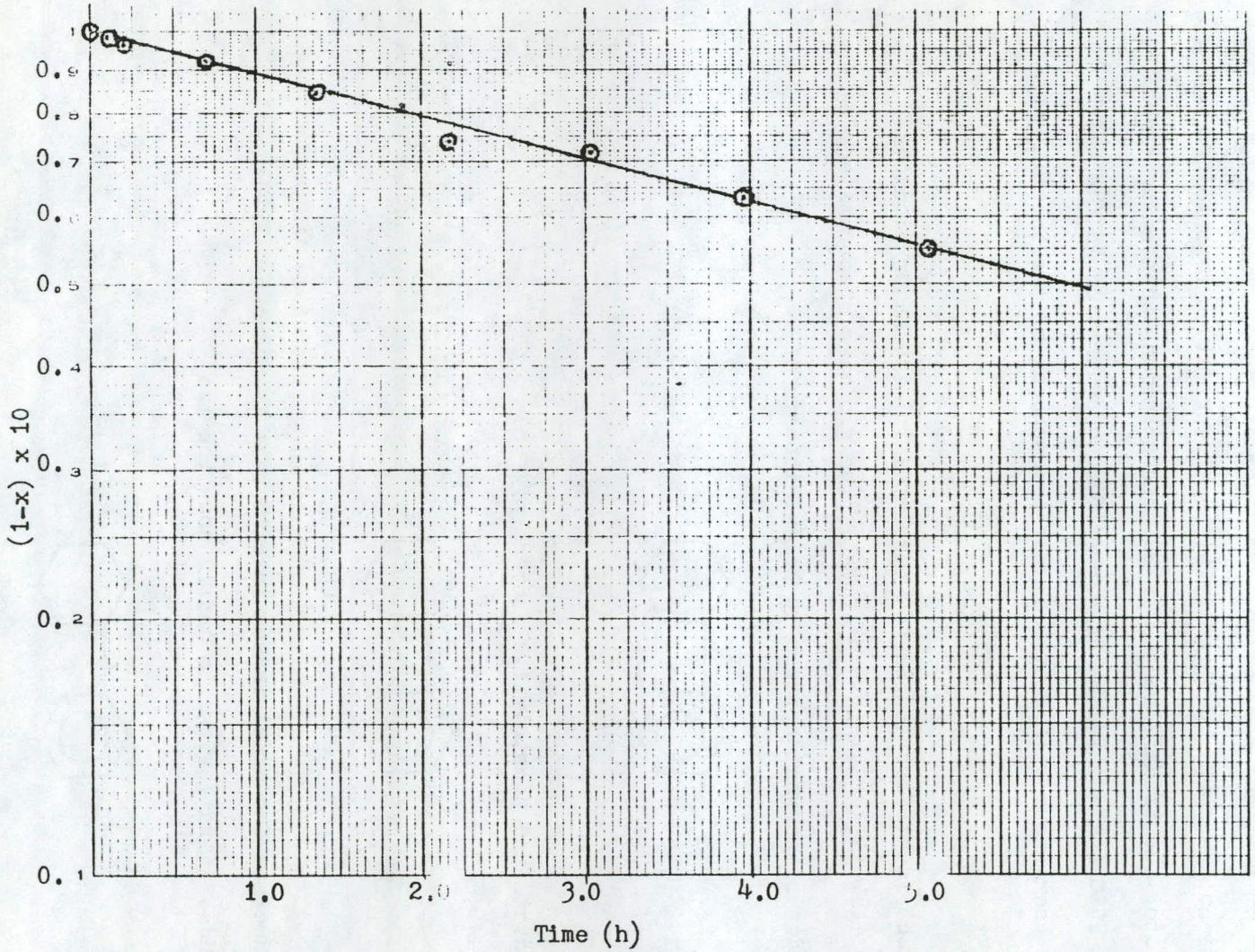

Fig. 15. First-order plot of hydrodesulfurization of 4,6-dimethyldibenzothiophene.

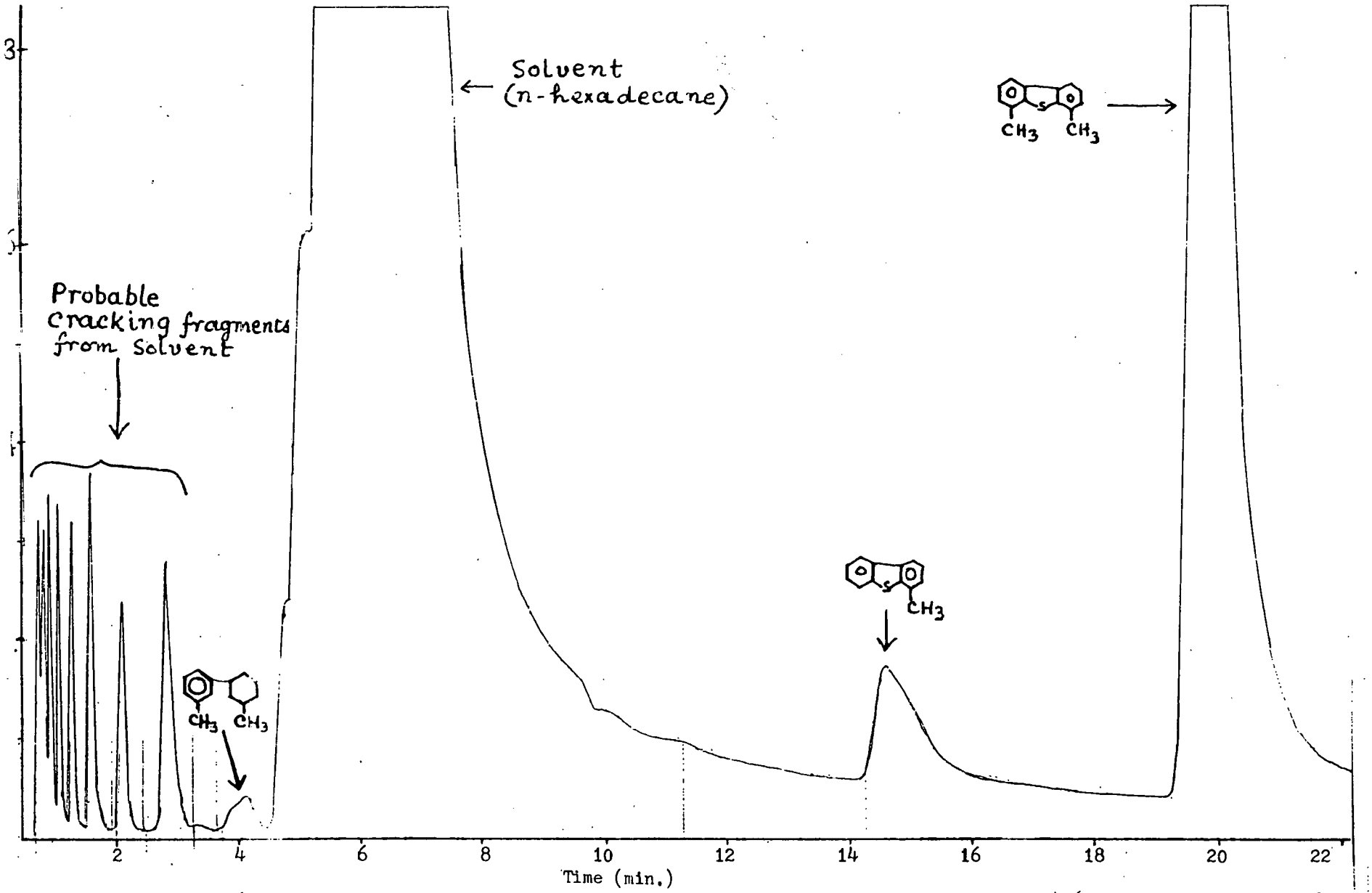

Fig. 16. Gas Chromatographic analysis of product sample from hydrodesulfurization of 4,6-dimethyl-

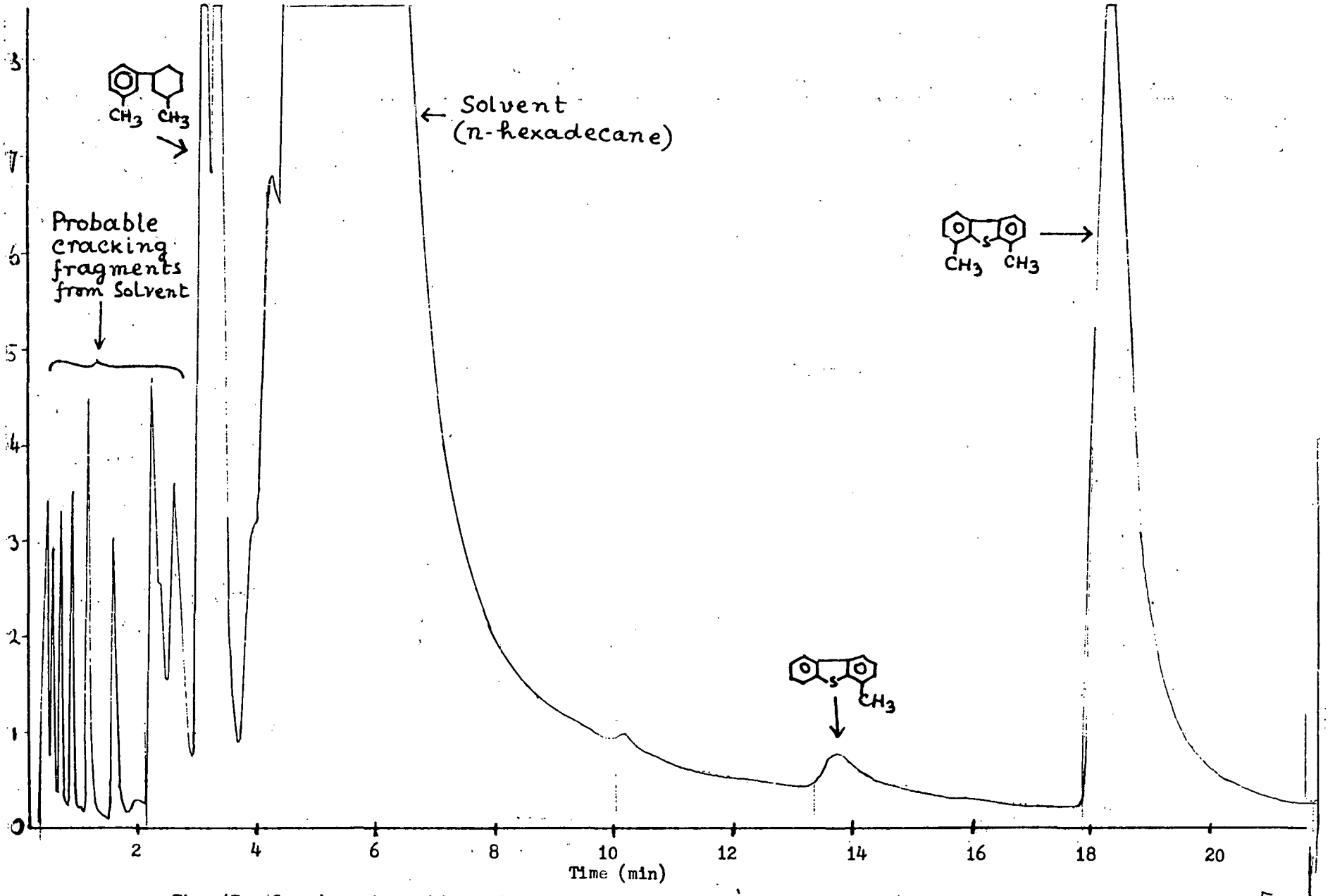

Fig. 17. Gas chromatographic analysis of product sample from hydrodesulfurization of 4,6-dimethyldibenzothiophene, long contact time (5.07 hr).

peaks at low and high levels of sulfur removal. The ratio of the areas of these two peaks remain nearly constant at 0.54. Second, the two peaks in the mass spec have the same molecular peak and fragments, but the relative intensity of the fragments is different for the two. Because 4-MeDBT was present in the reactant mixture as impurity, both

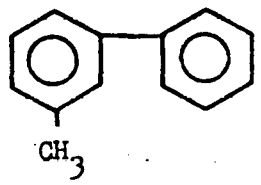

and

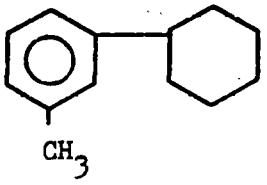

or

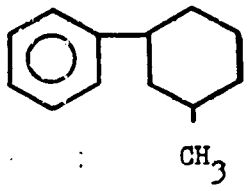

which were observed in the products cannot be ascribed to dealkylation of 4,6-diMeDBT without repeating the experiment with pure reactant.

Lumping the two

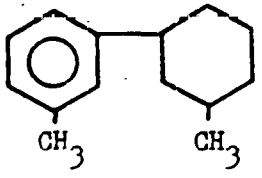

isomers together, assuming the same detector response as for 3,3'-diMeBP, and calculating the conversion to

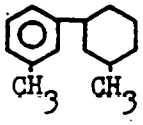

and 3,3'-diMeBP, percent selectivities based on disappearance of 4,6-diMeDBT is about 50 and 20% respectively. Clearly hydrogenation is much greater with 4,6-diMeDBT than with DBT (see 8th Quarterly Report, p. 28). Figure 18 shows concentration versus time data for the reactant and two major products. Whereas 3,3'-diMeBP, which appears to be a primary product,

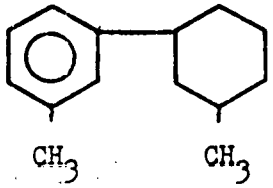

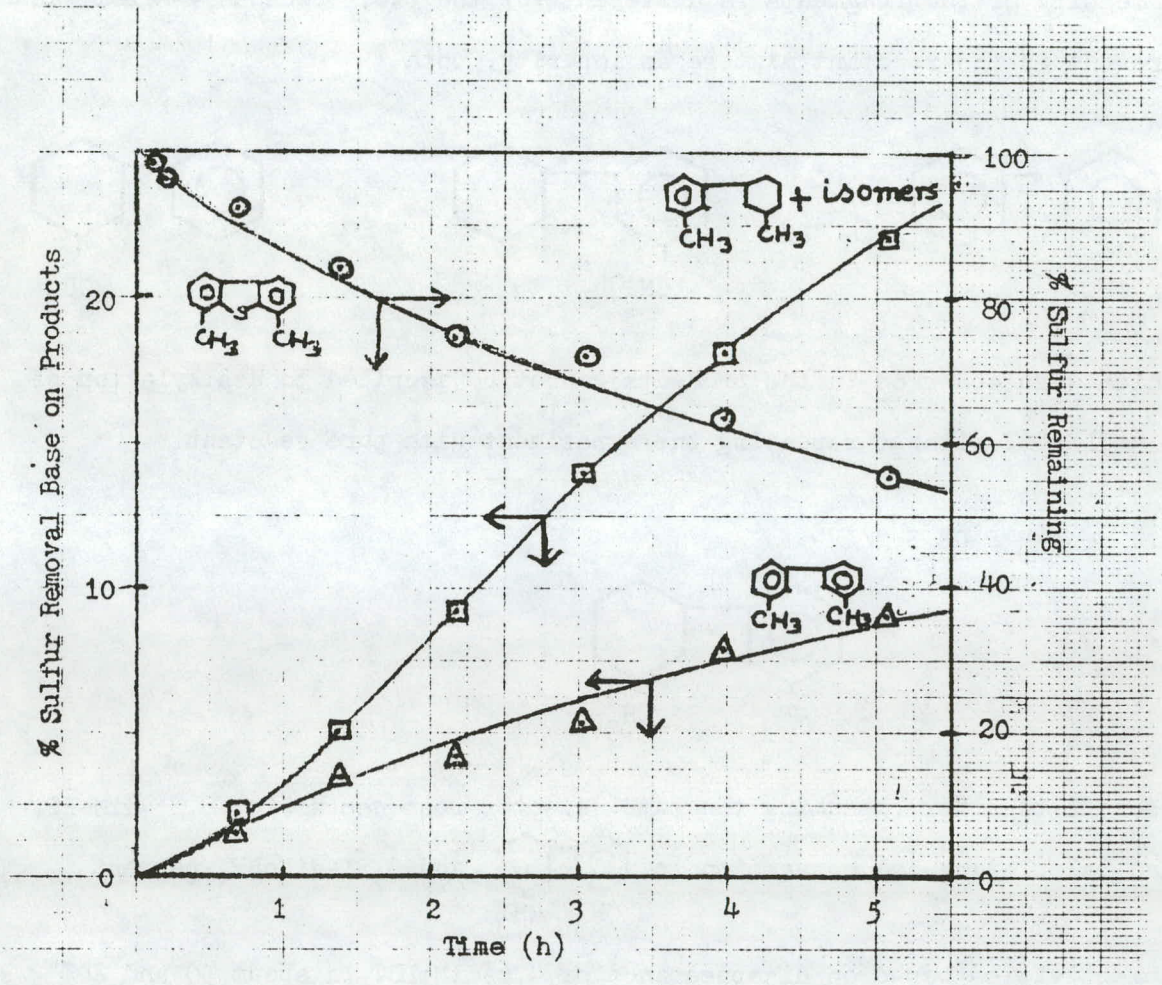

Fig. 18. Time dependence of reactant and product concentrations in the batch hydrodesulfurization of 4,6-dimethyldibenzothiophene over Co-Mo/γ-Al_2O_3.

is probably a secondary product. Thus assuming reaction pathways similar to DBT, the proposed reaction network for 4,6-diMeDBT is shown in Fig. 19. No sulfur intermediates have as yet been identified; thus the relative importance of pathways A and B is uncertain. As with DBT where hydrogenation of BP is slower than hydrogenation of DBT, path A may be the most important for producing the major products, isomers of

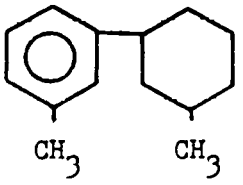

Further experiments and analyses are in progress to identify other products and intermediates since only roughly 70% of the 4,6-diMeDBT reacted has been accounted for in the major products. Likewise more insight into the relative rates of the various steps and pathways is being sought.

C. CATALYTIC HYDRODENITROGENATION

1. Benz[c]acridine

Benzacridines are planar molecules. The pyridine ring is sandwiched between one benzene and one naphthalene ring. The structures and numbering system of these compounds are shown below ("The Chemistry of Heterocyclic Compound," Vol. 9, Interscience Publishers, J. Wiley and Sons, New York, 1973).

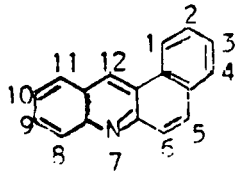

Benz[a]acridine

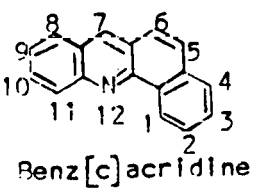

Benz[c]acridine

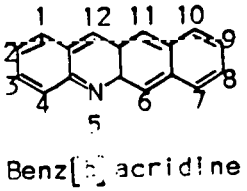

Benz[b]acridine

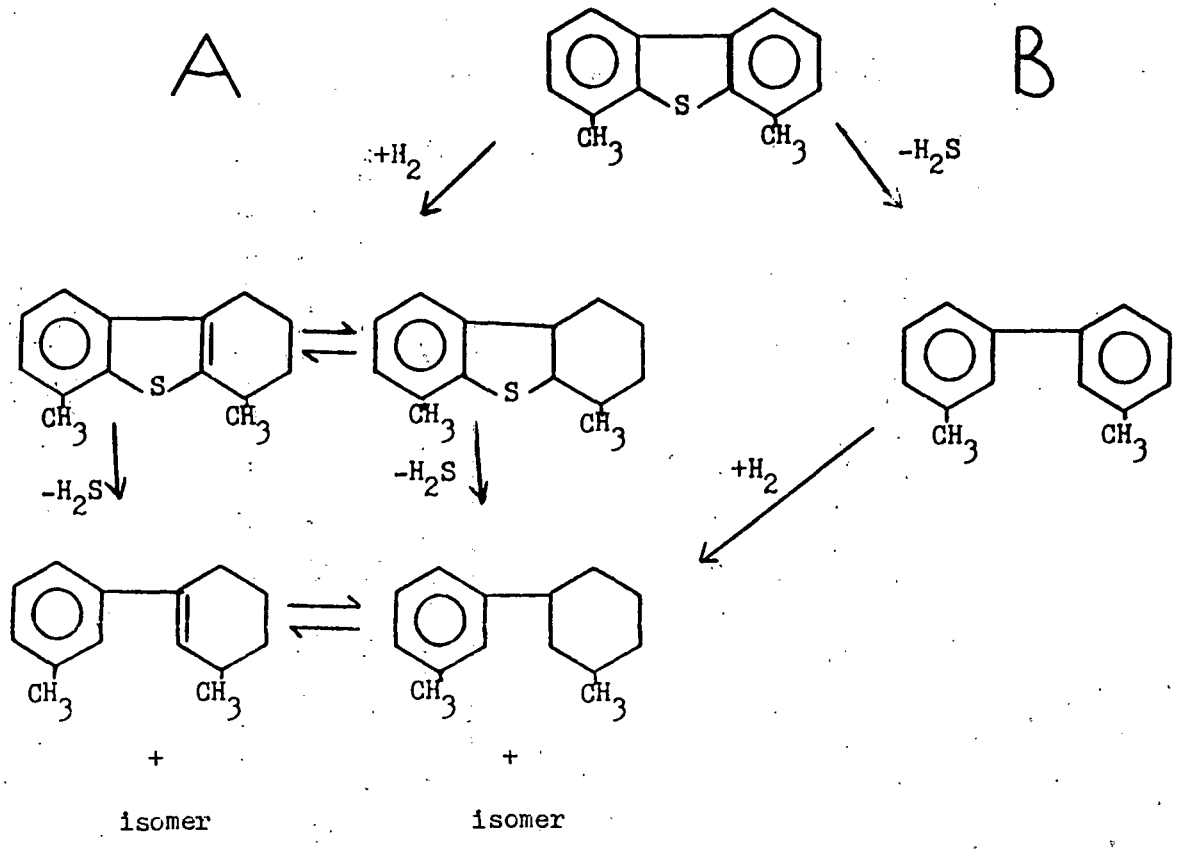

Fig. 19. Proposed reaction pathways for hydrodesulfurization of 4,6-dimethyldibenzothiophene.

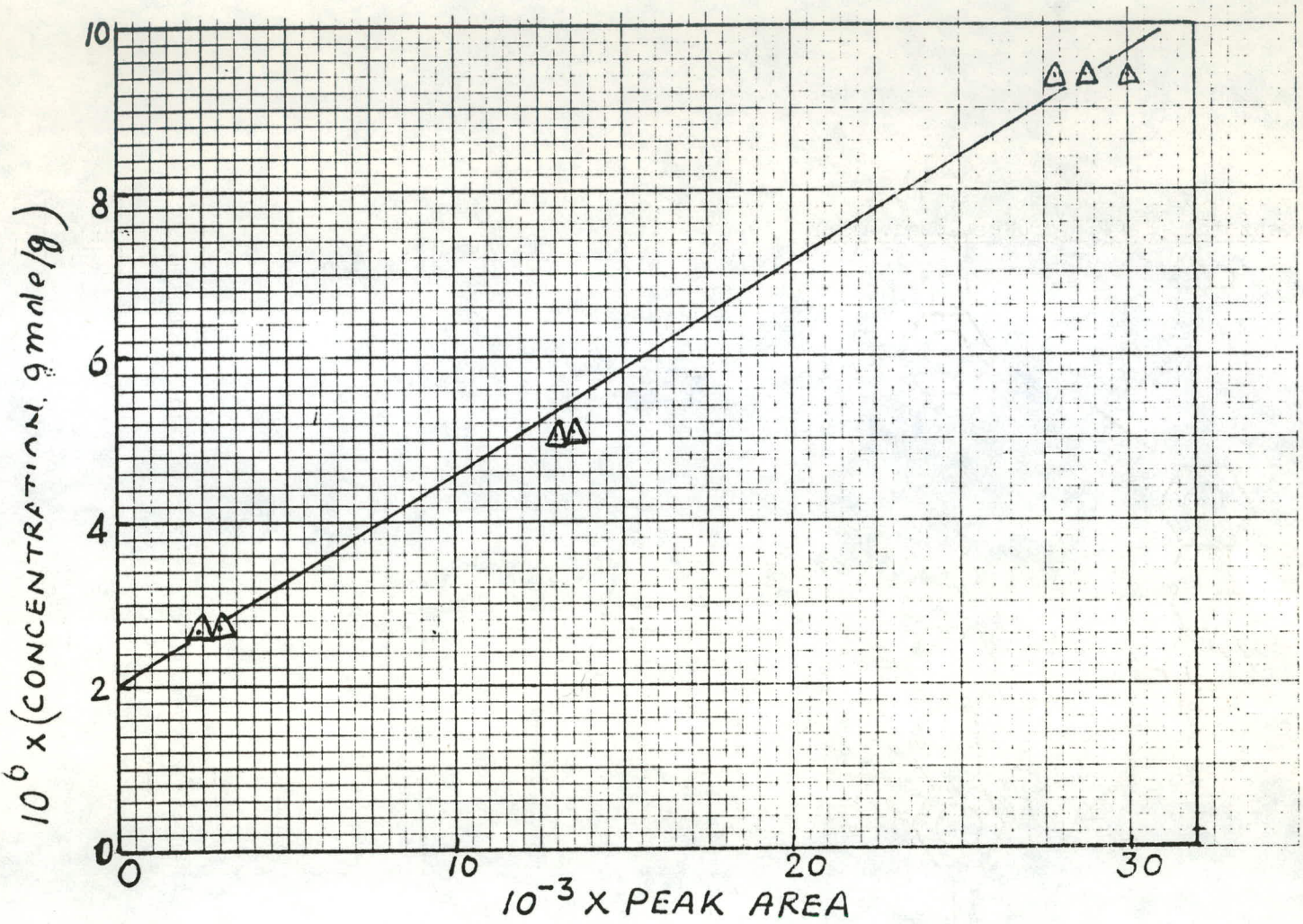

Figure 20: Calibration curve for high-pressure liquid chromatograph using benz[c]acridine.

THIS PAGE

WAS INTENTIONALLY

LEFT BLANK

Benz[c]acridine was subjected to catalytic hydrodenitrogenation, and the preliminary results are given below.

a. Experimental

Apparatus and procedure. The experiments were carried out in a one-liter stirred (1700 rpm) autoclave (Autoclave Engineers). The autoclave was operated in batch mode. Reactant and catalyst in carrier White Oil were injected into the autoclave, after it had been stabilized at the operating temperature and pressure. Typical operating conditions were:

Temperature:	367 ± 1°C
Total Pressure:	134 atm
Reactant concentration:	0.5 wt % in White Oil
Catalyst:	HDS-9A, Ni-Mo/γ-Al_2O_3, 0.5 wt % in White Oil 150-200 mesh; presulfided at 400°C in 10% H_2S in H_2 for 2 hours.
CS_2 loading:	0.05 wt % (= 1.4 vol % H_2S in the gas phase)

Liquid samples were taken periodically and analyzed.

Analysis. Reaction products were analyzed by means of gas-chromatography (Perkin Elmer - Model 3920B) equipped with a nitrogen specific detector (Perkin Elmer) and a glass capillary column (50m OV-101) at 210°C.

Separation of products. High-pressure liquid chromatography (DuPont) was used to separate reaction products. Several columns were tested under various conditions. The best results were obtained with the following conditions:

column	15 cm, ZORBAX ODS
pressure	116 atm
temperature	367°C
mobile phase	80% CH_3OH, 20% H_2O (by volume)
detector	UV photometer (254 nm)

Several solutions of benz[c]acridine in White Oil were used for calibration. Analysis showed that small amounts of benz[c]acridine was very strongly adsorbed on the column. Figure 20 shows the results obtained for standard solutions of benz[c]acridine.

Gas chromatographic analysis of reaction products showed that during hydrodenitrogenation a large number of nitrogen-containing compounds were produced as intermediate products; however these were very quickly reacted to give ammonia and the corresponding hydrocarbons. Figure 21 shows the typical chromatograms for samples taken after 3 and 240 minutes of catalytic reactions, respectively.

b. Results and Discussion

Total nitrogen removal from benz[c]acridine follows first-order kinetics as demonstrated in Figure 22.

The reactivity of benz[c]acridine as compared with that of other nitrogen-containing compounds under the same conditions (367°C, 136 atm, Ni-Mo/γ-Al_2O_3 catalyst is given below.

Reactant	Pseudo first-order rate constant for total nitrogen removal (g oil/min-g cat)
Benz[c]acridine	1.54
Acridine	1.62
Carbazole	2.43
Quinoline	2.52

The distribution of nitrogen-containing compounds produced during the hydrodenitrogenation of benz[c]acridine has been shown in Figs. 23 and 24.

The high-pressure liquid chromatography technique did not offer any better analysis (Fig. 25) than our gas chromatographic technique. The identification and quantification of the various products is under progress, and the results are expected during the next quarter.

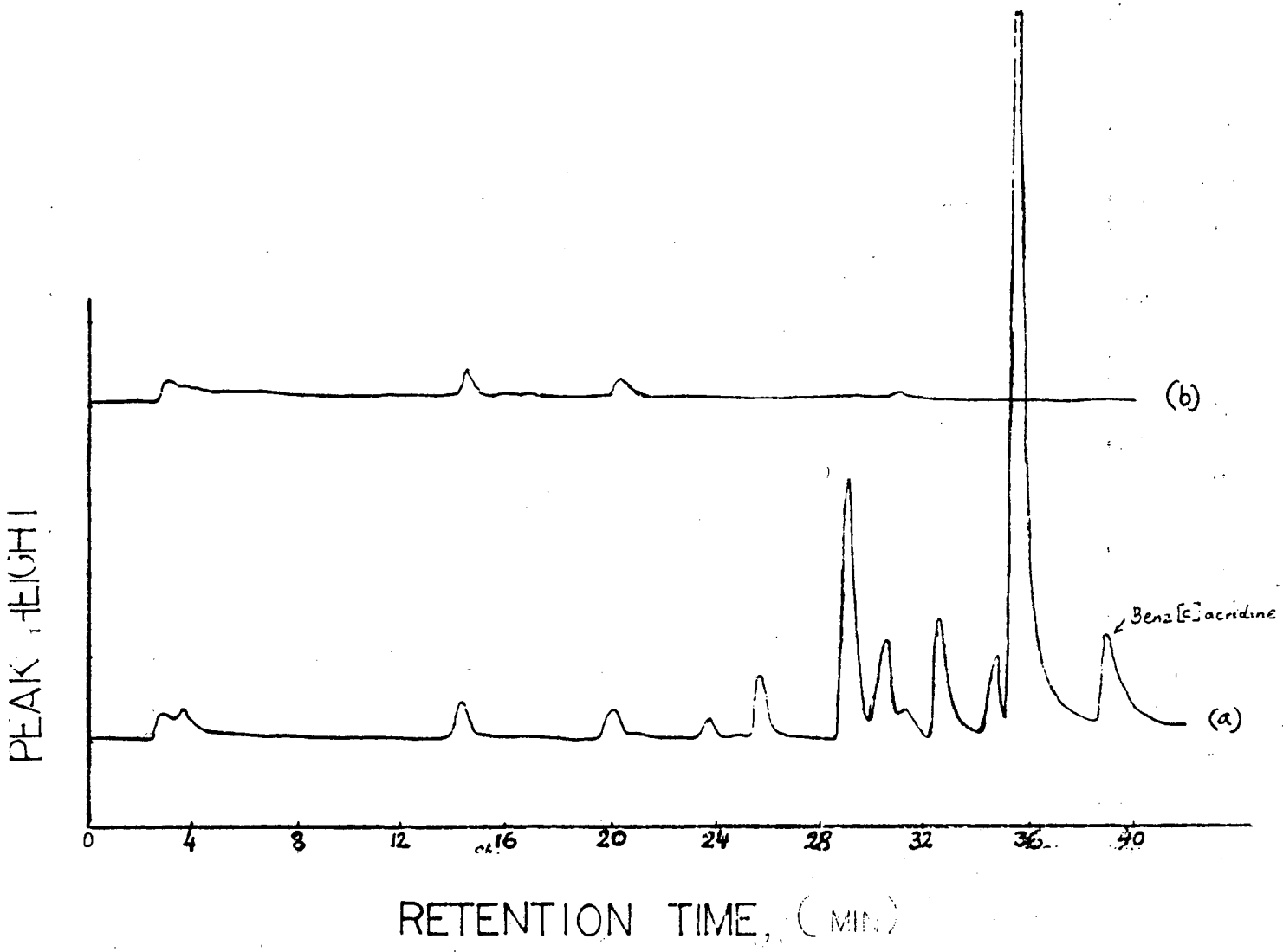

Figure 21: Gas chromatogram of samples from hydrogenation of benz[c]acridine taken (a) at 3 min and (b) at 240 min into a run in the batch autoclave at 367°C and 116 atm.

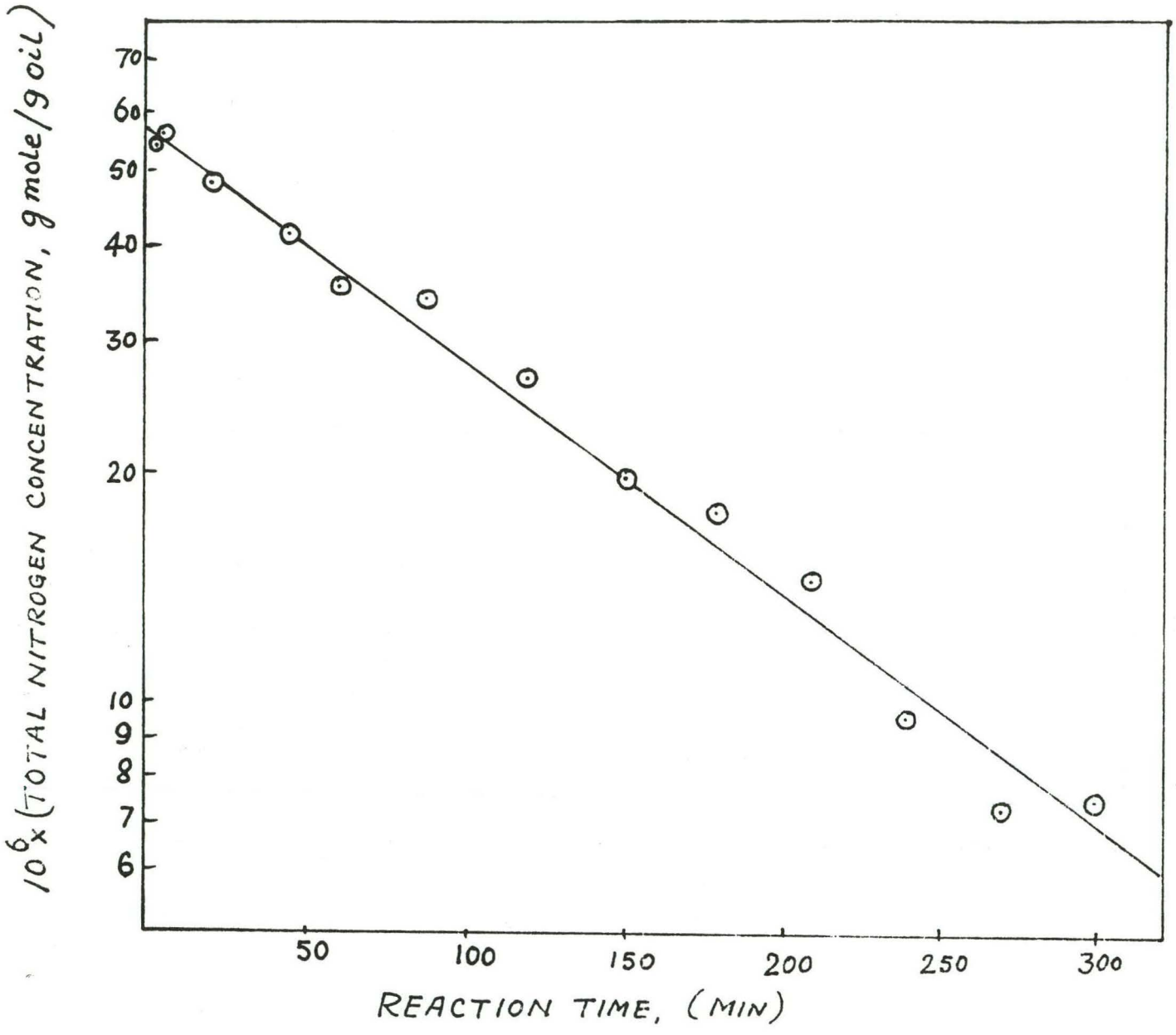

Figure 22: First-order rate plot for total nitrogen removal from Benz[c]acridine. Reaction conditions: 367°C, 136 atm, Ni-Mo/γ-Al_2O_3 catalyst.

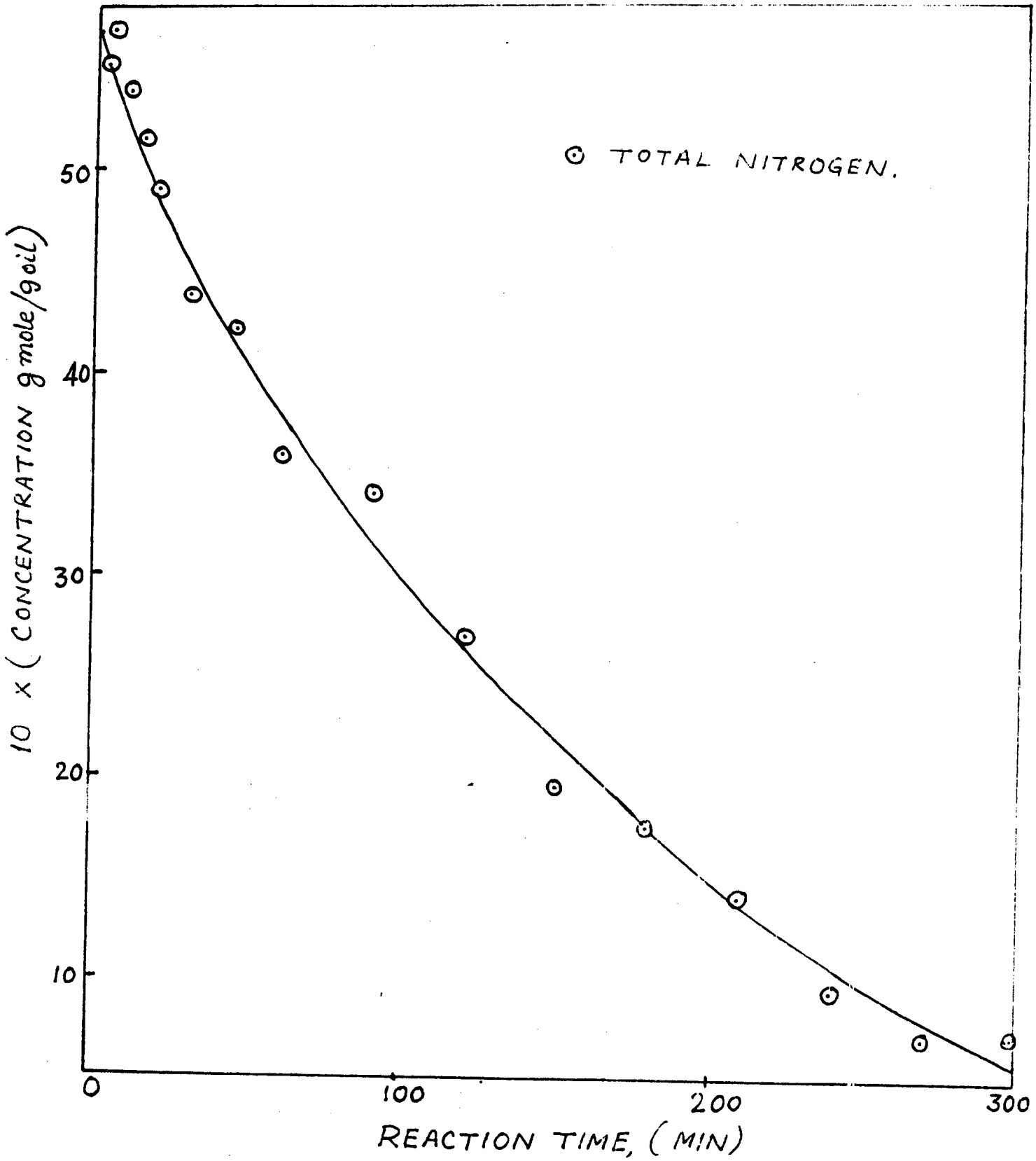

Figure 23: Reduction in total nitrogen concentration in batch hydrodenitrogenation of benz[c]acridine. Reaction conditions: 367°C, 136 atm, Ni-Mo/γ-Al_2O_3 catalyst.

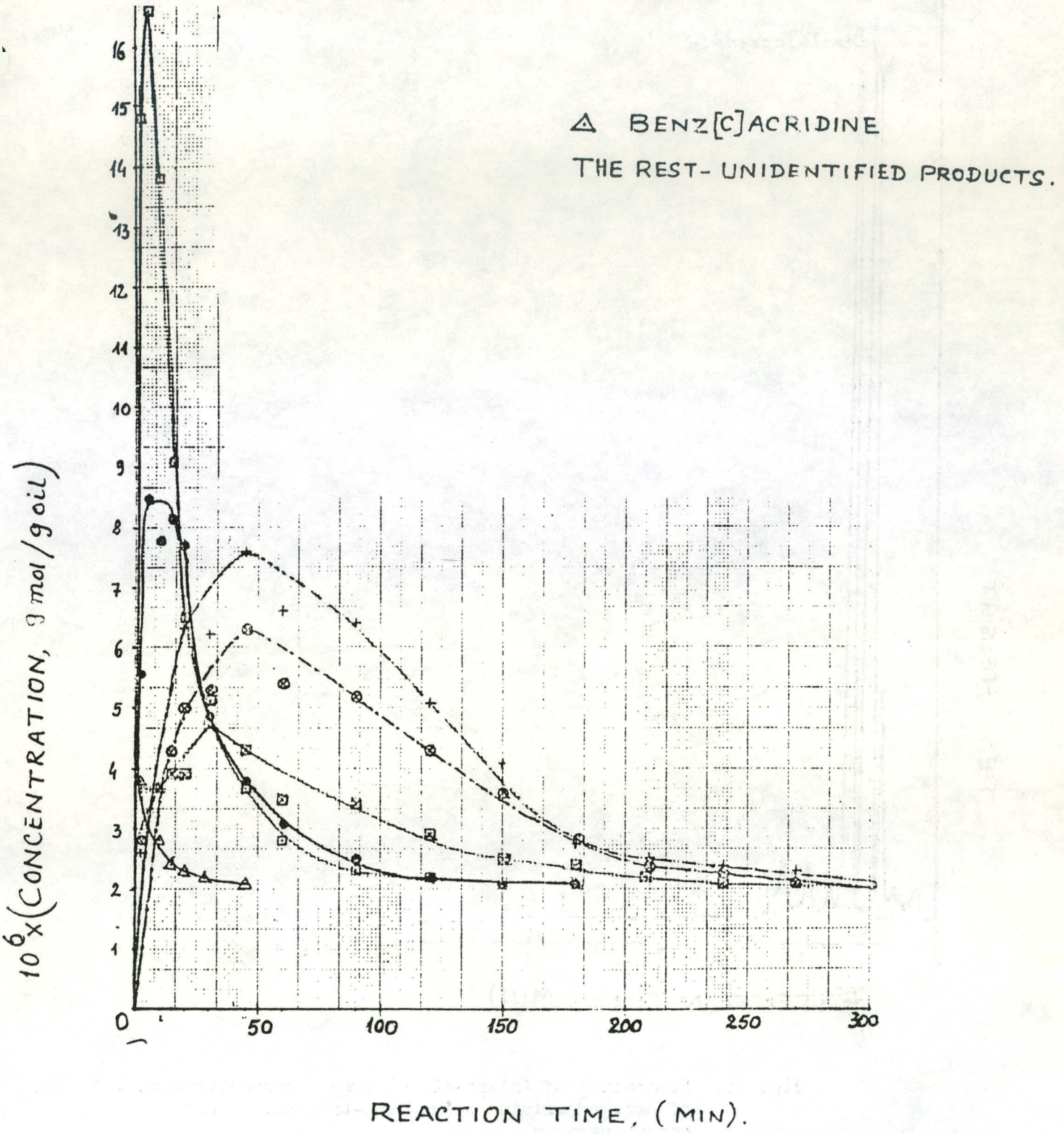

Figure 24: Intermediates observed in hydrodenitrogenation of benz[c]acridine in batch experiment. Reaction conditions: 367°C, 136 atm, Ni-Mo/γ-Al_2O_3.

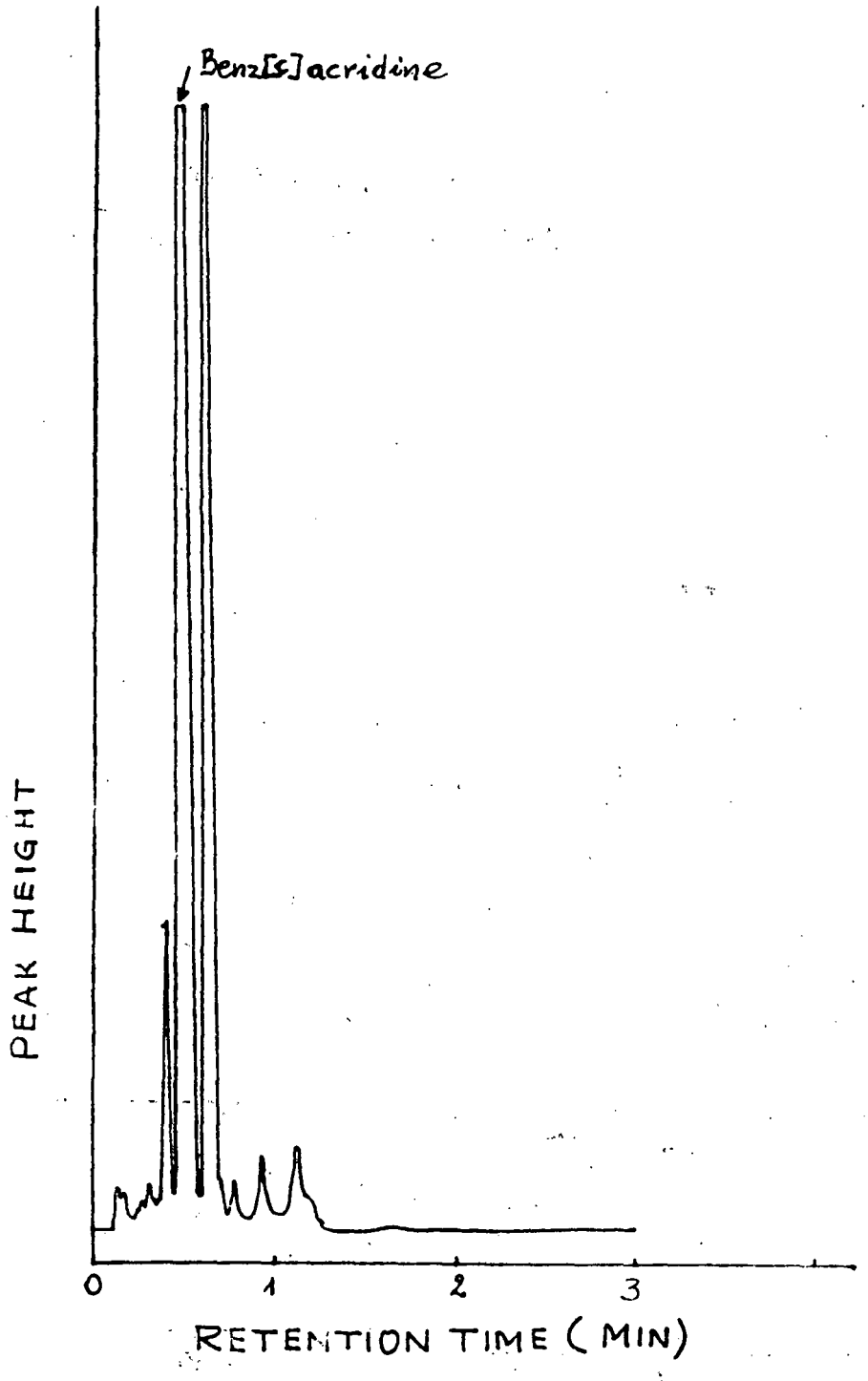

Fig. 25. Separation of intermediates from hydrodenitrogenation of benz[c]acridine using high-pressure liquid chromatography.

2. Reaction Network and Kinetics of Hydrodenitrogenation of Acridine

a. Introduction

Catalytic hydrotreating simultaneously removes sulfur, nitrogen and metals from the hydrocarbon feedstock. Catalytic hydrodenitrogenation seems to be more important because nitrogen-containing compounds are more refractory and the substituted feedstocks derived from coal, tar sands and oil shale contain more nitrogen than in petroleum feedstock. Hydrodenitrogenation is also more complex than hydrodesulfurization. Moreover, there is limited understanding of the catalytic chemistry and engineering of the hydrodenitrogenation process. Our approach is to study the reactivity and the reaction network associated with the removal of nitrogen from representative nitrogen-containing compounds found in various natural and processed feedstocks. Cox and Berg (1962), Sonnemans (1973), Goudriaan (1974), Mayer (1974) and Cocchetto (1974) have studied hydrodenitrogenation of unsaturated nitrogen-containing ring compounds. This work demonstrated that hydrodenitrogenation involves ring hydrogenation followed by carbon-nitrogen bond rupture. However except for pyridine the reaction networks and reaction kinetics have not been determined for the important nitrogen-containing compounds found in heavy petroleum, coal-derived liquids or shale oil. Recently Shih et al. (1977) have determined the reaction network and reaction kinetics associated with quinoline hydrodenitrogenation.

The objective of this study is to determine the reaction network and reaction kinetics of acridine hydrodenitrogenation under high-pressure liquid-phase conditions.

The experiments were carried out in a one-liter stirred autoclave (Autoclave Engineers) which was operated in batch mode. A schematic of the reactor setup is given elsewhere (Shih et al., 1977).

For a typical run the autoclave was brought to reaction temperature and pressure while periodically purging the system with dihydrogen. When the autoclave was at operating conditions, the oil-catalyst-reactant mixture was injected into the autoclave. There was an initial temperature drop that lasted at most 10 min. Liquid samples were withdrawn periodically and were analyzed by gas chromatography.

Unless stated otherwise, the experimental conditions were as stated in Table 5.

Experimental materials. Acridine (Aldrich Chemical Co.) was over 99% purity and was used as received. C.P. grade hydrogen (Matheson) was purified by passing through a DEOXO column (Engelhard Minerals & Chemicals Corp.) and a molecular sieve column to remove trace amounts of oxygen and water respectively. Perhydroacridine was prepared by hydrogenation of acridine. The white oil (Parol 70, Pereco Division of Penzoil Co.) was a prehydrotreated, highly paraffinic oil which was free of sulfur- and nitrogen-containing compounds and aromatics. Its boiling range was 315 to 455°C, and it contained mainly C_{18} to C_{36} hydrocarbons.

The catalyst used was Ni-Mo/γ-Al_2O_3, designated HDS-9A, from American Cyanamid Co. It contained 3.0-4.0 wt % NiO; 17.5-18.5 wt % MoO_3, 0.04 wt % N_2O and 0.05 wt % Fe. It had a surface area of 149 m^2/g and a pore volume of 0.46 cm^3/g. The catalyst was presulfided at 425°C for two hr

TABLE 5

Operation Conditions

- Standard Conditions
  - * Reactor: batch, 1ℓ autoclave, stirring speed 1700 rpm
  - * Catalyst: Ni-Mo/γ-Al_2O_3 (HDS-9A, American Cyanamid)
  - * Carrier oil: hydrotreated white oil
  - * Catalyst loading: 2 in 500 cm^3 of white oil, 150-200 mesh, presulfided for 2 hr at 425°C in 160 cm^3 per min in 10% H_2S/H_2 to give a 10-fold stoichiometric excess of sulfur
  - * Initial acridine concentration: 0.5 wt % in white oil
  - * Temperature: 367°C
  - * Total pressure: 136 atm
- Operation Variables
  - * Temperature: 317°C to 365°C
  - * Pressure: 54.4 to 172 atm
  - * Initial acridine conc.: 0.5 to 1 wt %

in a flow of 160 cm^3/min of 10% H_2S in H_2. This represents a ten-fold stoichiometric excess of sulfur. Unless indicated otherwise 0.05 wt % CS_2, which was rapidly converted to H_2S, was added to the reaction mixture to maintain the catalyst in a sulfided state during reaction.

Analytical Techniques. The concentration of the nitrogen-containing reaction products determined by gas chromatograph (Perkin Elmer Model 3920B) equipped with a nitrogen-phosphorous specific detector, consisting of a rubidium silicate bead placed above the jet of a conventional FID detector. The nitrogen-specific detector eliminates interference by hydrocarbons. An appropriate concentration standard was injected initially and after each fire samples to saturate active sites on the column. For acridine product analysis a glass column and oven temperature of 220°C was used.

A concentration vs. peak area calibration curve was constructed for acridine and was verified before, during and after the analysis of each run. In all cases, the samples were analyzed in a random manner. Repeated injections of the same sample showed a ±10% variation in the concentration of nitrogen compounds.

Acridine is a planar molecule consisting of three linear condensed aromatic rings in which a pyridine moity is flanked by two benzenoid structures as shown in [1] where the positions of substitution have been numbered according to common usage:

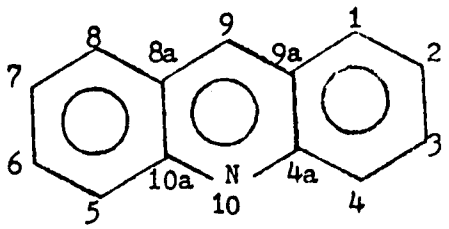

[1]

Kinetic runs of the catalytic hydrodenitrogenation of this substrate were carried out in the stirred autoclave. Table 5 shows the standard operating conditions and the range of operating variables studied. Under these conditions, acridine was rapidly hydrogenated to 1,2,3,4-tetrahydroacridine (THA) and 1,2,3,4,9,10,4a,9a-octahydroacridine (OHA). Several other intermediates also were observed including 1,2,3,4,5,6,7,8- (symmetric) octahydroacridine (SOHA), perhydroacridine (PHA), o-methyl- (cyclohexyl) aniline (MCA) and a trace amount of 1,2-dihydroacridine (DHA). Figures 26 and 27 show the concentration profiles for total nitrogen (sum of all nitrogen-containing compounds), acridine and some of the identifiable reaction intermediates under the standard run conditions of 367°C and 136 atm.

Although the hydrodenitrogenation of acridine is a complex reaction, it exhibits relatively clean first-order behavior with respect to the total nitrogen content as shown in Figure 26. Consideration of the structures of the reaction intermediates observed, clearly indicates that acridine hydrodenitrogenation involves preliminary hydrogenation of aromatic rings followed by hydrogenolysis of saturated carbon-nitrogen bonds.

A proposed reaction network based on the identifiable intermediates is given in Table 6. The first order-rate constants for each reaction

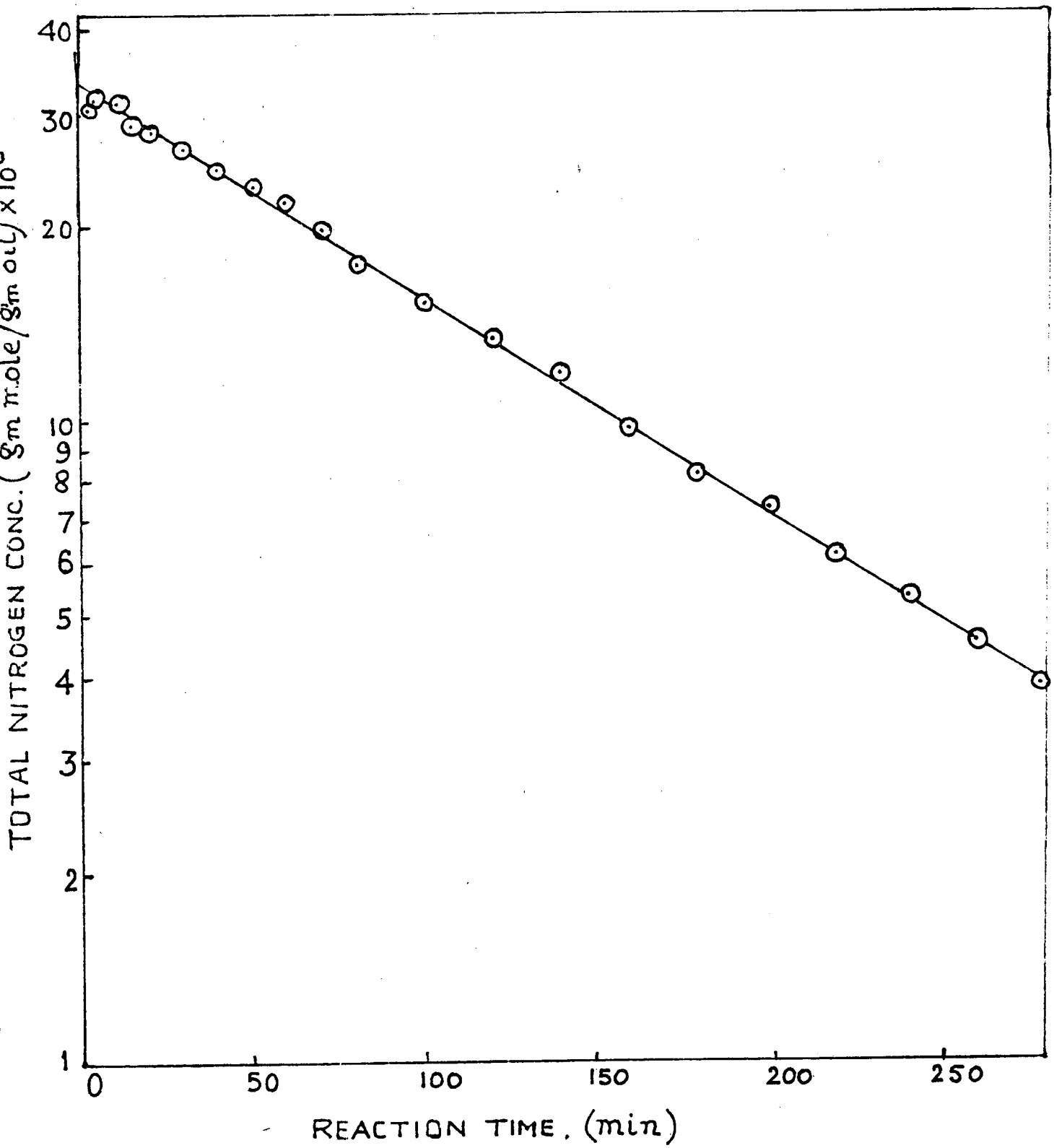

Figure 26: First-order dependence of total nitrogen removal for hydrodenitrogenation of acridine. Reaction conditions: 367°C, 136 atm, Ni-Mo/γ-Al_2O_3.

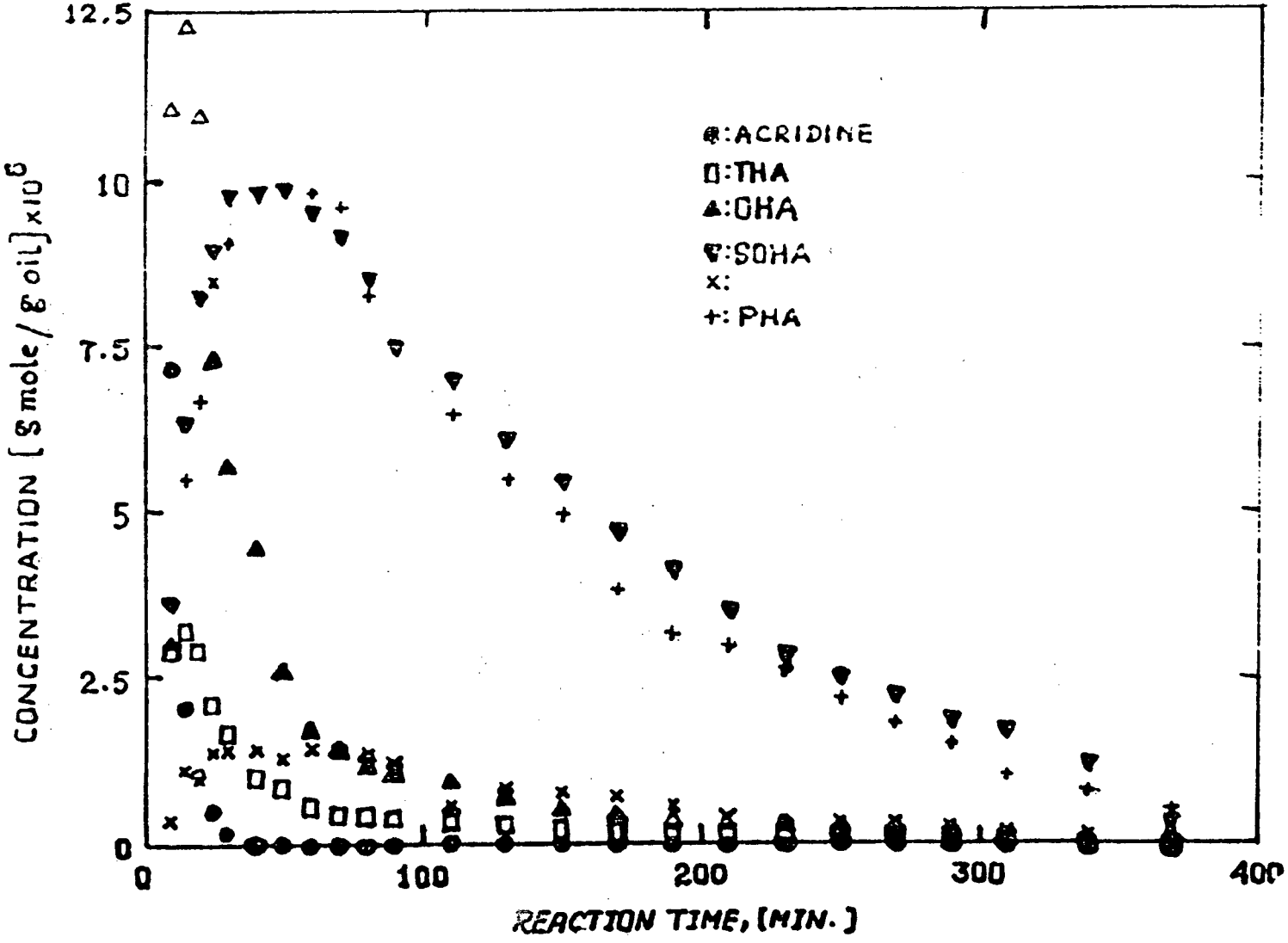

Fig. 27. Behavior of intermediates observed in hydrodenitrogenation of acridine.

TABLE 6

Reaction Network of HDN of Acridine and First-Order Rate Constants*

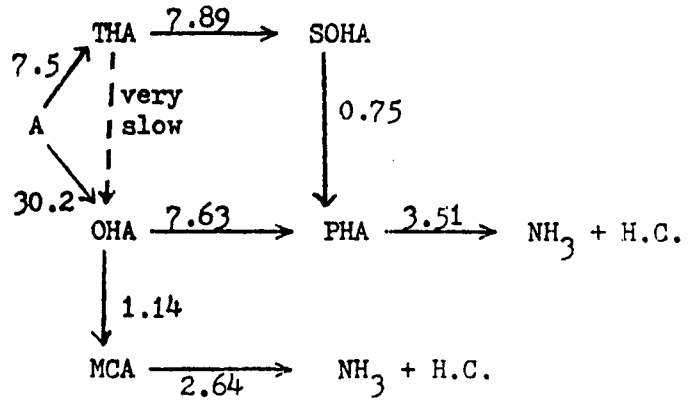

*First order rate constants are in $min.^{-1}$.

**A : acridine
THA : 1,2,3,4-tetrahydroacridine
OHA : 1,2,3,4,9,10,4a,9a-octahydroacridine
SOHA: 1,2,3,4,5,6,7,8-octahydroacridine
PHA : perhydroacridine
MCA : o-cyclohexyl-methyl aniline
H.C.: hydrocarbon

***Operation conditions:

364°C, 136 atm total pressure, Ni-Mo/γ-Al_2O_3 (HDS-9A), 140-200 mesh catalyst conc. = 0.5 wt %, CS_2 conc. = 0.05 wt %, solvent = white oil.

in the reaction network were calculated from the concentration vs. time data. Since the system showed first-order kinetic behavior with respect to the removal of acridine and with respect to total nitrogen content, pseudo first-order kinetics was used in modeling each reaction in the acridine reaction network. The pseudo first-order rate constants were defined by

$$\frac{M_o}{M_c} \frac{d C_i}{dt} = -K_{i,j} C_i$$

where

M_o = mass of oil, g
M_c = mass of catalyst, g
C_i = concentration of species i, gmoles i/g oil
t = time, min
$K_{i,j}$ = pseudo first-order rate constant for compound i in the jth reaction, (g oil) (g cat-min)$^{-1}$ min^{-1}.

The numerical values of the first-order rate constants for each reaction under the standard conditions (Table 5) are given in Table 6.

Increasing hydrogen pressure results in a non-linear increase in the rate of acridine hydrodenitrogenation over the range of 54.4 to 172 atm as shown by the behavior of the pseudo first-order rate constant for total nitrogen removal (Figure 28). The effect of hydrogen pressure on the pseudo first-order rate constant for each reaction in the reaction network is shown in Figures 29, 30, 31 and 32.

Acridine hydrodenitrogenation is strongly dependent on temperature; a total rate of nitrogen removal has an activation energy of 35 kcal/mole (Figure 33). The Arrhenius plots for the intermediate reactions in the acridine hydrodenitrogenation reaction network are presented in Figure 34 and Figure 35 and the activation energies are summarized in Table 7.

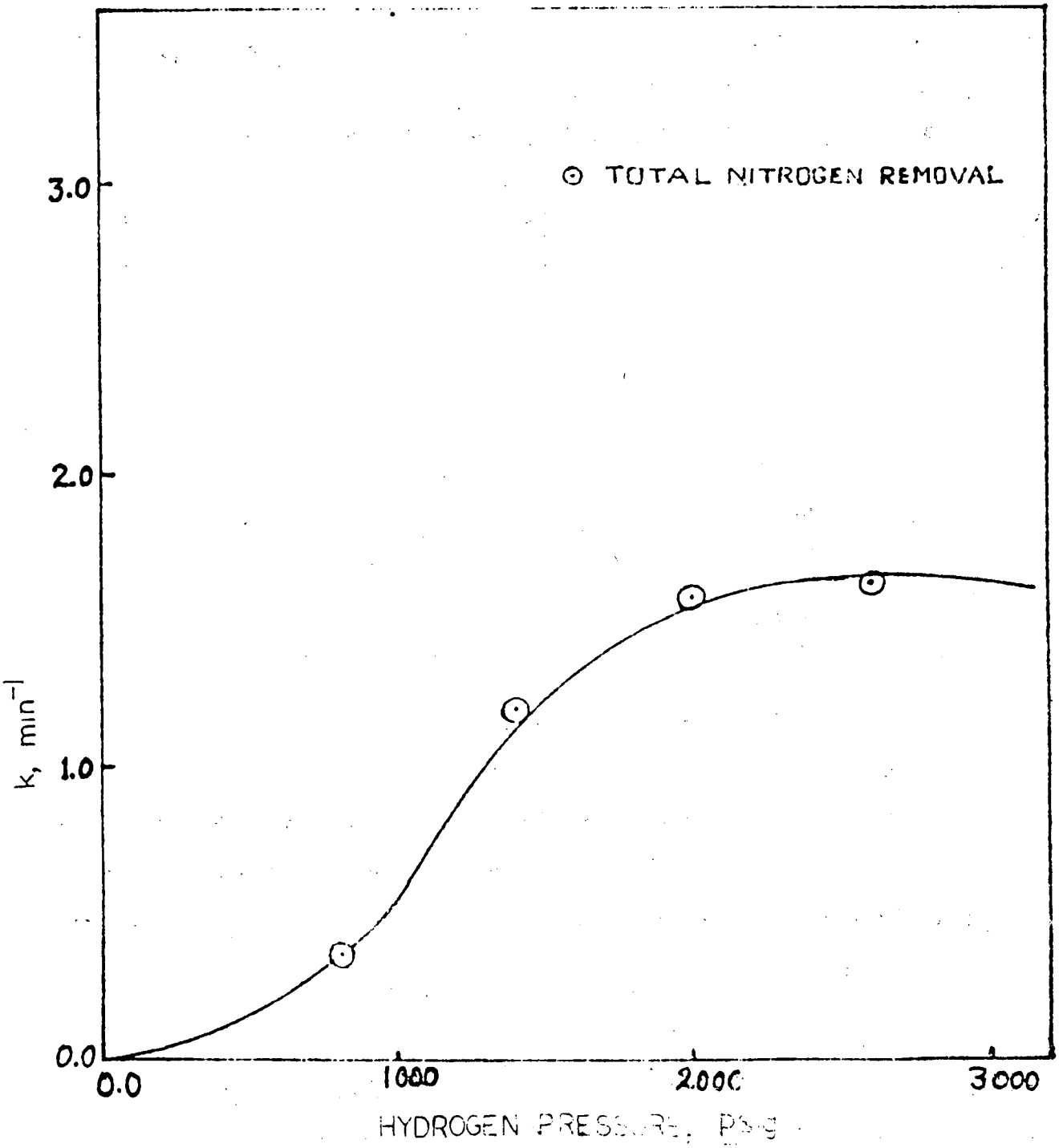

Fig. 28. Effect of hydrogen pressure on the pseudo first-order rate constant for hydrodenitrogenation of acridine. Reaction conditions: 367°C, Ni-Mo/γ-Al_2O_3 catalyst, batch reactor.

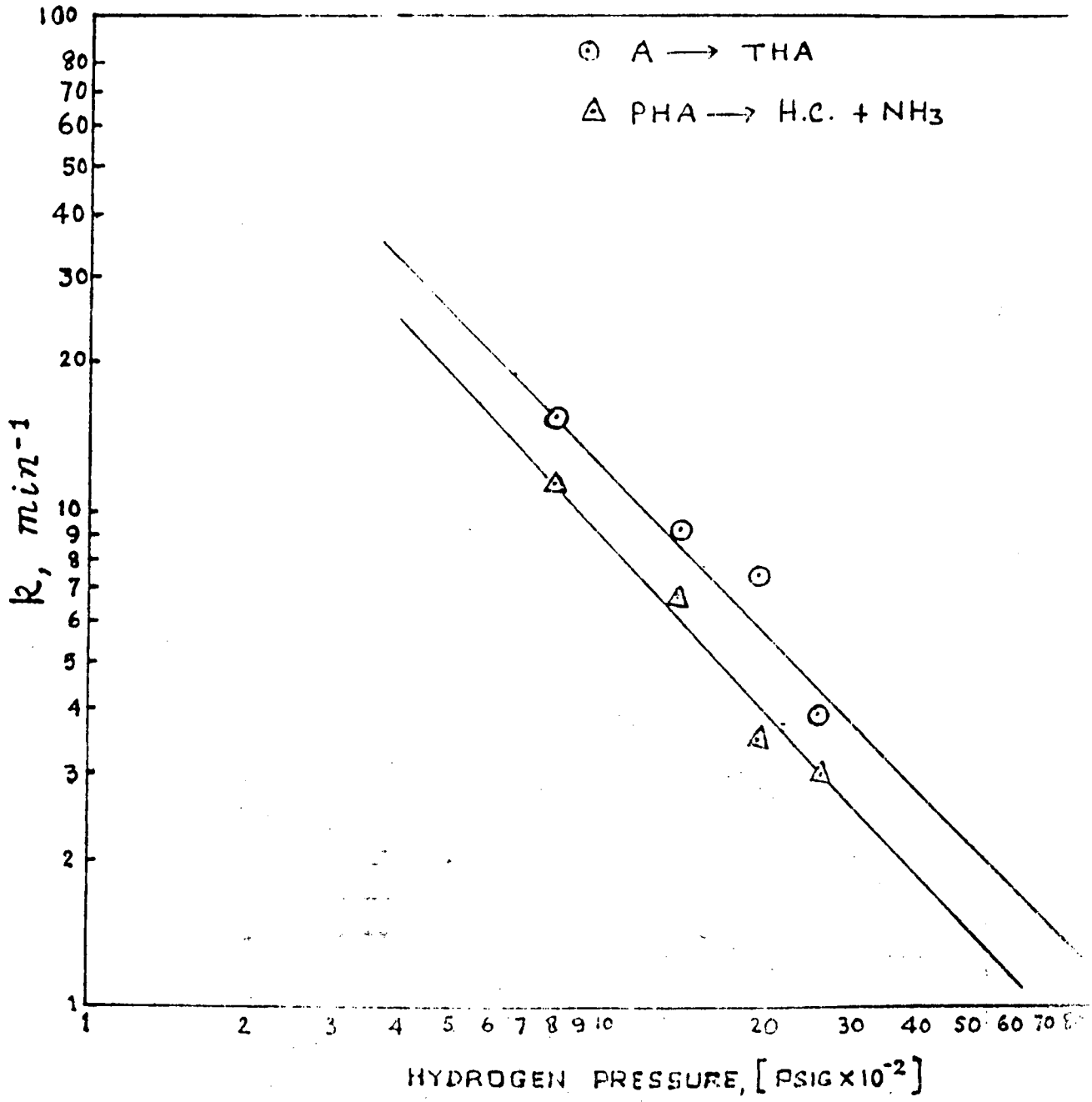

Fig. 29. Effect of hydrogen pressure on pseudo first-order rate constant for conversion of acridine to tetrahydroacridine and of perhydroacridine to hydrocarbons and ammonia in hydrodenitrogenation of acridine. Reaction conditions: 367°C, Ni-Mo/γ-Al_2O_3.

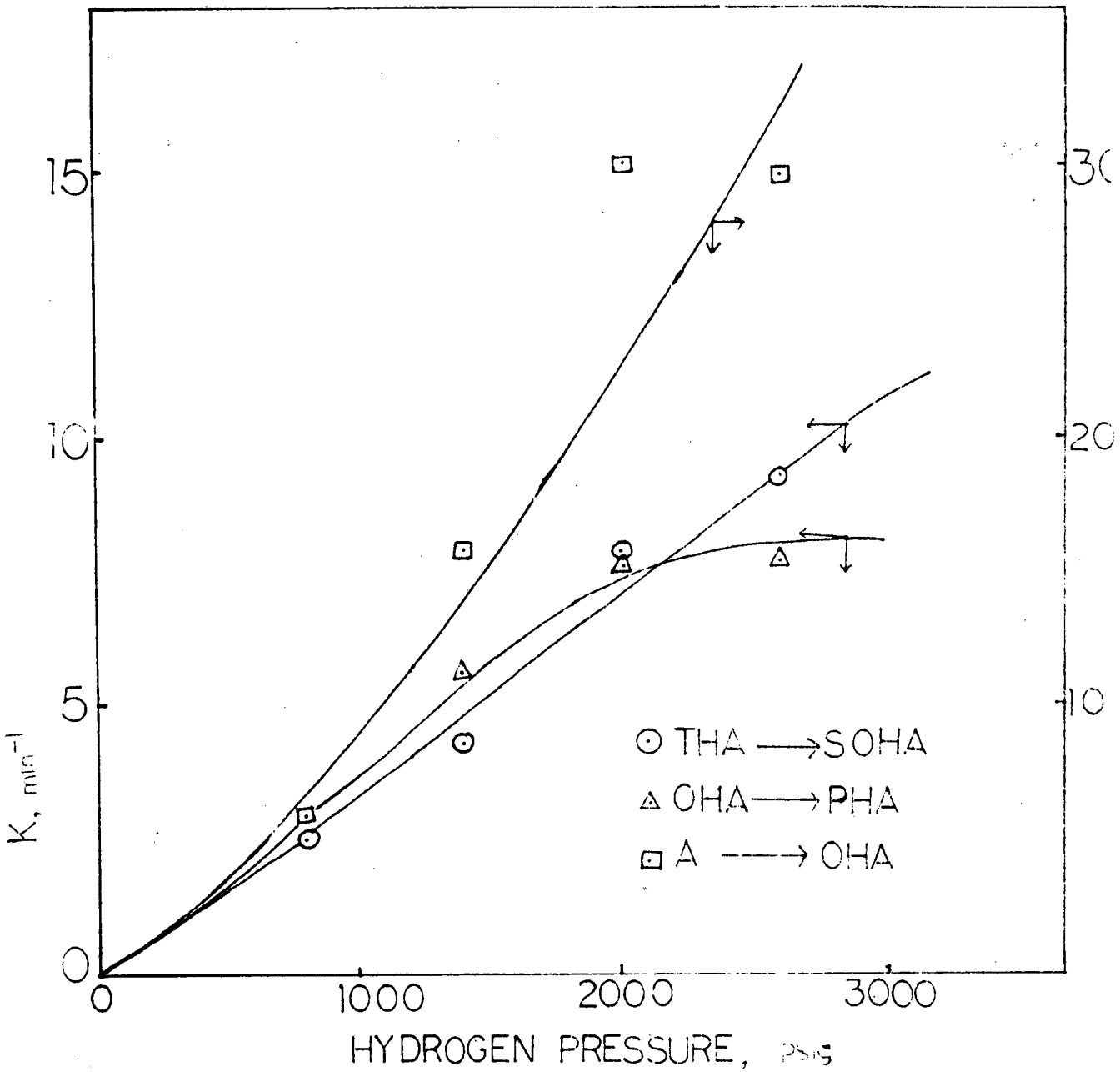

Figure 30: Effect of hydrogen pressure on hydrogenation steps in hydrodenitrogenation of acridine. Reaction conditions: 367°C, Ni-Mo/γ-Al_2O_3.

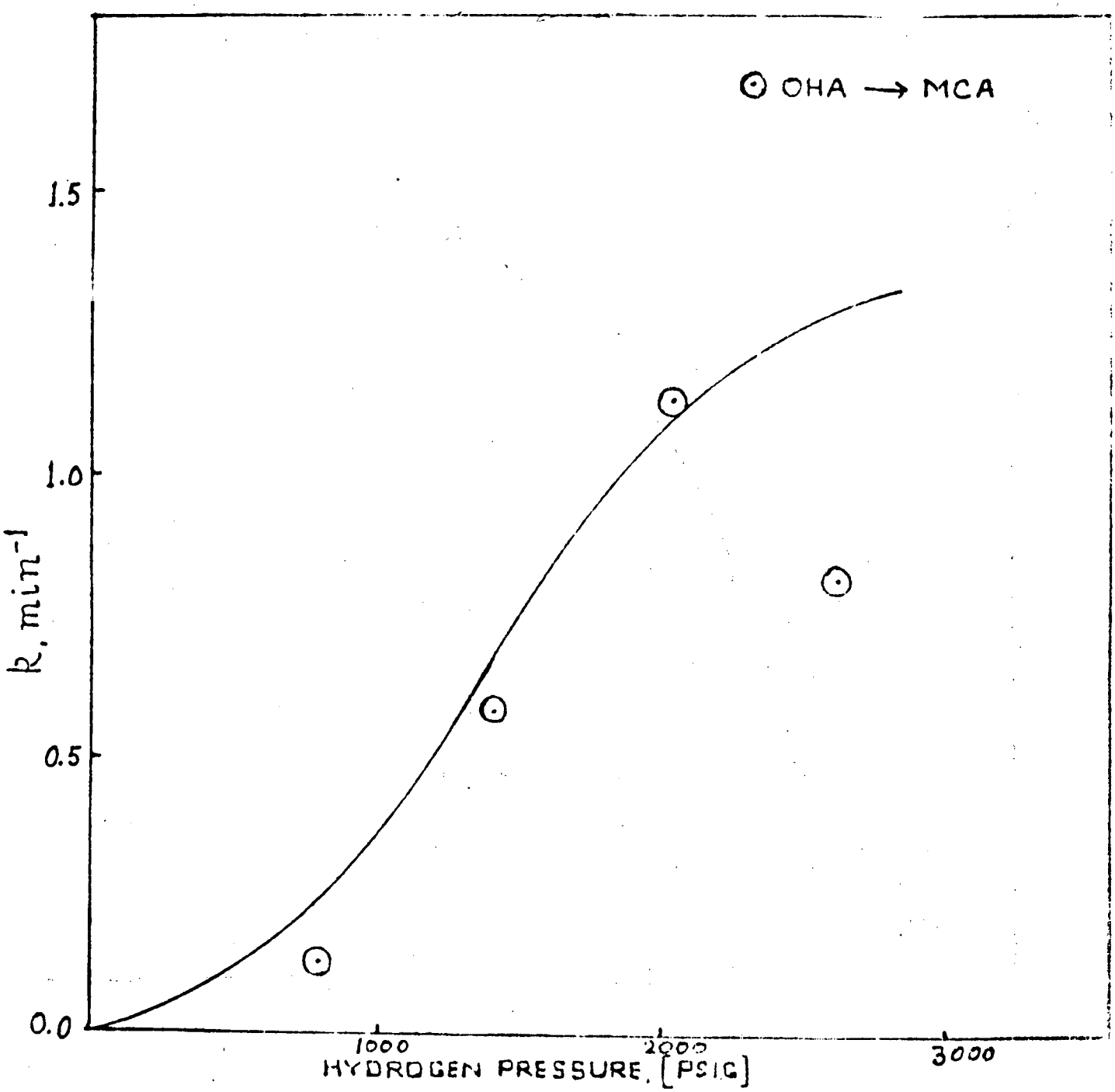

Fig. 31. Effect of hydrogen pressure on conversion of octahydrcacridine to o-methyl-(cyclohexyl) aniline in hydrodenitrogenation of acridine. Reaction conditions: 367°C, Ni-Mo/γ-Al_2O_3 catalyst.

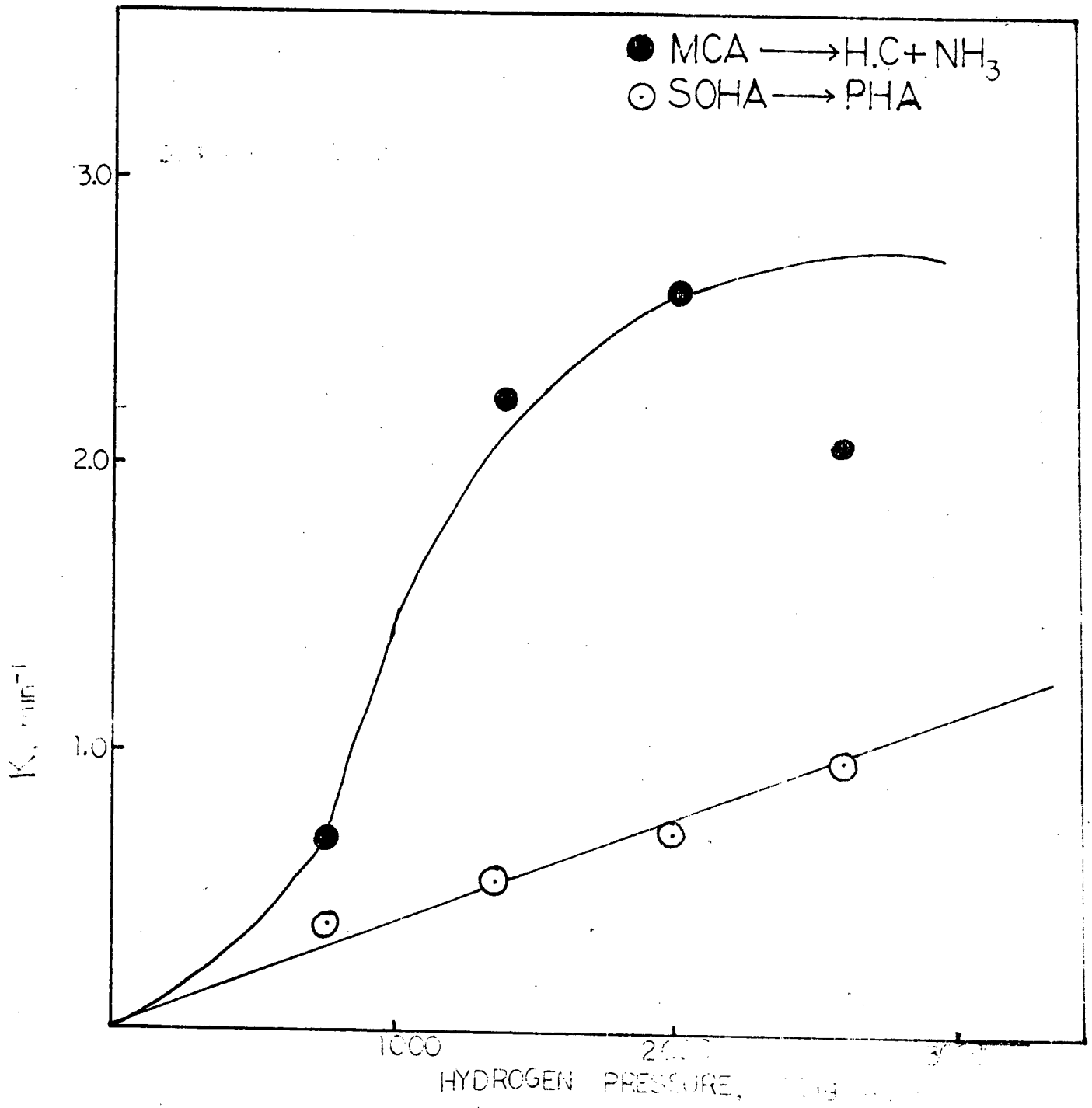

Figure 12: Effect of hydrogen pressure on pseudo-first-order rate constant for conversion of o-methyl-(cyclohexyl) aniline to hydrocarbon and ammonia and of symmetric octahydroacridine to perhydroacridine in hydrodenitrogenation of acridine. Reaction conditions: 367°C, Ni-Mo/γ-Al_2C_3 catalyst.

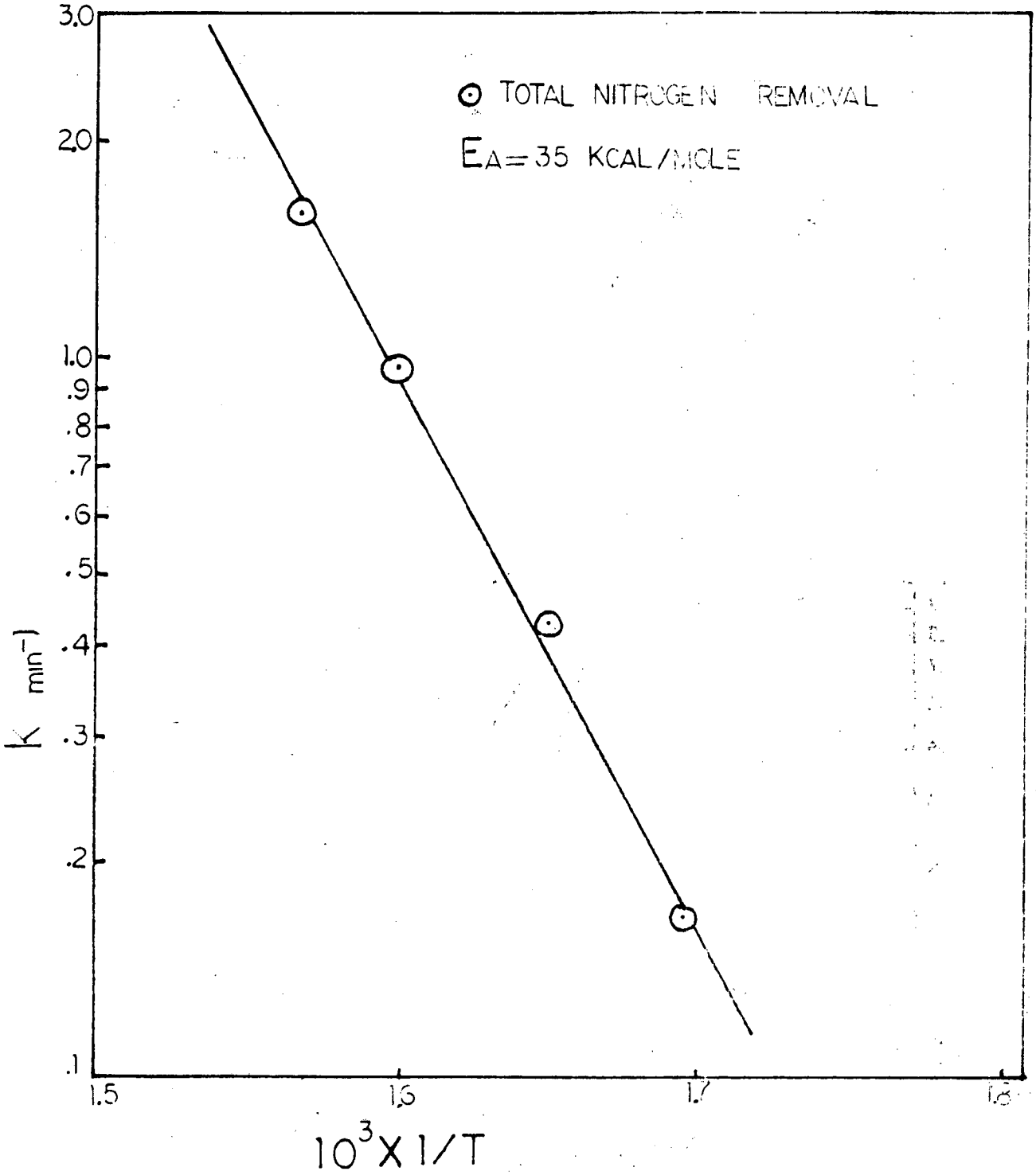

Figure 33: Temperature dependence of total nitrogen removal in hydrodenitrogenation of acridine. Reaction conditions: 136 atm, Ni-Mo/γ-Al_2O_3 catalyst.

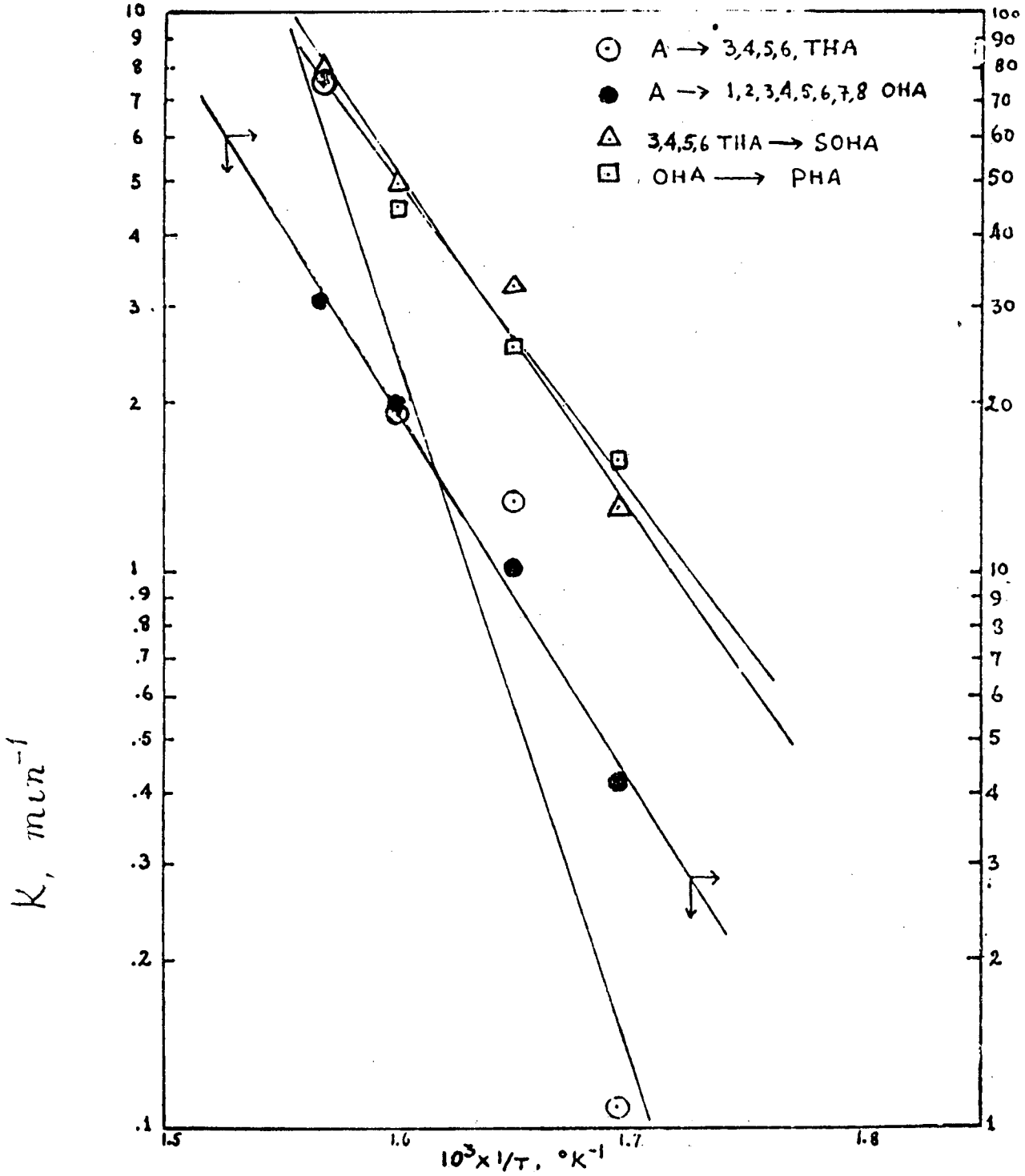

Figure 34: Temperature dependence of intermediate hydrogenation reaction steps in acridine hydrodenitrogenation. Reaction conditions: 136 atm, Ni-Mo/γ-Al_2O_3 catalyst.

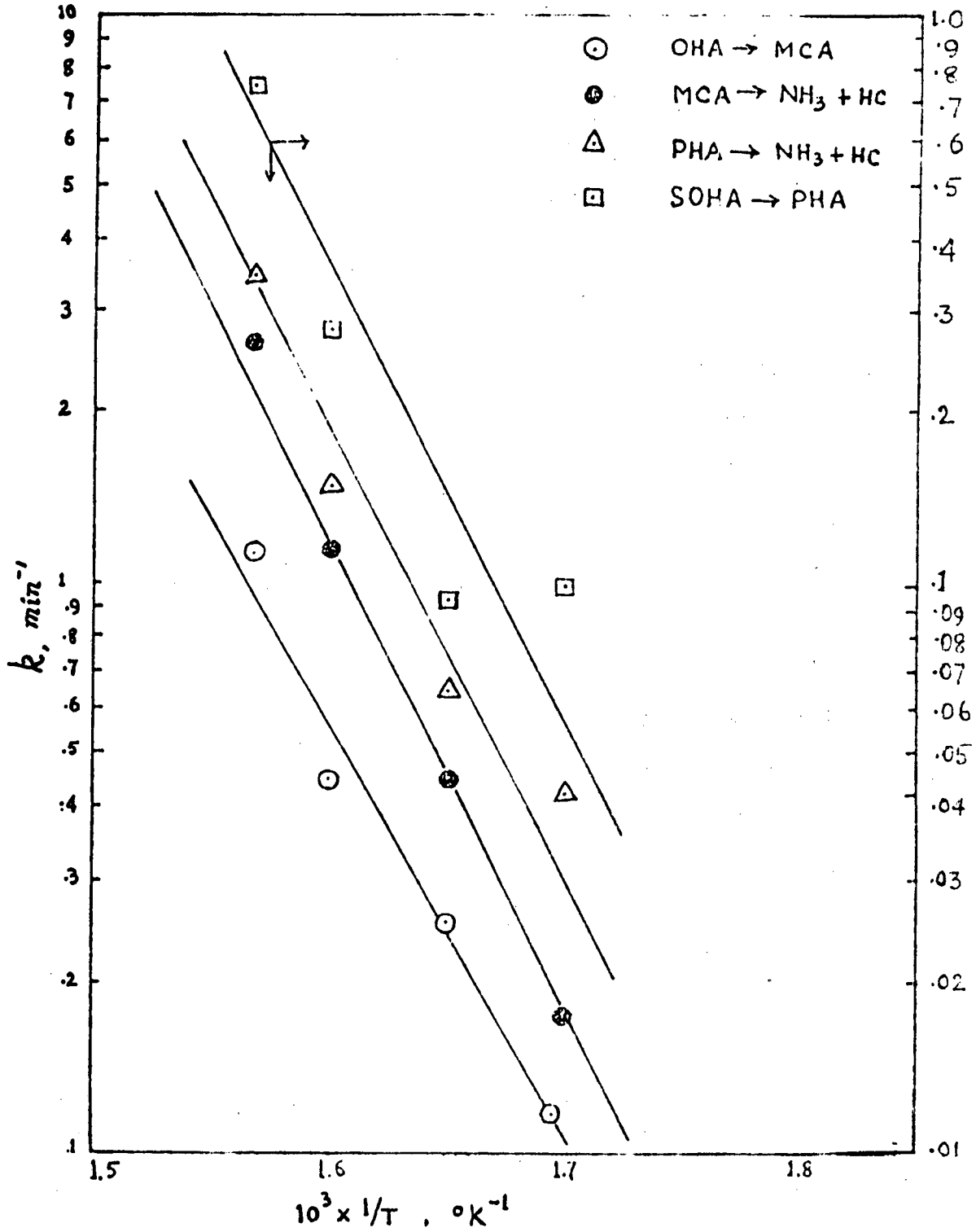

Figure 35: Temperature dependence of the C-N bond scission steps (except one) in acridine hydrodenitrogenation. Reaction conditions: 136 atm, Ni-Mo/γ-Al_2O_3 catalyst.

TABLE 7

Activation Energies of the HDN of Acridine

Reaction	E, kcal/mole
Total Nitrogen Removal	35.9
A → THA	57.7
A → OHA	30.8
THA → SOHA	28.0
OHA → PHA	25.2
SOHA → PHA	36.9
OHA → MCA	31.6
MCA → NH_3 + H.C.	37.4
PHA → NH_3 + H.C.	36.4

As in the case of pyridine and quinoline hydrodenitrogenation (McIlvried, 1970; Shih et al., 1977) the corresponding rate of the acridine reaction is found to be sensitive to the initial reactant concentration. Table 8 illustrates a comparison between two runs with initial concentrations of 0.5 wt % and 1.0 wt % acridine. Acridine hydrodenitrogenation is inhibited by the basic nature of the acridine and by all basic reaction intermediates.

b. Discussion

Acridine is a nitrogen-containing compound whose lone pair of electrons on the nitrogen atom are extensively delocalized over the three rings by resonance, thus accounting for its weak basicity. It is slightly more basic than pyridine and quinoline, and considerably less basic than ammonia (Table 9). However, with respect to the hydrodenitrogenation reaction, acridine is more refractory than quinoline. It requires more severe reaction conditions than quinoline as shown in Table 10.

Both the benzenoid and pyridine rings in the molecule are very reactive toward hydrogenation leading to partially hydrogenated intermediates. Indeed, acridine was very rapidly hydrogenated to tetrahydroacridine (THA) and octahydroacridine (OHA). The occurrence of 1,4-dihydroacridine (1,4-DHA) as a detectable transient species suggests that the route of hydrogenation of acridine to tetrahydroacridine follows equation [11]

$$A \rightarrow 1,4\text{-DHA} \rightarrow THA \qquad [11]$$

The formation 1,4-DHA was very rapid and seemed to attain thermodynamic equilibrium. Justification of the establishment of thermodynamic

TABLE P

Effects of Acridine Initial Conc. on the

[illegible] Denitrogenation of [illegible]

	k, $min.^{-1}$	
	1.0 wt%[a]	0.5 wt%[a]
Total Nitrogen-Removal	0.994	1.59
A → THA	5.9	7.5
A → OHA	21.7	30.7
THA → SOHA	5.28	7.89
OHA → PHA	3.85	7.63
SOHA → PHA	0.22	0.75
OHA → MCA	0.70	1.14
MCA → NH_3+H.C.	1.68	2.64
PHA → NH_3+ H.C.	2.48	3.51

Operating Conditions: standard operation conditions 367°C, [illegible] atm.

[a]wt % acridine added at zero time.

Table 9

pK_a (in H_2O) of Nitrogen-Containing Compounds*

Compound	pK_a (H_2O)*
piperidine	11.11**
cyclohexylamine	10.6**
ammonia	9.27
acridine	6.5
pyridine	5.6
quinoline	4.94
pyrrole	0.4

*Richter (1952)

**Roberts (1971)

TABLE 10

Comparison of Reactivity of Quinoline and Acridine

	Quinoline	Acridine
First-order rate constant of total N-removal	0.55 $min.^{-1}$	0.50 $min.^{-1}$
Temperature	342°C	342°C
Hydrogen pressure	34 atm	136 atm

equilibrium was difficult to achieve, however, due to the rapid reaction and the few data points available in most of these runs. However, in a run carried out at low hydrogen pressure (57.8 atm) a clear indication of the presence of thermodynamic equilibrium was established.

In view of the fact that the hydrogenation (Table 11) of acridine produces a stronger base and that rapid formation of dynamic equilibrium between acridine and 1,4-dihydroacridine is observed, it was not surprising that the hydrogenation step is inhibited by increasing hydrogen pressure as is shown in Figure 31. Since the hydrogenation products are more strongly adsorbed on the catalyst than the less basic reactant acridine, the greater the concentration of hydrogenation product accumulated the slower the rate of acridine hydrogenation.

As stated earlier, acridine is rapidly hydrogenated to octahydroacridine (OHA) in addition to tetrahydroacridine (THA). The formation of octahydroacridine was presumed to proceed through the 9,10-dihydroacridine (9,10-DHA) (equation [12]), although 9,10-dihydroacridine was only a transient and not directly observable.

$$A \rightarrow [9,10\text{-DHA}] \rightarrow OHA \qquad [12]$$

Systematically, tetrahydroacridine can be hydrogenated to octahydroacridine and symmetrical octahydroacridine. However, kinetic analysis indicated that the rate of hydrogenation of tetrahydroacridine to octahydroacridine was negligible. This reaction apparently is hindered by the adjacent, bulky cyclohexyl ring. Hydrogenation of tetrahydroacridine to octahydroacridine involves the hydrogenation of the sandwiched pyridine ring.

TABLE 11

The Establishment of Thermodynamic Equilibrium Between Acridine and 1,4-Dihydroacridine

Reaction Time min.	$C_{1,4\text{-DHA}}/C_A$
10	0.26
20	0.67
30	0.61
40	0.59
50	0.67
60	0.55
70	0.51
80	0.54
90	0.63
110	0.44
120	Beyond Detectability

Hydrogenation of the flanking benzenoid rings to tetrahydroacridine is obviously a sterically less-hindered reaction. On the other hand, the results show that the hydrogenation of tetrahydroacridine to symmetrical octahydroacridine is relatively rapid. Steric hindrance can also be invoked to explain the high selectivity to symmetrical octahydroacridine when hydrogenation occurs over noble metal catalysts (Vierhapper and Eliel, 1975). A similar steric effect markedly diminishes the hydrogenation reactivity of symmetrical octahydroacridine to perhydroacridine.

Octahydroacridine, which consists of one benzenoid ring and a saturated pyridine moiety, was subjected to further hydrogenation in an effort to effect saturation of the benzenoid ring and hydrogenolysis of the C-N bond, leading to perhydroacridine and o-methyl-(cyclohexyl) aniline (MCA) respectively. However, under standard operating conditions (136 atm and 367°C) octahydroacridine was selectively hydrogenated to perhydroacridine (1:7 ratio of hydrogenolysis to hydrogenation). As, in the case of aniline and o-propylaniline (Flinn, 1962; Shih, 1977) MCA proved to be highly resistant to the hydrodenitrogenation reaction. Finally, perhydroacridine, a fully-saturated compound, was denitrogenated through hydrogenolysis of its carbon-nitrogen bond with formation of an aliphatic amine. Aliphatic amines undergo hydrodenitrogenation very rapidly. Consequently only the non-nitrogeneous compounds derived from the hydrogenolysis of perhydroacridine could be detected in this study.

Acridine hydrodenitrogenation was promoted by increasing the hydrogen pressure. The hydrogen pressure is a unique process variable by means of which the reaction path may be altered. Since major denitrogenation

takes place only through the hydrogenolysis of perhydroacridine, total nitrogen-removal is more or less completely correlated with the rate of formation and the rate of decomposition of the perhydroacridine. There are, in fact, two routes for the formation of perhydroacridine which are delineated in the reaction network (Table 6).

$$A \rightarrow THA \rightarrow SOHA \rightarrow PHA \qquad [13]$$

$$A \rightarrow OHA \rightarrow PHA \qquad [14]$$

At high hydrogen pressures, perhydroacridine was selectively formed through A → OHA → PHA, and this preference may be a consequence of the concomitant fact that the formation of tetrahydroacridine, the alternative path to perhydroacridine, was inversely proportional to the hydrogen pressure. As shown in Figures 29 and 30, lowering the hydrogen pressure shifts the selectivity between tetrahydroacridine and octahydroacridine; the selectivity at several hydrogen pressures is shown in Table 12. In the A → THA → SOHA → PHA route, symmetrical octahydroacridine is a very refractory compound which is only slowly hydrogenated to perhydroacridine.

Whereas increasing of hydrogen pressure ordinarily promotes the hydrogenation reactions, hydrogenolysis of perhydroacridine was severely retarded by increasing the hydrogen pressure. A similar phenomenon was found in the hydrodenitrogenation of quinoline under similar conditions (Shih et al., 1977); in the hydrodenitrogenation of quinoline, the rate of hydrogenolysis of decahydroquinoline decreased with increasing hydrogen pressure.

The two mechanistic possibilities considered previously for hydrogenolytic denitrogenation differ only as regards the rate determining

TABLE 12

Selectivity of Acridine Hydrogenation

Total pressure, atm	$K_{A \rightarrow THA}/K_{A \rightarrow OHA}$
54.4	1.99
95.2	0.60
136	0.23
177	0.13

*First-order rate constant, $min.^{-1}$

**Reaction temperature: 367°C

cleavage of the carbon-nitrogen bond. In the Hoffman type E-2 elimination mechanism (Eq. 15) coordination of the nitrogen as an anionic catalyst vacancy preceeds concerted carbon-nitrogen bond breaking and β-hydrogen abstraction by a hydrogen acceptor catalyst site. In the E-1 (so-called, carbonium ion) elimination mechanism (Equation 16) coordination of the nitrogen at the anionic catalyst vacancy preceeds a rate-determining cleavage or ionization of the carbon-nitrogen bond without necessity for assistance by a catalyst site in the subsequent, fast β-hydrogen abstraction. The observed, strong negative dependence of the hydrogenolysis of perhydroacridine on the hydrogen pressure is in accord with both of these mechanisms of hydrogenolysis, in that, increased hydrogen pressure results in decreased availability of anionic catalyst vacancies for coordination of the nitrogen unshared pairs.

Based on the considerations discussed above, an S-shaped relationship between the first-order rate constant of the total nitrogen removal and the hydrogen pressure is to be anticipated. Figure 28 illustrates how closely the data fulfills this expectation.

The activation energy for total nitrogen removal from acridine was 35 kcal/mole, which is slightly higher than that found for the quinoline hydrodenitrogenation (25 kcal/mole). The high activation energy for the total nitrogen removal is partly a reflection of the high activation requirements of the prior hydrogenation reactions which ranged from 25 kcal/mole to 35 kcal/mole. These values are to be compared to those for the hydrodenitrogenation of quinoline, where activation energies of the hydrogenation reactions were around 20 kcal/mole. These differences can be correlated with steric factors which are responsible for hindrance to hydrogenation

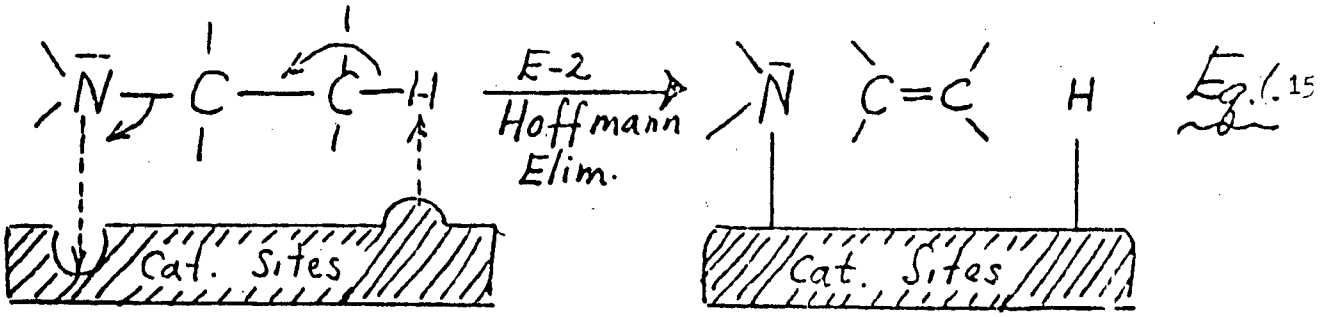
E-2
Hoffmann
Elim.
Cat. Sites
Cat. Sites

Eq. (15)

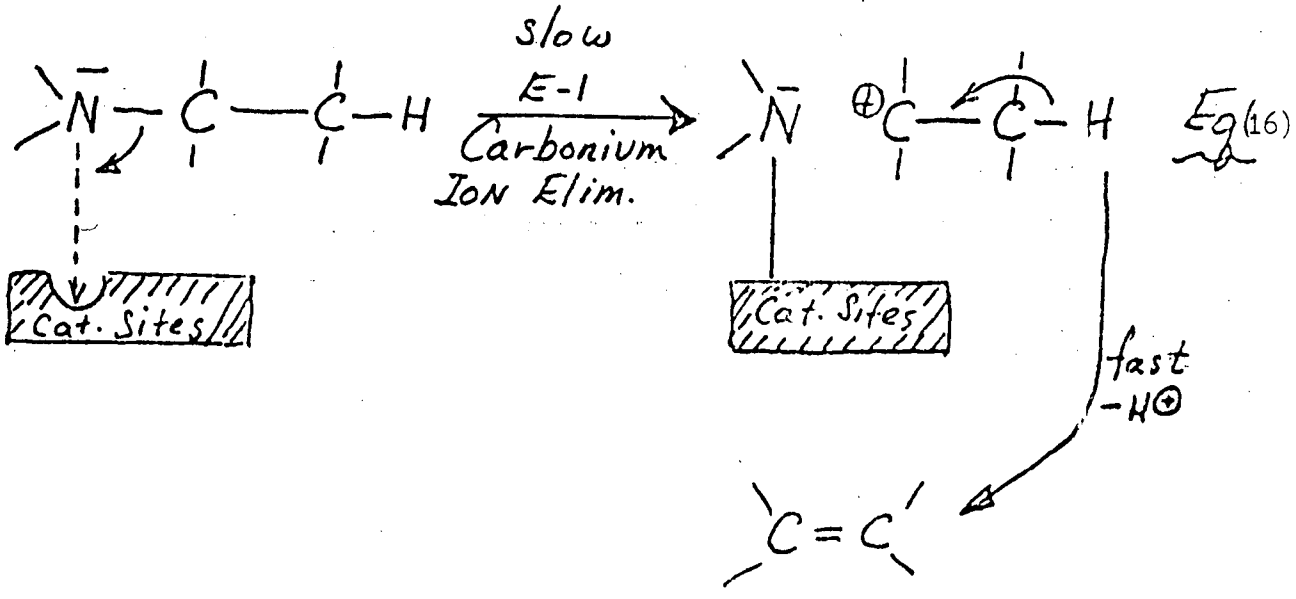
Slow
E-1
Carbonium
Ion Elim.
Cat. Sites
Cat. Sites
fast
-H⊕

Eq (16)

in acridine and its partially hydrogenated derivatives, and which, as a result, are attended by higher entropy barriers than in the more simply-structured quinoline substrate. Thus, the activation energy for hydrogenolysis of perhydroacridine (ca. 35 kcal), was found to be comparable to that for the hydrogenolysis of decahydroquinoline which is the most sterically hindered of the hydrogenated intermediates among the quinoline derivatives.

c. Conclusions

Acridine hydrodenitrogenation involves a complex series of hydrogenation and hydrogenolysis reactions. The reaction network of acridine hydrodenitrogenation is similar to that of quinoline hydrodenitrogenation, where hydrogenation of the pyridine ring is necessary for the removal of nitrogen. However, acridine hydrodenitrogenation requires more severe operating conditions. The reaction path is strongly dependent on hydrogen pressure, and is very subject to steric hindrance. The results presented afford considerable insight into the details of the hydrodenitrogenation reaction network in polycondensed nitrogen-containing compounds. This information can provide quantitative guidance for process development and catalyst improvement.

3. Studies on the Interaction Between Various Nitrogen, Sulfur and Aromatic (Hydrocarbon) Compounds

During this quarter, reaction network and kinetic studies involving interactions between heteroatom-containing compounds and aromatic compounds were initiated. Since quinoline is a typical nitrogen-containing compound present in coal-derived liquids and reaction network and kinetics of hydrodenitrogenation of quinoline have been studied in great detail in our prior work, we have chosen quinoline as a typical compound for the interactions studies. Four different sets of experiments are being done in the preliminary parts of the interaction work. These are:

a. Basic and Non-Basic Nitrogen-Containing Compounds

The quinoline-indole pair was chosen for these studies. Three runs were carried out in our standard batch autoclave reactor at 342°C and 34 atm dihydrogen with Ni-Mo/γ-Al_2O_3 (HDS-98) catalyst; 0.05 wt % CS_2 was added to the reaction mixture.

Although analytical work is not fully completed, preliminary results indicate that indole alone is less reactive ($K_{I,TN}$ = 0.7 min^{-1} at 342°C and 37 atm) than is quinoline alone ($K_{Q,TN}$ = 0.8 min^{-1}). When indole and quinoline are present together, the total nitrogen removal rate from quinoline-type compounds (reaction intermediates) is unaffected, but the rate of total nitrogen removal from indole-type compounds is reduced by 10-20%. The pseudo first-order rate constants for the competing compound experiment are

$$K_{I,TN} \cong 0.57 \text{ min}^{-1} \text{ and } K_{Q,TN} = 0.8 \text{ min}^{-1}.$$

b. Aromatic Compounds and Basic Nitrogen-Containing Compounds

Preliminary studies of the interaction between naphthalene and quinoline have been carried out in hexadecane carrier and analyzed utilizing the FID because of the need to analyze for the aromatic compounds, partially saturated compounds and fully saturated compounds. All reactions were carried out at 342°C and 37 atm with 0.05 wt % CS_2 in the feed. The concentration of quinoline was 0.5 wt %. Naphthalene alone was studied at the 5 wt % concentration level, and competitive reaction was carried out with 0.5 wt % quinoline and 5 wt % naphthalene in hexadecane.

Naphthalene alone hydrogenates rapidly to tetralin and equilibrium is essentially established after two hours at reaction conditions. A small quantity of tetralin further hydrogenates to decalin. The naphthalene-tetralin equilibrium strongly favors tetralin. The pseudo first-order rate constant K_N for hydrogenation of naphthalene to tetralin at the reaction conditions is about 5 min^{-1}.

When quinoline and naphthalene are present together, hydrogenation of naphthalene is retarded drastically. The pseudo first-order rate constant for naphthalene hydrogenation to tetralin is reduced about 20-fold by the presence of quinoline. However, the rate of total nitrogen removal from quinoline compounds is not affected by the presence of naphthalene in the feed.

In the next quarter, kinetic analysis of the above-mentioned systems will be completed, and the effect of interactions on individual rate constants in the reaction networks will be determined.

The two other types of interactions to be studied include:

- Interaction between nitrogen-containing and sulfur-containing compounds.
- Interaction among nitrogen-containing compounds, sulfur-containing compounds and aromatic compounds.

Preliminary studies of these interactions will begin during the next quarterly period with dibenzothiophene being used as the typical sulfur-containing compound.

D. POISONING REACTION ENGINEERING

1. Introduction

In the last quarterly report, coking effect on the catalyst deactivation in H-coal process has been examined with a specific mechanism of independent fouling. The model including the effect of pore blockage caused by coke laydown and the effect of hindered diffusion of larger molecules in the partially closed pores shows that sometimes improvement in catalyst life and activity level can be obtained by proper selection of the pore size.

Since the coke content on H-coal® catalyst is very high, coke deposition may be the major factor for catalyst deactivation, especially in the initial stage of operation. Literature describing the effects of coke laydown on both physical and chemical properties of the catalysts are few. The decisive effects have not been reported.

This report continues to concern physical rather than chemical properties of the catalyst. Prototype mechanisms of series, parallel and

independent reaction networks for coke formation are studied. The accumulation and propagation of coke laydown in the catalyst for these three reaction networks are investigated and compared. The theoretical model of the effect of coke formation on the performance in the H-coal process is similar to that described in last report, but some additional criteria have been included to consider the general phenomena of coke formation.

In the H-coal® process pulverized coal is mixed with slurry oil and heated in the preheater with compressed make-up hydrogen before being led to the H-coal® reactor. The first step in liquefaction occurs principally as an uncatalyzed reaction, and the resulting asphaltene will then be transformed to the desired products via hydrogenation, hydrocracking, etc., by catalytic reaction with hydrogen. The essence of the H-coal® process, therefore, can be modeled simply as a slurry reactor as shown in Fig. 36. Owing to the complex compositions in the coal slurry and the possibly numerous side reactions which will contribute to the coke formation such as polymerization and aromatization etc., description of the coking mechanism is difficult. Nevertheless, understanding of some basic aspects of coking mechanism will enable the process to be characterized with a traceable phenomenon and promote better reaction design and longer catalyst life.

Material balances characterizing the fluid phases both inside and outside the catalyst pellet for specific reaction network in H-coal reactor are summarized in Table 13 with appropriate boundary conditions. The implicit assumption made in formulation for Table 13 is that the time constant for the deterioration of the catalyst is relatively longer than that of residence and reactions, and therefore, quasi-steady state can be

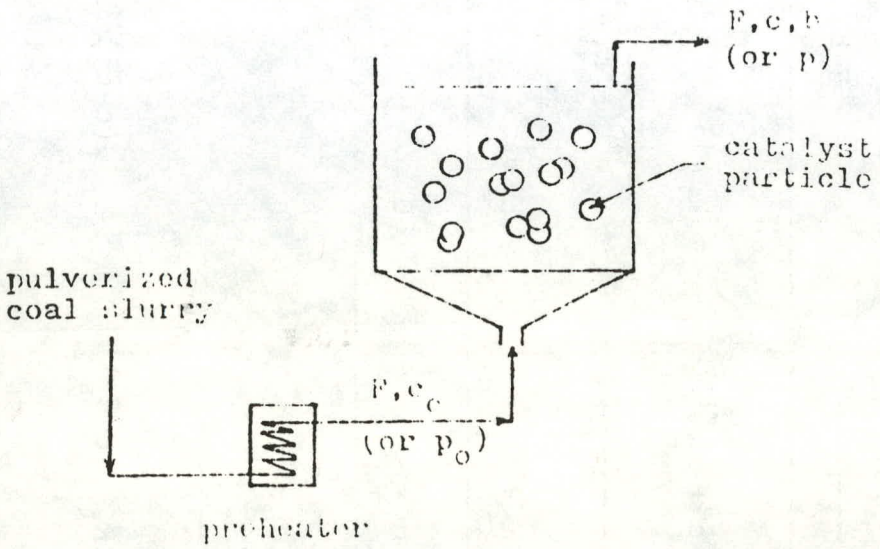

Fig. 36. Catalyst-slurry reactor of H-coal hydroprocessing.

TABLE 13: Material Balances for H-coal Reactor

	$c \xrightarrow{1} b$, $c \xrightarrow{2} \bar{p}$	$c \xrightarrow{1} b \xrightarrow{2} \bar{p}$	$c \xrightarrow{1} b$, $p \xrightarrow{2} \bar{p}$
Fluid phase outside catalyst pellet :			
$K_{f,1} \cdot S \cdot (c - \tilde{c}_s) =$	$F \cdot c_o - F \cdot c$	$F \cdot c_o - F \cdot c$	$F \cdot c_o - F \cdot c$
$K_{f,2} \cdot S \cdot (x - \tilde{x}_s) =$	———	$- F \cdot b$	$F \cdot p_o - F \cdot p$
Inside catalyst pellet :			
$\frac{1}{r^2}\frac{\partial}{\partial r}(r^2 D_{e,1}\frac{\partial \tilde{c}}{\partial r}) =$	$K_1 \theta^{\alpha} \tilde{c}^{\beta} + K_2 \theta^{\delta} \tilde{c}^{\gamma}$	$K_1 \theta^{\alpha} \tilde{c}^{\beta}$	$K_1 \theta^{\alpha} \tilde{c}^{\beta}$
$\frac{1}{r^2}\frac{\partial}{\partial r}(r^2 D_{e,2}\frac{\partial \tilde{x}}{\partial r}) =$	———	$K_2 \theta^{\delta} \tilde{b}^{\gamma} - K_1 \theta^{\alpha} \tilde{c}^{\beta}$	$K_2 \theta^{\delta} \tilde{p}^{\gamma}$
$\frac{\partial \bar{p}}{\partial t} =$	$K_2 \theta^{\delta} \tilde{c}^{\gamma}$	$K_2 \theta^{\delta} \tilde{b}^{\gamma}$	$K_2 \theta^{\delta} \tilde{p}^{\gamma}$
Initial condition :			
$\bar{p}\big\|_{t=0} =$	0	0	0
Boundary conditions :			
$\frac{\partial \tilde{c}}{\partial r}\big\|_{r=0} =$	0	0	0
$\frac{\partial \tilde{x}}{\partial r}\big\|_{r=0} =$	———	0	0
$D_{e,1}\frac{\partial \tilde{c}}{\partial r}\big\|_{r=r_c} =$	$K_{f,1} \cdot (c - \tilde{c}_s)$	$K_{f,1} \cdot (c - \tilde{c}_s)$	$K_{f,1} \cdot (c - \tilde{c}_s)$
$D_{e,2}\frac{\partial \tilde{x}}{\partial r}\big\|_{r=r_c} =$	———	$K_{f,2} \cdot (x - \tilde{x}_s)$	$K_{f,2} \cdot (x - \tilde{x}_s)$

** x represents either b or p.

assumed. At the same time, it is assumed that excess hydrogen is available from dissolved molecular liquid phase and also from the donor solvent. Consequently, the potential exterior mass transfer limitation will be at the liquid-solid interface. The catalyst looses activity by blockage with coke, and the fractional activity of the catalyst is defined to be:

$$\theta = 1 - \frac{\bar{p}}{\bar{p}_s} \qquad [17]$$

where $\bar{p}_s$ is the saturated coke level required to deactivate the catalyst.

The pores decrease in size with coke deposition, and this decrease will affect significantly the transport properties, particularly the effective diffusivity of large molecules. The relatively high content of asphaltenes in coal liquid, which are molecules commensurate to the catalyst pore size, implies that the configurational diffusion limitation will become significant, particularly when coupled with the effect of pore blockage caused by coke laydown.

To demonstrate the pore plugging effect in a simple way, consider a catalyst with cylindrical pores of uniform radius, R_o, and assume the coke laydown is monotonous as shown in Fig. 37. The shrinkage of the effective pore size as a function of catalyst activity can be described to be

$$(\frac{R}{R_o})^2 = 1 - \frac{(1-\theta)}{NPU} \qquad [18]$$

where NPU characterizes the number of poisoning units and is defined as follows:

$$NPU = \frac{\bar{p}_{max}}{\bar{p}_s} \qquad [19]$$

Here $\bar{p}_{max}$ specifies the maximum amount of coke laydown when the catalyst

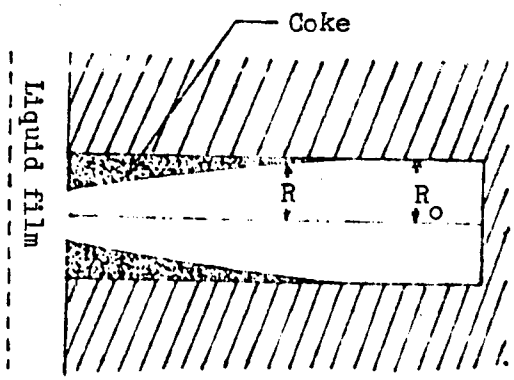

Fig. 37. Deposition of coke in a cylindrical catalyst pore.

pores are filled with coke completely. The actual catalyst does not have cylindrical pores, but the exclusion effect is handled in the same manner.

The parameter λ_i is defined to be the geometrical ratio of the radius of the ith component to the catalyst pore dimension, i.e.,

$$\lambda_i = \frac{r_i}{R} \qquad [20]$$

Then Equation [18] will be rearranged to be:

$$\lambda_i \frac{\lambda_{o,i}}{\sqrt{1 - \frac{(1-\theta)}{NPU}}} \qquad [21]$$

where $\lambda_{o,i}$ is evaluated for ith component and initial pore radius. From Equation [21], it is concluded that the catalyst life will be terminated unless the following criterion holds true at the catalyst surface, i.e.,

$$\lambda_i < 1 \qquad [22]$$

The passage of the reactant molecules will be hindered when λ_i approaches unity (greater than 0.1). The molecules absolutely can not pass if λ_i is greater than unity. Therefore, the catalyst will be considered to be dead if condition [22] does not hold true.

Considering the geometrical exclusion effect of the diffusion process of a large molecule through a fine pore, the empirical equation proposed by Satterfield et al., (1973) can be applied,

$$D_{e,i} = \frac{D_{o,i} f}{\tau'} e^{-4.6\lambda_i} \qquad \text{for } \lambda_i < 1 \qquad [23]$$

Where f is the fractional void volume and τ' is the tortuosity factor. It is apparent in Equation [23] that the correction for geometrical exclusion

will be significant when λ_i is greater than 0.1. This correction will be particularly important when $\lambda_{o,i}$ for fresh catalyst is already large enough that any further decline in pore size due to coke deposition will reduce the effective diffusivity significantly.

The effects of both pore plugging and geometrical exclusion on the effective diffusivity can be combined into a single correction factor. This factor is defined as the ratio of the effective diffusivity in aging catalyst to that in fresh catalyst:

$$Cd_i = 1 - \frac{(1-\theta)}{NPU} \quad \exp \frac{-4.6\,\lambda_{o,i}}{\sqrt{1-\frac{(1-\theta)}{NPU}}} \qquad [24]$$

Using groups defined clearly in Nomenclature, the original equations characterizing the catalyst behavior in H-coal reactor can be rearranged to be the dimensionless forms shown in Table 14.

The effect of coke deposit on the main reaction can be characterized by an effectiveness factor defined as the ratio of the observed reaction rate to the initial rate in the absence of mass transfer resistance.

$$\eta(\tau) = \frac{\int_0^1 \phi_1^2\, \theta^\alpha\, \tilde{C}^\beta\, \xi^2 d\xi}{\int_0^1 \phi_1^2\, \theta^\alpha\, \tilde{C}_s^\beta\, \xi^2 d\xi\Big|_{\tau=0}} \qquad [25]$$

which can be rearranged to be

$$\eta(\tau) = \frac{\bar{\gamma}A}{\gamma AS(\tau=0)} \qquad [26]$$

The total activity is simply related to the fraction of the initial effectiveness factor which remains after the coking has started. This fractional activity ratio is then defined to be:

TABLE 14 : Dimensionless Material Balances for H-coal Reactor

	$C \xrightarrow{1} B$, $C \xrightarrow{2} \bar{P}$	$C \xrightarrow{1} B \xrightarrow{2} \bar{P}$	$C \xrightarrow{1} B$, $P \xrightarrow{2} \bar{P}$
Fluid phase outside catalyst pellet :			
$\tilde{C}$ =	$\dfrac{B_{o,1}^{-1} + \Omega_1 \tilde{C}_s}{B_{o,1}^{-1} + \Omega_1}$	$\dfrac{B_{o,1}^{-1} + \Omega_1 \tilde{C}_s}{B_{o,1}^{-1} + \Omega_1}$	$\dfrac{B_{o,1}^{-1} + \Omega_1 \tilde{C}_s}{B_{o,1}^{-1} + \Omega}$
$\tilde{X}$ =	———	$\dfrac{\Omega_2 \tilde{B}_s}{B_{o,2}^{-1} + \Omega_2}$	$\dfrac{B_{o,2}^{-1} + \Omega_2 \tilde{P}_s}{B_{o,2}^{-1} + \Omega_2}$
Inside catalyst pellet :			
$Cd_1 \cdot \nabla^2 \tilde{C} + \dfrac{\partial Cd_1}{\partial \phi} \cdot \dfrac{\partial \tilde{C}}{\partial \phi}$ =	$\phi_1^2 \theta^\alpha \tilde{C}^\beta + \phi_2^2 \theta^\delta \tilde{C}^\gamma$	$\phi_1^2 \theta^\alpha \tilde{C}^\beta$	$\phi_1^2 \theta^\alpha \tilde{C}^\beta$
$Cd_2 \cdot \nabla^2 \tilde{X} + \dfrac{\partial Cd_2}{\partial \phi} \cdot \dfrac{\partial \tilde{X}}{\partial \phi}$ =	———	$\phi_2^2 \theta^\delta \tilde{B}^\gamma - \phi_1^2 \theta^\alpha \tilde{C}^\beta$	$\phi_2^2 \theta^\delta \tilde{P}^\gamma$
$\dfrac{\partial \theta}{\partial \tau}$ =	$-\theta^\delta \tilde{C}^\gamma$	$-\theta^\delta \tilde{B}^\gamma$	$-\theta^\delta \tilde{P}^\gamma$
Initial condition :			
$\theta \mid_{\tau=0}$ =	1	1	1
Boundary conditions :			
$\dfrac{\partial \tilde{C}}{\partial \phi}\Big\|_{\phi=0}$ =	0	0	0
$\dfrac{\partial \tilde{X}}{\partial \phi}\Big\|_{\phi=0}$ =	———	0	0
$Cd_1 \dfrac{\partial \tilde{C}}{\partial \phi}\Big\|_{\phi=1}$ =	$\dfrac{1 - \tilde{C}_s}{B_{o,1}^{-1} + \Omega_1}$	$\dfrac{1 - \tilde{C}_s}{B_{o,1}^{-1} + \Omega_1}$	$\dfrac{1 - \tilde{C}_s}{B_{o,1}^{-1} + \Omega_1}$
$Cd_2 \cdot \dfrac{\partial \tilde{X}}{\partial \phi}\Big\|_{\phi=1}$ =	———	$\dfrac{-\tilde{B}_s}{B_{o,2}^{-1} + \Omega_2}$	$\dfrac{1 - \tilde{P}_s}{B_{o,2}^{-1} + \Omega_2}$

** X represents either B or P.

$$A(\tau) = \frac{\eta(\tau)}{\eta(0)} \qquad [27]$$

The least complex form for demonstrating the use of relative activity is for a series reaction network. The conversion for main component is given as

$$\phi(\tau) = \frac{\bar{Y}A}{LHSV} \qquad [28]$$

From Equations [26] and [27], consequently the relative activity is equivalent to

$$A(\tau) = \frac{\phi(\tau)}{\phi(0)} \qquad [29]$$

This simple equation can be confirmed from the data on Figures 39 and 42. The definition of relative activity can be extended to the other two networks. The relative activity shows how the original capacity for useful reaction diminishes with time. The function is dependent on the history of the catalyst deactivation.

The propagation of coke laydown per unit mass of catalyst can be derived to be:

$$W(\tau) = \left(\frac{3 \cdot \ell_o \rho_p}{\rho_e}\right) \cdot \int_0^1 \frac{(1-\theta)}{NPU} \cdot \phi^2 d\phi \qquad [30]$$

Taking into account the effect of pore plugging and hindered diffusion, the deviation of the effective diffusivity can be elucidated by considering the average correction factor as follows:

$$\tilde{C}d_i = 3\int_0^1 Cd_i \cdot \phi^2 d\phi \qquad [31]$$

This average correction factor is not related to the effective in any simple way but instead provides a qualitative means of the contribution of hindered diffusion to the behavior of the system. There is no simple weighting which will permit a corrected diffusivity to be used in the conventional thiele modulus; the correction depends on the specific problem.

These ideas are illustrated with some specific numerical examples. For the sake of demonstrating the effect of coke on the catalyst behavior in the H-coal reactor, typical exponents with $\alpha = \beta = \delta = \gamma = 1$ in the power-law reaction mechanism are considered. And some secondary parameters are assumed empirically as follows:

$$B_{o,i} = 100$$

$$\text{LHSV} = 1 \text{ hr}^{-1}$$

$$V_e = 0.5$$

$$\tau_{p,i} = 1 \text{ hr}$$

where i = 1,2.

The coupled, non-linear equations are solved by the Orthogonal Collocation Method (Villadsen and Stewart, 1967). The results are shown in Figs. 38 to 46. Some qualitative observations about these results are given below.

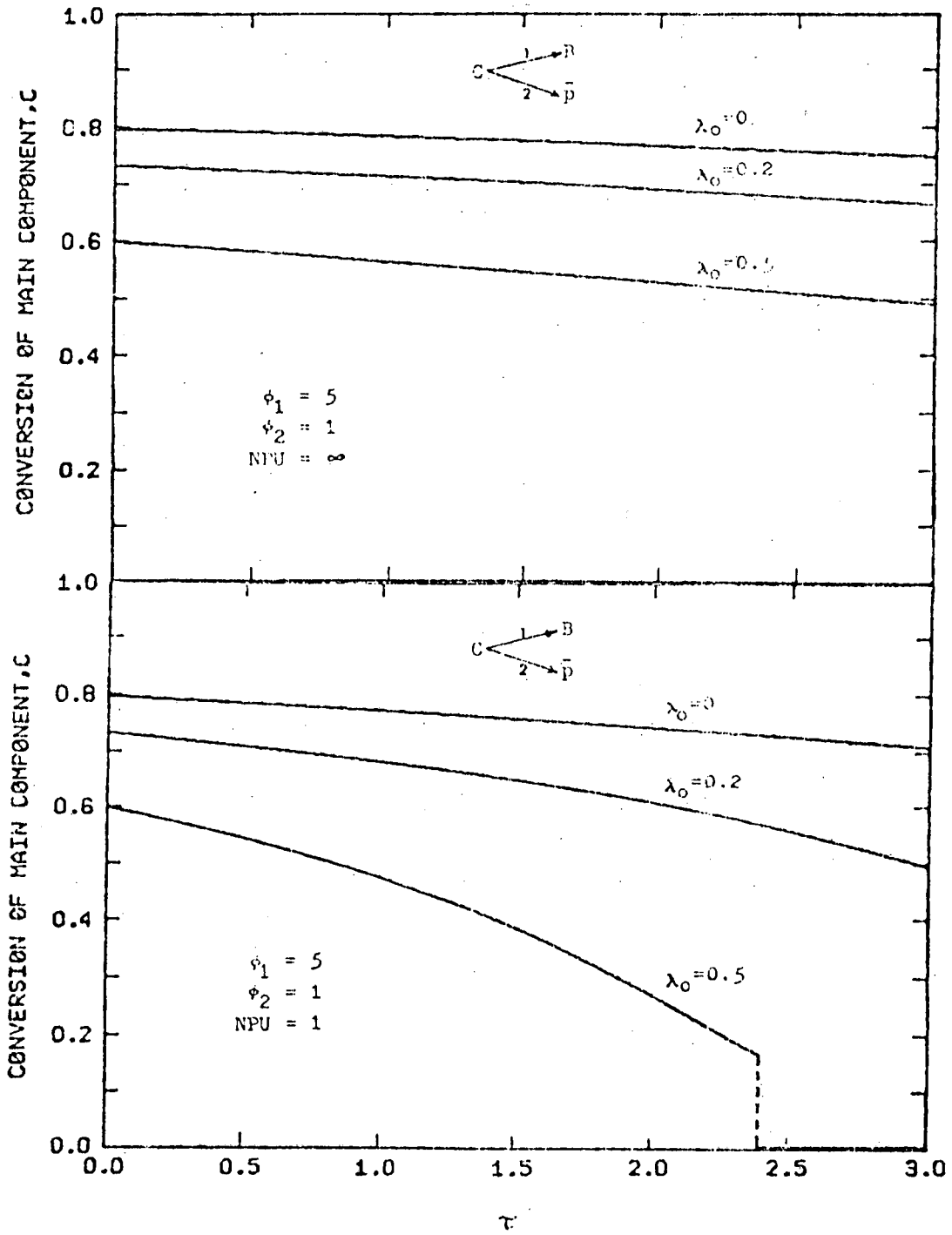

Fig. 38. Variation of conversion of main component with time as a function of λ_o for parallel mechanism.

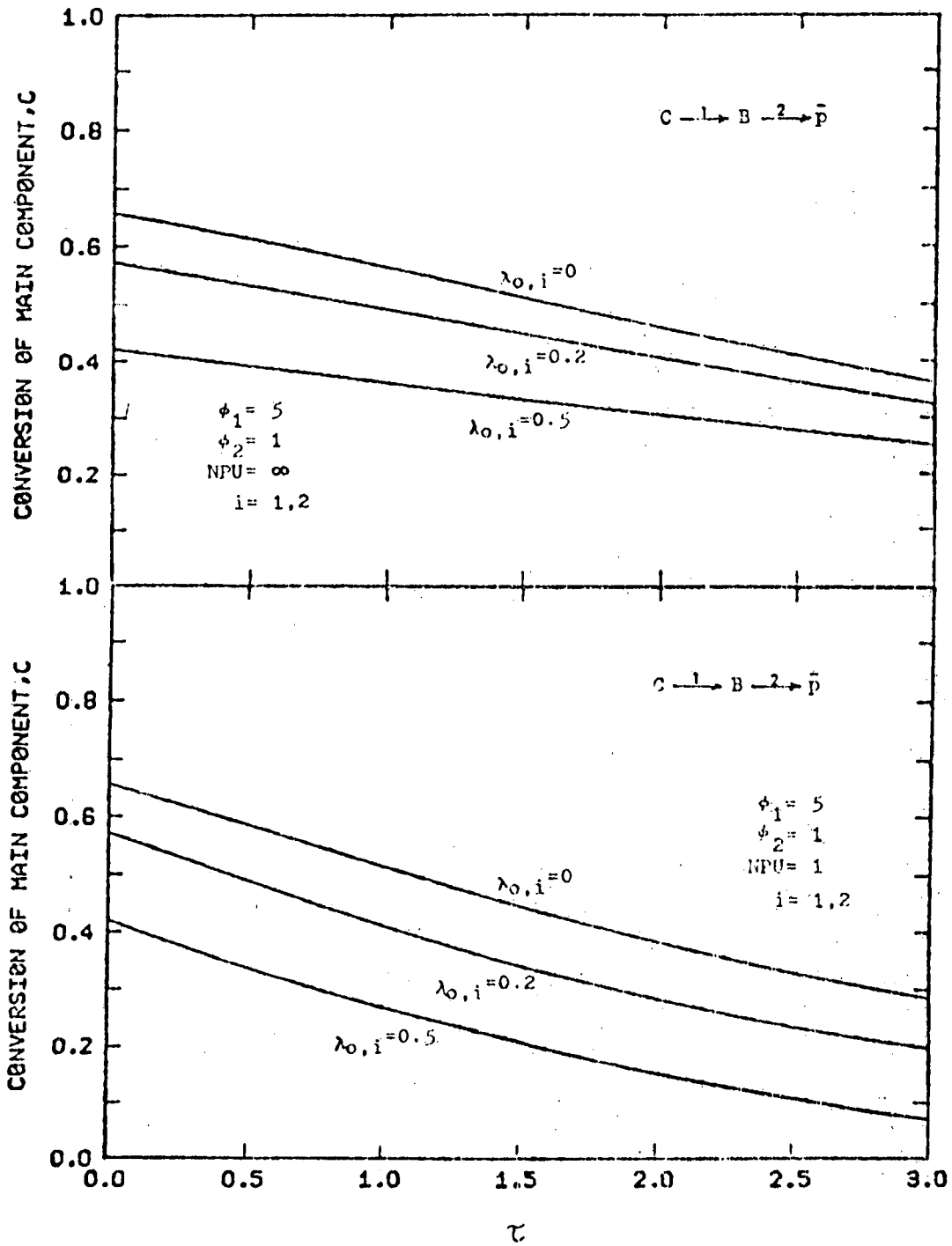

Fig. 39. Variation of conversion of main component with time as a function of $\lambda_{o,i}$ for series mechanism.

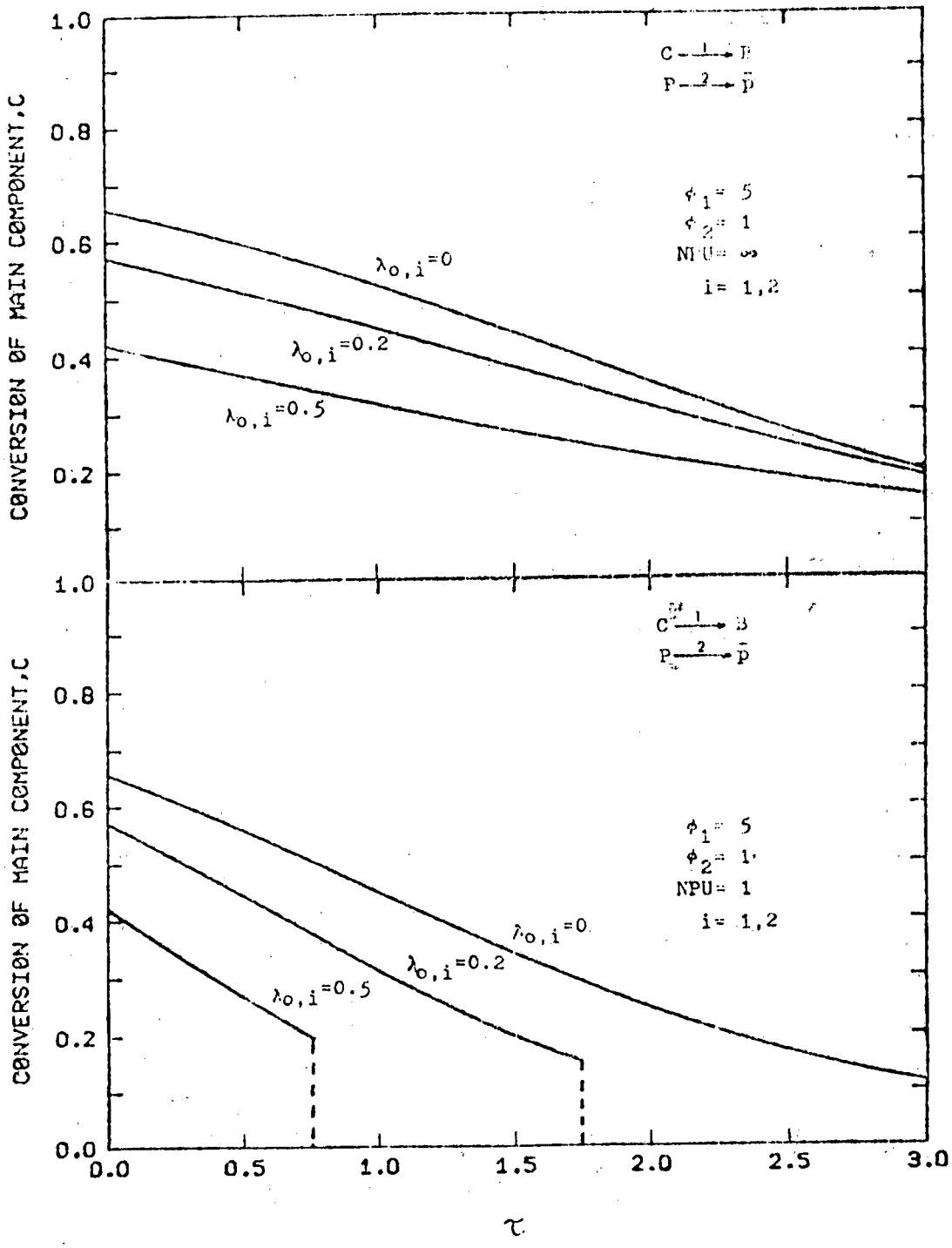

Fig. 40. Variation of conversion of main component with time as a function of $\lambda_{o,i}$ for independent reactions.

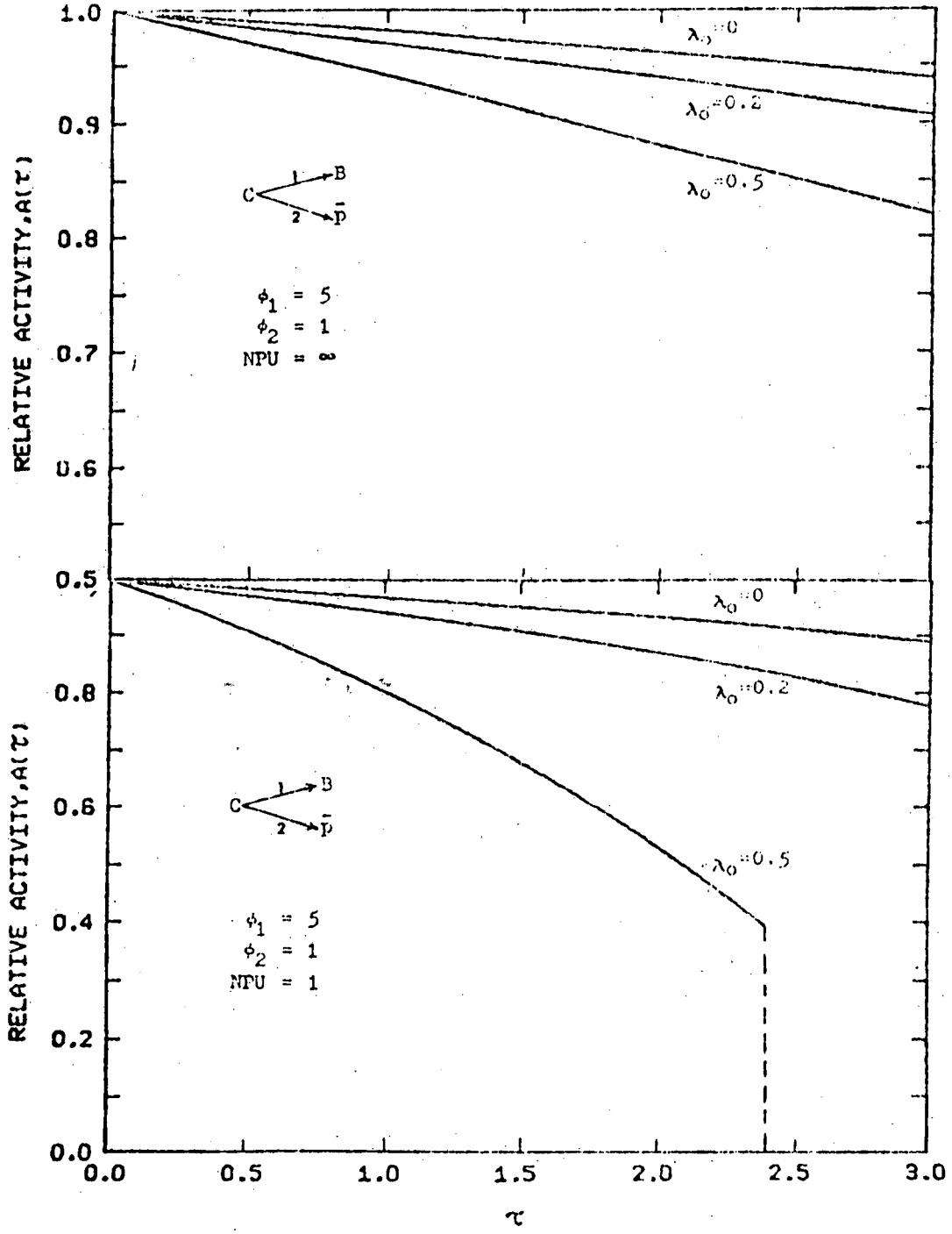

Fig. 41. Time change of relative activity as a function of λ_o for parallel mechanism.

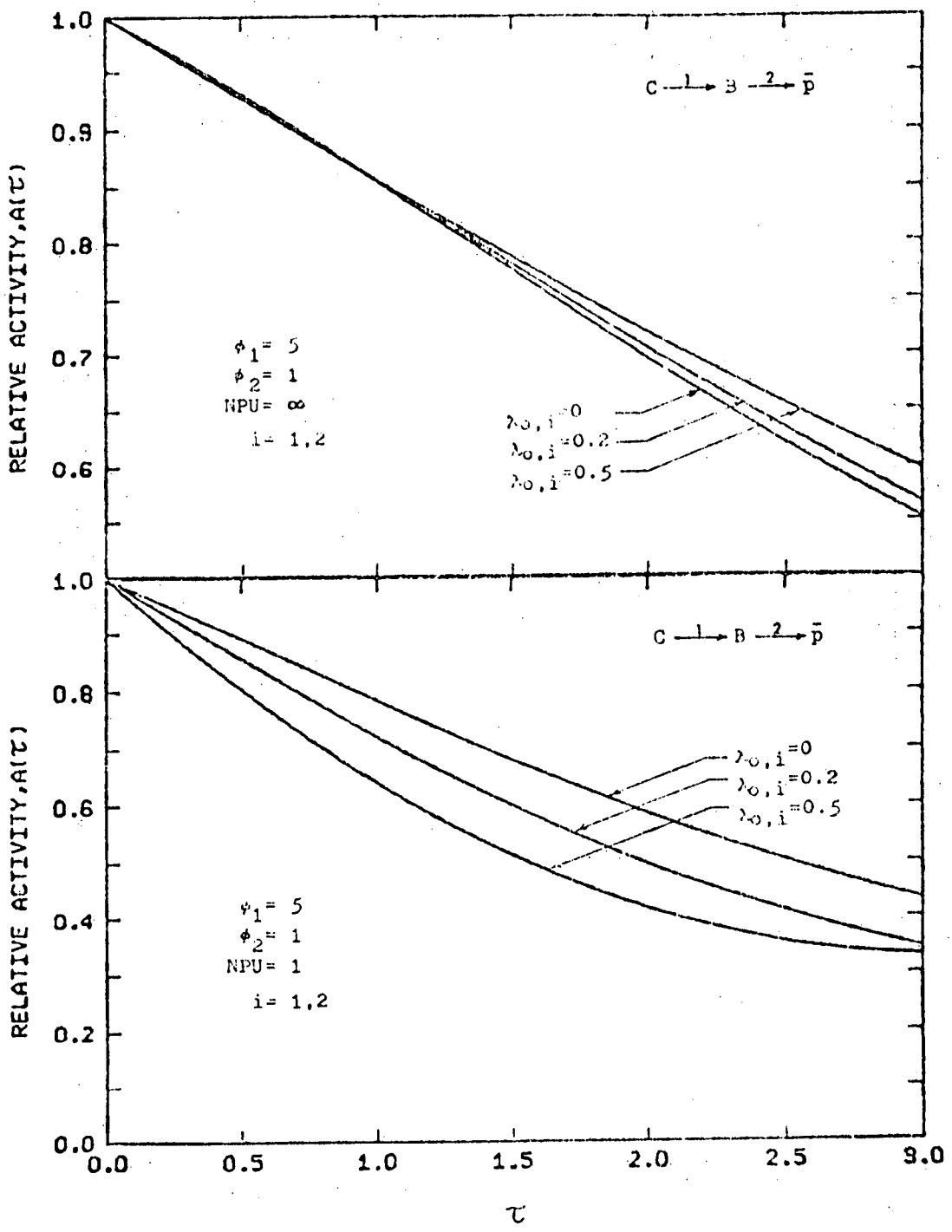

Fig. 42. Time change of relative activity as a function of $\lambda_{o,i}$ for series mechanism.

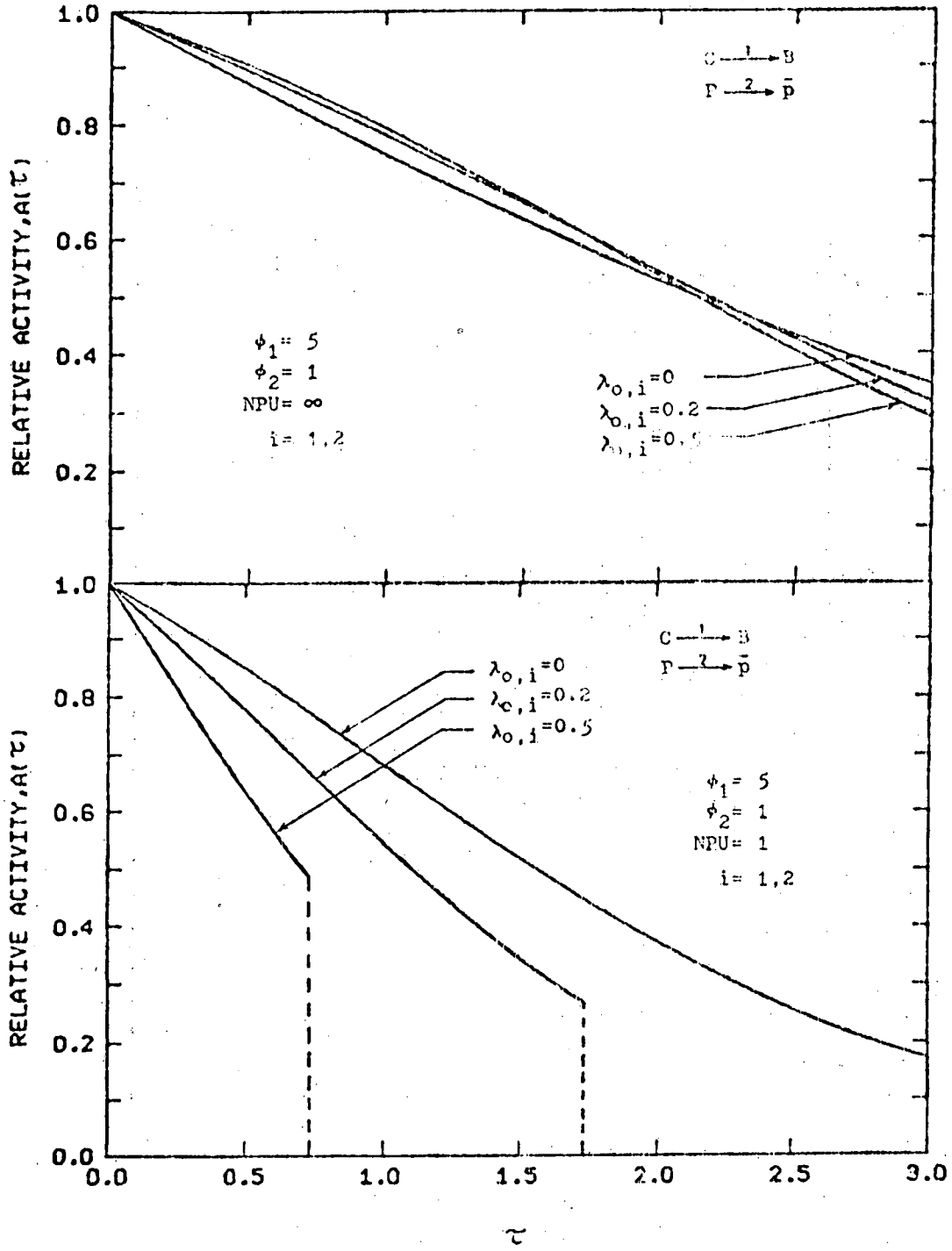

Fig. 43. Time change of relative activity as a function of $\lambda_{o,i}$ for independent mechanism.

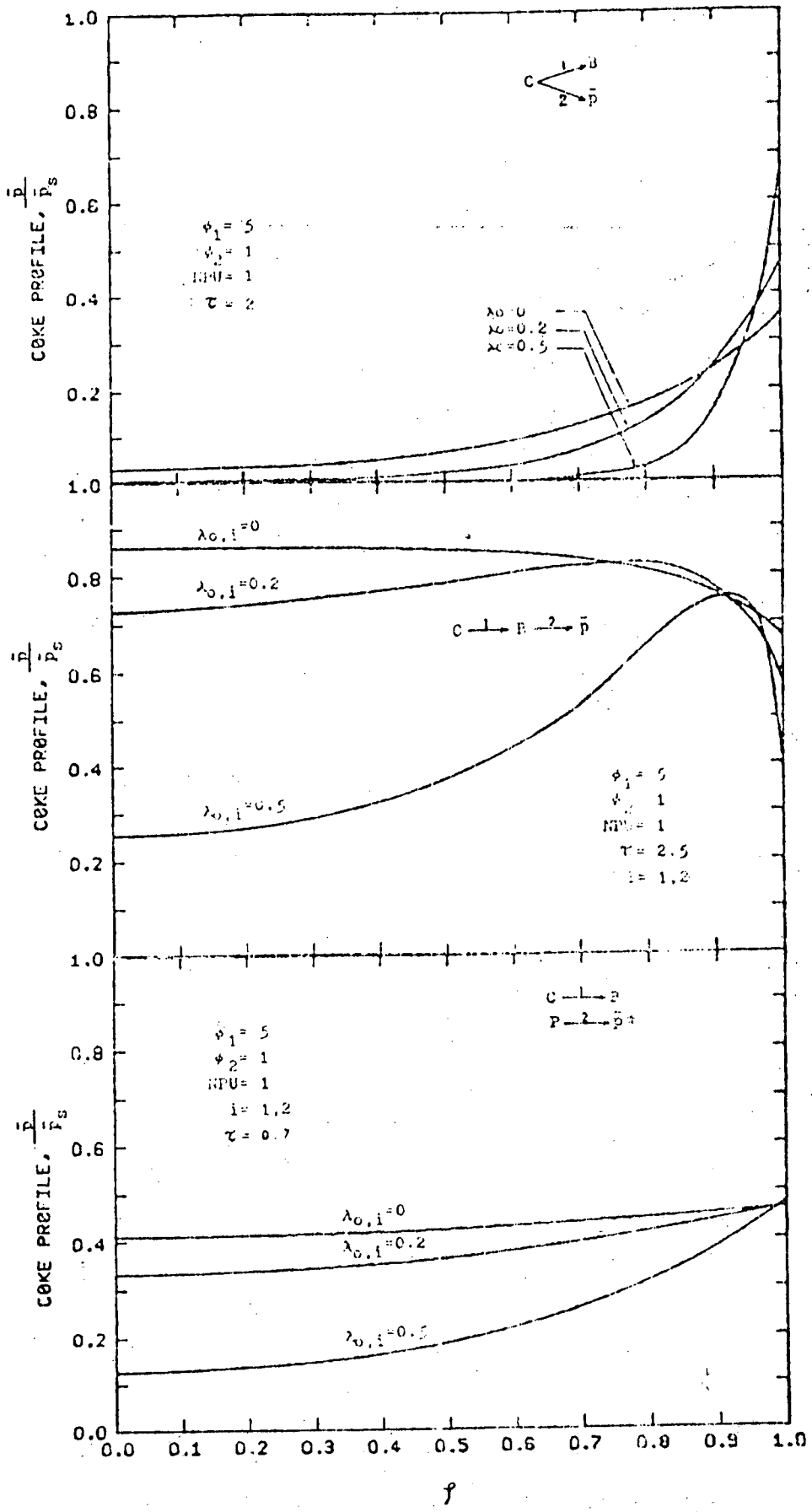

Fig. 44. Coke profiles inside the catalyst particle as a function of $\lambda_{o,i}$ for parallel, series and independent networks at a certain fixed time.

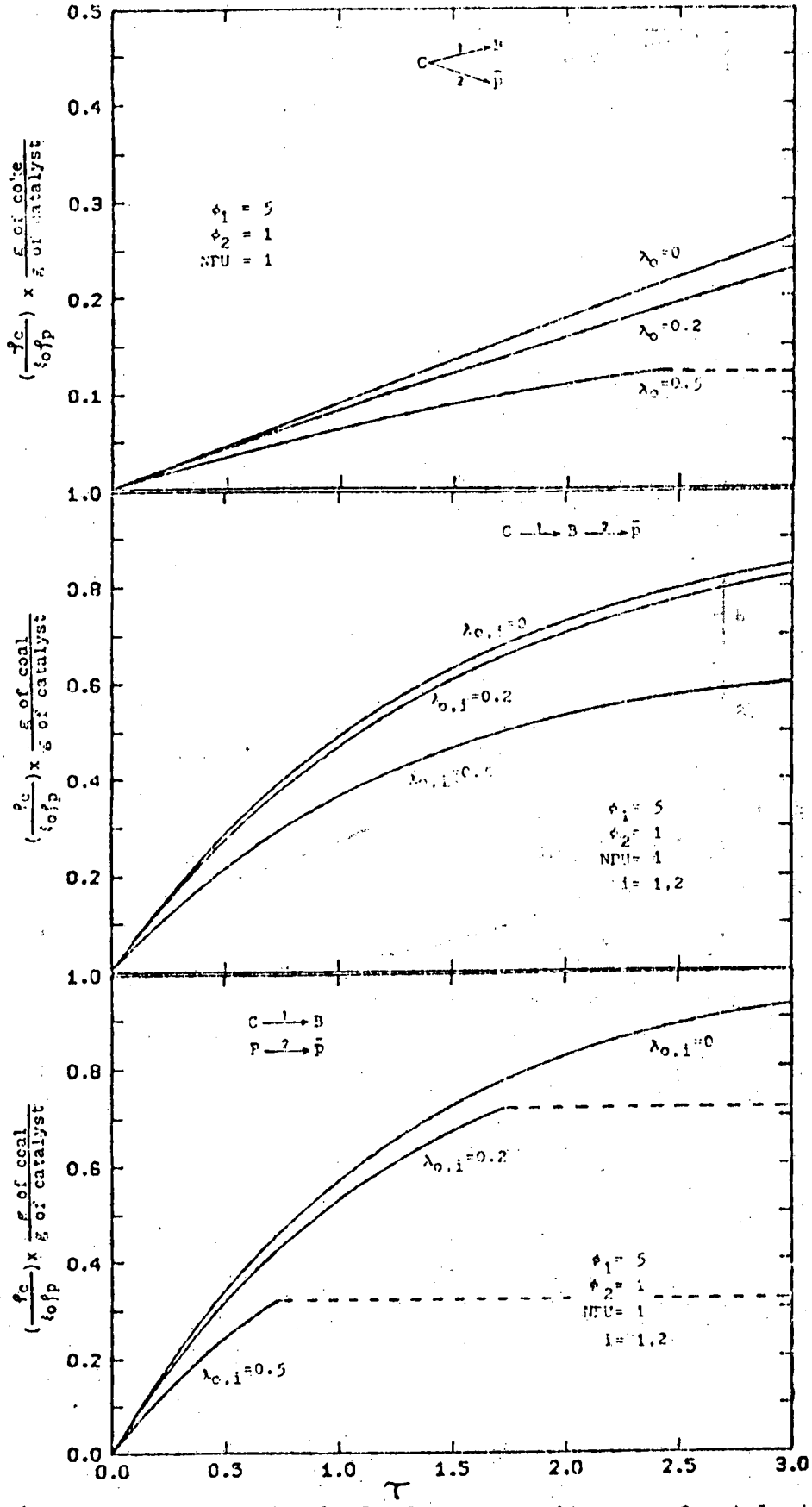

Fig. 45. Propagation of coke laydown per unit mass of catalyst as a function of $\lambda_{o,i}$ for parallel, series and independent networks.

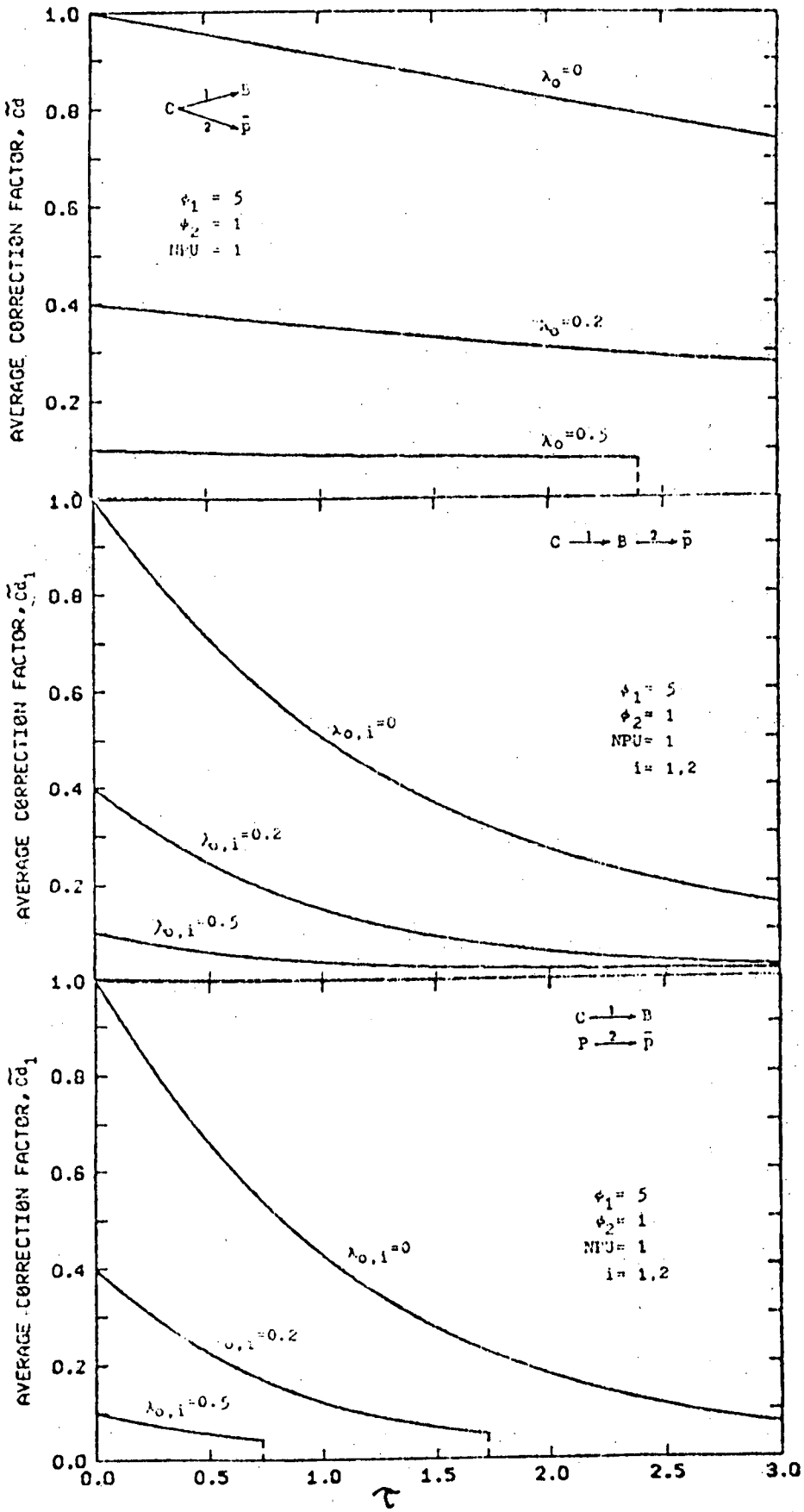

Fig. 46. Time change of the average correction factor for effective diffusivity as a function of $\lambda_{o,i}$ for three different mechanisms.

2. Results and Discussion

In the following paragraph some of the important effects of the pore plugging and geometrical exclusion on the catalyst behavior in H-coal process will be presented. Typical mechanisms of coke formation by parallel, series and independent networks are examined. For the sake of simplicity, the initial geometrical ratios, $\lambda_{o,i}$, are assumed to be the same for both main reactant and coke precursors in the following analysis. Figs. 38 to 40 show the time change of conversion of the main component, c, in H-coal® hydroprocessing. The case that NPU approaches infinity specifies the condition for clean pore structure. No pore plugging effect will be observed for this extreme case. The conversion of main reactant, therefore, is dominated by the intrinsic, configurational diffusion limitation, and the results shown on the top of Figs. 38 to 40 demonstrate that the geometrical exclusion has a decisive effect on the conversion of the main component. However, for longer operating time, the dependence on this effect will not be significant for both series and independent networks, this is due to the rapid decline of the effectiveness factor for these mechanisms with small value of $\lambda_{o,i}$. When NPU is unity, strong pore plugging phenomenon will be observed. The consequent decline of the pore size will further aggravate the geometrical exclusion significantly. The catalyst life will be terminated when the pore is finally choked by coke deposit to prevent access of the reactant to the interior of the catalyst active sites, even though portions of the catalyst are still highly active. The occurrence of choking phenomena depends strongly on the reaction mechanisms, the possibility of decreases in the order: independent > parallel > series as shown in Figs. 38 to 40. The dotted lines indicate the termination of

the catalyst life by the blockage of coke at pore mouth. Owing to the relative rapid coke-building rate, the catalyst blocking will occur easily for independent mechanism. The choking of catalyst will occur only for large value of λ_o for parallel mechanism, while the phenomenon is not observed for series network under the same conditions examined. The comparison between the two extreme cases of NPU shows that the effect of hindered diffusion coupled with pore plugging will reduce the catalyst life substantially with increasing value of $\lambda_{o,i}$. Therefore, initially larger pore catalyst will be preferable for higher conversion and longer catalyst life.

Figs. 41 to 43 show the complicated effects of pore plugging and hindered diffusion on the relative activity of catalyst. The effect of hindered diffusion alone is demonstrated in the upper part of these figures The action of geometrical exclusion only eliminates the access of the molecules through the pore; consequently, the activity of the catalyst remains high. The effectiveness factor depends not only on the mass flux of reactant into the catalyst particle but also on the activity of catalyst remaining. Therefore, in Fig. 42 an increase in the relative activity may be observed with the increase of $\lambda_{o,i}$. The total result indicates the effect of hindered diffusion alone is not significant on the relative activity for the networks studied. The results for the coupled effects of pore plugging and geometrical exclusion also are shown in the same figures for NPU=1. The dotted line specifies that the evaluation of relative activity is meaningless after the catalyst life is terminated. From these figures, it is found that relative activity decreases significantly for

both parallel and independent networks when pore plug by coke laydown is taken into account. The result for series network suggests the activity is less sensitive to the coke plugging and geometrical exclusion effects.

Fig. 44 demonstrates the typical coke profiles at specific operating time in catalyst particle for three different networks. The profile for the parallel model shows a sharp gradient toward the core of catalyst, and there will be no coke at all near the center of the catalyst particle for large value of λ_o. The relatively high content of coke at pore mouth suggests the catalyst life may be terminated by pore blockage with high interior activity remaining.

The coke profile for series model shows some interesting aspects. There exists a "peak" of coke profile inside the catalyst particle. The position of this peak propagates toward the center of the catalyst pellet with decreasing value of $\lambda_{o,i}$. Choking of the pore may occur inside the catalyst particle instead of at pore mouth. However, the pore blockage is not observed for the present example concerned, although interior blockage can occur for other sets of parameters.

Similarly the coke profile for the independent model shows a relative rapid coke build-up and the coke profile appears much uniform. Consequently, the catalyst pore mouth will be choked relatively early. This conclusion is consistent with the observations in the previous figures. From these observations, it is concluded that coke laydown will be eliminated toward the core of catalyst for all mechanisms when $\lambda_{o,i}$ are large. The physical properties of both catalyst and reactants will affect the coke propagation substantially, especially for series type.

Fig. 45 shows the accumulation of coke laydown per unit mass of catalyst used. The dotted line specifies that coke formation will cease when the catalyst life is terminated. The amount of coke laydown decreases in the order: independent > series > parallel. Further increase of $\lambda_{o,i}$ will generally prevent the formation of coke, especially when the initial value of $\lambda_{o,i}$ is greater than 0.2. Therefore, proper choice of catalyst pore size can in principle be used to eliminate the coke formation.

The significant decrease of effective diffusivity is shown in Fig. 46 in terms of average correction factor. The substantial decline in the effective diffusivity demonstrates the important effects of pore plug and geometrical exclusion. However, serious misinterpretation of the kinetic information will result without considering these correction factors coupled with the specific reaction network.

3. Conclusion

The effects of pore plugging and geometrical exclusion on the catalytic behavior in H-coal® hydroprocess has been studied. A kinetic model correlating the decline of effective diffusivity with hindered diffusion and coke laydown is proposed. The results demonstrate that physical properties of both catalyst and reacting molecules have a decisive effect on the loss of the catalyst life and the nature of coke formation. The profiles for coke laydown demonstrate the dramatic effects of pore plugging coupled with geometrical exclusion. Although a complete modeling of hydroprocessing must include the effect of coke deposit on the main hydroprocessing reactions such as HDS, HDN and HDM etc., this study of three models for coke deposition yield the basic characterization for more complicated systems. There is potential of improving hydroprocessing processes by control of catalyst physical properties.

E. PROGRESS IN THE SYNTHESIS AND CHARACTERIZATION OF SULFUR AND NITROGEN SUBSTRATES

Benz[c]acridine was synthesized by the following route using o-toluidine hydrochloride and 1-naphthol (see Ullmann (1904))

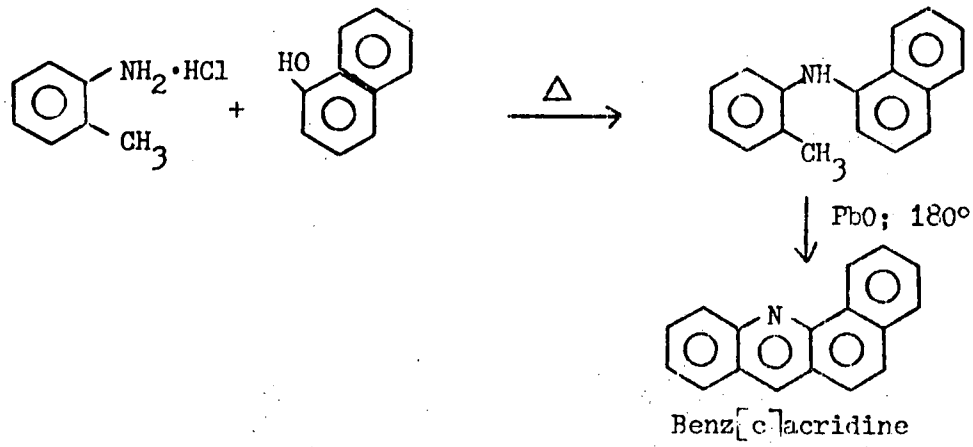

Benz[c]acridine

Benz[a]acridine was similarly obtained from o-toluidine hydrochloride and 2-naphthol (see Ullmann (1904))

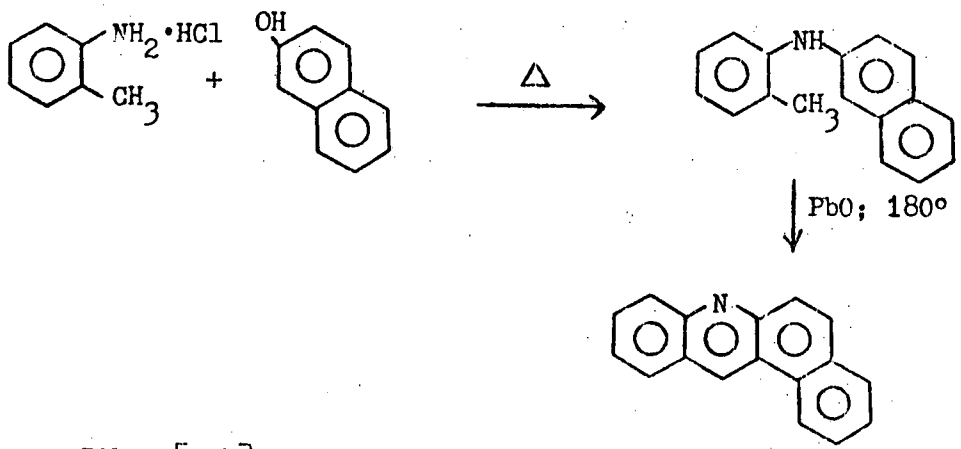

Dibenz[c,h]acridine was obtained from 1-naphthol, 1-naphthylamine and paraformaldehyde (see Jacquignon (1973))

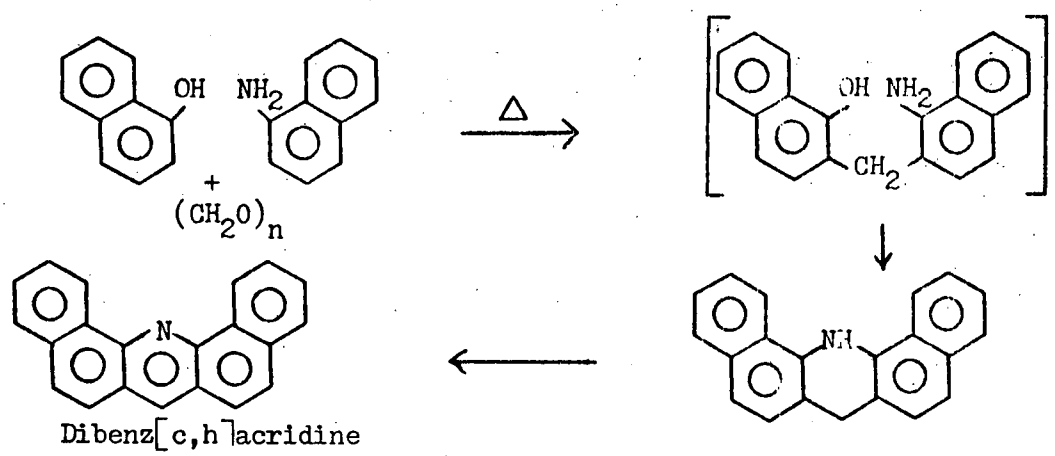

Dibenz[c,h]acridine

Benzo[b]naphtho[2,3-d]thiophene has been synthesized by the following route (see Campaigne, (1968))

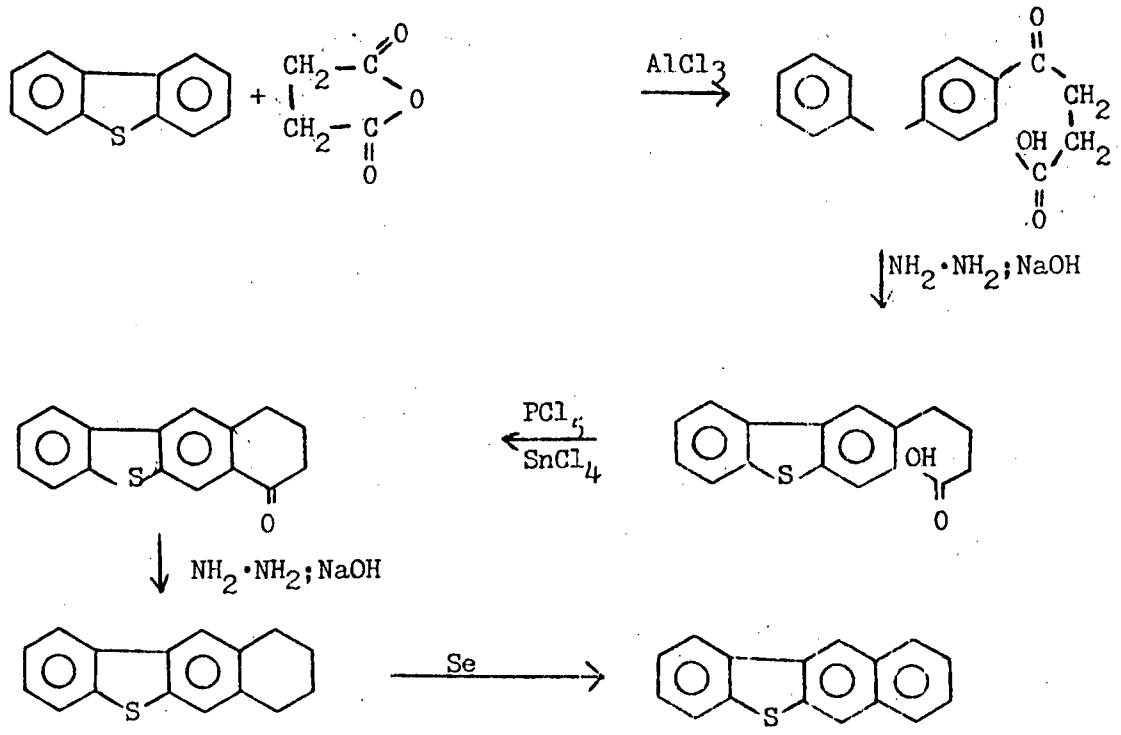

7-Methylbenzo[b]naphtho[2,3-d]thiophene has been obtained by the following procedure (see Campaigne et al. (1969))

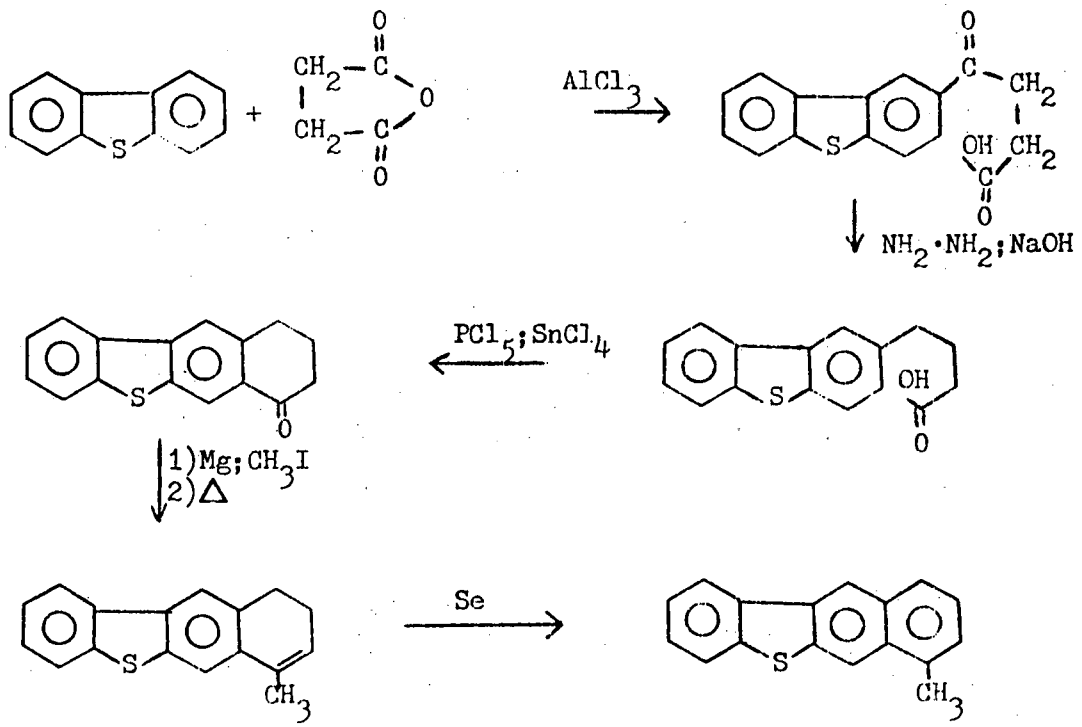

The preparation of Acridine N-oxide from acridine is underway (see Acheson (1968))

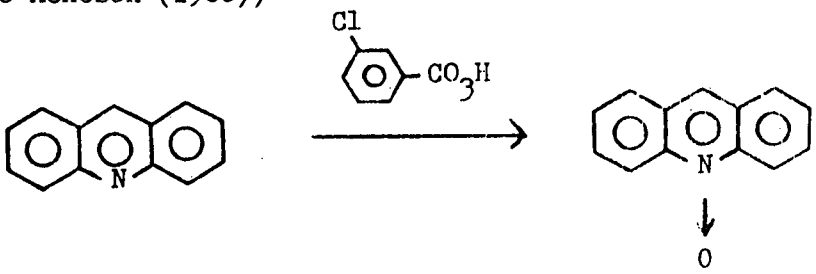

4-Methylbenzo[b]naphtho[2,3-d]thiophene will be prepared by methylation of the parent compound (see Litvinov et al. (1970))

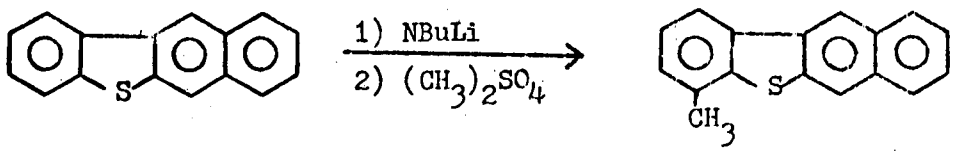

Phenanthro[4,5-bcd]thiophene will be obtained from phenanthrene and hydrogen sulfide (see K. L. Klemm et al. (1969, 1970, 1976))

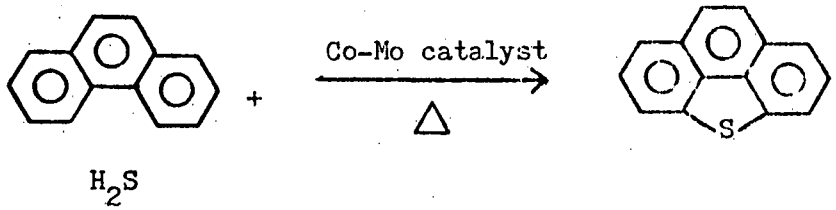

6-Methylbenzo[b]naphtho[2,3-d]thiophene will be synthesized by the following sequence of reactions (see Campaigne et al. (1969))

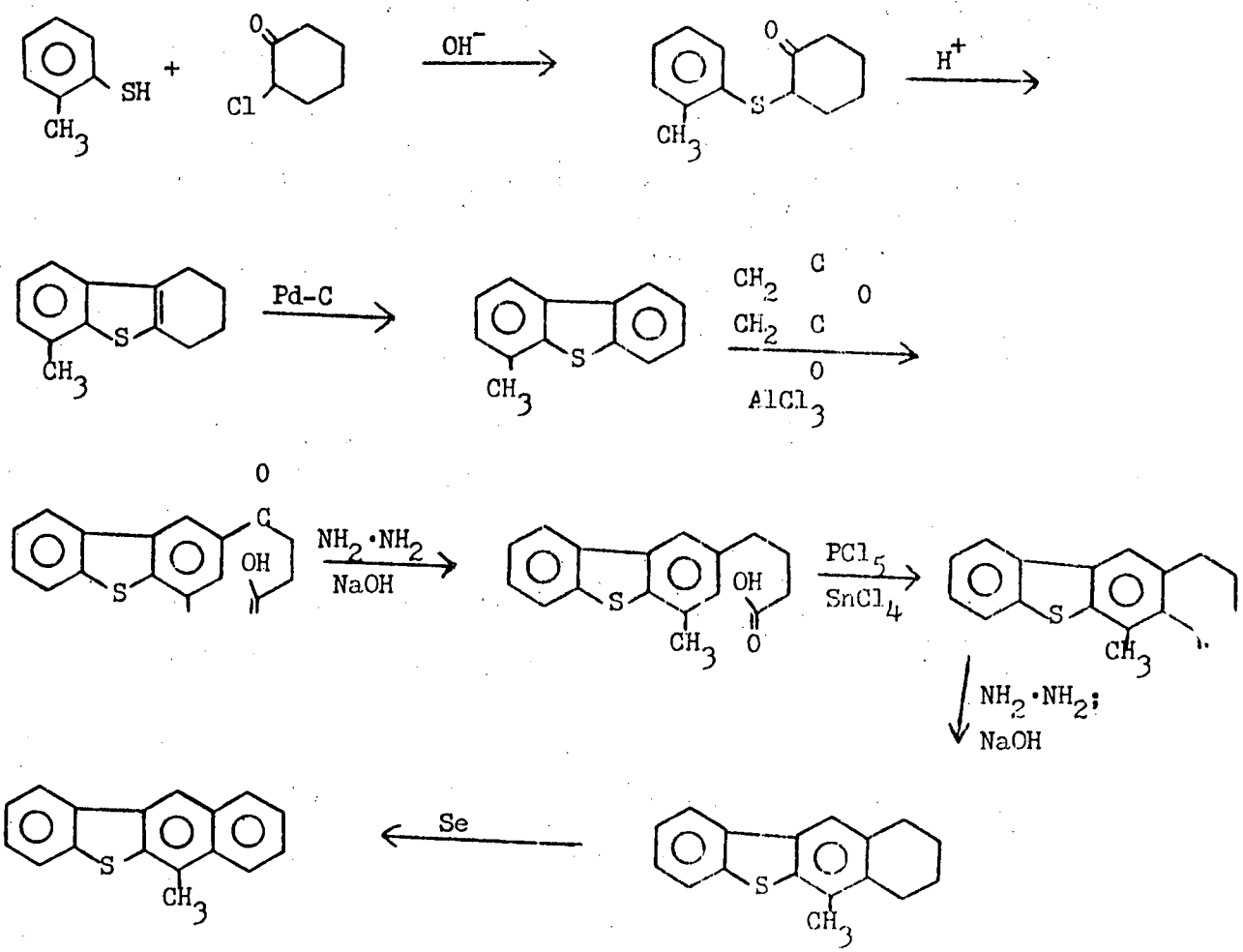

Thioxanthene will be obtained by reduction of Thioxanthen-9-one (see Wechter (1963))

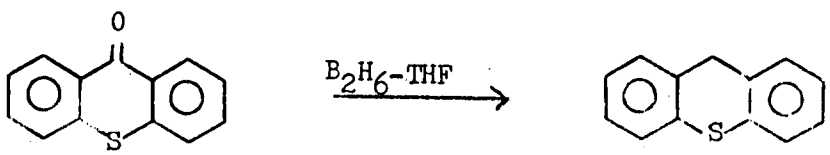

V. NOMENCLATURE

$A(\tau)$: Fractional activity as defined in equation (10).

b : Concentration of main product in fluid phase outside the catalyst pellet.

$\tilde{b}$: Concentration of main product in fluid phase inside the catalyst pellet.

$B_{o,i}$: Biot number for ith component, $\frac{K_{f,i} r_c}{D_{e,i}}$.

c : Concentration of reactant in fluid phase outside the catalyst pellet.

$\tilde{c}$: Concentration of reactant in fluid phase inside the catalyst pellet.

c_o : Concentration of reactant at entrance of reactor.

C : Dimensionless concentration of reactnat in fluid phase outside the catalyst pellet, c/c_o.

$\tilde{C}$: Dimensionless concentration of reactant in fluid phase inside the catalyst pellet, $\tilde{c}/c_o$.

Cd_i : Correction factor for effective diffusivity for ith component.

$\tilde{Cd}_i$: Average correction factor for effective diffusivity for ith component as defined in equation (12).

$D_{o,i}$: Bulk diffusivity for ith component.

$D_{e,i}$: Effectivity diffusivity as defined in equation (7).

F : Volumetric flow rate.

K_1 : Rate constant for main reaction.

K_2 : Rate constant for coking reaction.

$K_{f,i}$: Mass transfer coefficient at liquid-solid interface.

LHSV : Liquid hour space velocity, hr^{-1}.

NPU : Number of poisoning unit as defined in equation (3).

p : Concentration of coke precursors in fluid phase outside the catalyst pellet for independent coking mechanism.

$\tilde{p}$: Concentration of coke precursors in fluid phase inside the catalyst pellet for independent coking mechanism.

p_o : Concentration of coke precursor at entrance of reactor.

P : Dimensionless conenetration of coke precursor in fluid phase outside the catalyst pellet, p/p_o.

$\tilde{P}$: Dimensionless concentration of coke precursor in fluid phase inside the catalyst pellet, $\tilde{p}/p_o$.

$\bar{p}$: Coke deposition on catalyst surface, g-mole coke/cm^3 of catalyst.

$\bar{p}_s$: Saturated coke deposition on catalyst surface.

$\bar{p}_{max}$: Maximum amount of coke deposition to fill the entire pores of catalyst.

R : Radius of pore in aging catalyst.

R_o : Radius of pore in fresh catalyst.

r_c : Radius of catalyst pellet.

r : Spatial variable of catalyst radius.

V_A : Average reaction rate inside the catalyst pellet for main component.

V_{As} : Reaction rate of main component at surface conditions.

t : Time variable

V : Volume of H-coal reactor.

V_c : Fractional volume of catalyst in H-coal reactor.

$W(\tau)$: Relative coke laydown, g of coke/g of catalyst.

Greek symbols

α, β : Exponents of the main reaction expression.

δ, γ : Exponents of the coking reaction expression.

τ : Dimensionless time, $\frac{(t \cdot K_2 \cdot y_o^{\gamma})}{P_o}$, where y_o represents c_o for series and parallel mechanisms and p_o for independent coking network.

ζ :

ε : Free cross section area of pore.

ε_o : Porosity of fresh catalyst particle.

τ' : Tortuosity factor.

θ : Catalyst activity as defined in equation (1).

ϕ_1 : Thiele modulus for main reaction, $r_c \sqrt{\frac{K_1 c_o^{\beta-1}}{D_{e,1}}}$.

ϕ_2 : Thiele modulus for coking reaction, $r_c \sqrt{\frac{K_2 \cdot y_o^{\gamma-1}}{D_{e,2}}}$, where y_o indicates c_o for series and parallel mechanisms and p_o for independent network.

η : Effectiveness factor as defined in equation (9).

f : Dimensionless radius of catalyst particle, r/r_c.

ρ_c : Density of catalyst.

ρ_p : Density of coke deposition.

λ_i : Geometrical ratio of the radius of reactant to the radius of catalyst pore as defined in equation (4).

$\tau_{p,i}$: Time constant for diffusion in catalyst particle for ith component, $\frac{r_c'}{3 \cdot D_{e,i}}$, hr.

Ω_i : Dimensionless group defined to be $\frac{V_c}{LHSV \cdot \tau_{p,i}}$

Subscripts

s : Concentrations on external catalyst surface.

VI. LITERATURE CITED

1. Acheson, R. M., J. Chem. Soc. (c) 1045 (1968).

2. Campaigne, E., and Osborn, S. W., J. Heterocyclic Chem., 5, 655 (1968).

3. Campaigne, E., Ashby, J. and Osborn, S. W., J. Heterocyclic Chem., 36, 885 (1969).

4. Cocchetto, J. F., S. M. Thesis, M.I.T., Cambridge (1974).

5. Cox, K. E., and Berg, L., CEP 56, No. 12, 54 (1962).

6. Farcasiu, M., Fuel 1977, 56, 9.

7. Flinn, R. A., Larson, O. A., and Beuther, H., Hydrocarbon Proc. and Pet. Refiner 42, No. 9, 129 (1962).

8. Gates, B. C., Katzer, J. R., Olson, J. H., Kwart, H., and Stiles, A. B. "Kinetics and mechanisms of Desulfurization and Denitrogenation of coal derived liquids," Contract E(49-18)-2028, June 1977.

9. Goudriaan, F., Ph.D. Thesis, Twente Technical Institute, The Netherlands (1974).

10. Himmelblau, D. M., Jones, C. R. and Bischoff, K. B., Ind. Eng. Chem. Fundamentals, 6, 539 (1967).

11. Jacquignon, P., Bull. Soc. Chem. Fr., 2, 2131 (1973).

12. Kang, C. C., and Johanson, E. S., Liquid Fuel from Coal, Academic Press, 1977, 89.

13. Klemm, K. L. et al. J. Heterocyclic Chem. 6, 813 (1969); ibid, 7, 1347 (1970); ibid, 13,1245 (1976).

14. Litvinov, V. P., Gverdstsitch, D. D. and Lubuzh, E. D. IZV. Akad. Nauk SSSR. Ser. Khim (Eng.) p. 70 (1972).

15. Mayer, J. T., Sc.D. Thesis, M.I.T., Cambridge (1974).

16. Richter, F. P., Caesar, P. D., Meisel, S. E., and Offenhauer, P. D., Ind. Eng. Chem. 44, 2601 (1952).

17. Roberts, J. D., Stewart, R., and Caserio, M. C., Organic Chemistry, Benjamin Inc., Menlo Park, CA (1971).

18. Satterfield, C. N., Colton, C. K., and Pitcher, W. H., Jr., AIChE J. 1973, 19, 628.

19. Shih, S. S., Katzer, J. R., Kwart, H., and Stiles, A. B., "Quinoline Hydrodenitrogenation: Reaction Network and Kinetics," submitted to J. Catal, 1977.

20. Sonnemans, J., Ph.D. Thesis, Twente University of Technology, The Netherlands (1973).

21. Sternberg, H. W., Raymond R., and Schweighardt, F. K., Science, 1975 188, 49.

22. Uplmann, F., and Torre, A. L., Ber. 3, 2924 (1904).

23. Vierhapper, F. W., and Eliel, E. L., J. Org. Chem. 40, 2779 (1975).

24. Villadsen, J. V., and Stewart, W., Chem. Eng. Sci., 1967, 22, 1483.

25. Wechter, W. J., J. Org. Chem., 28, 2935 (1963).

VII. PUBLICATIONS

1. Stanulonis, J. J., B. C. Gates, and J. H. Olson, "Catalyst Aging in a Process for Liquefaction and Hydrodesulfurization of Coal," A.I.Ch.E. Journal 19, 417 (1976).

2. Ellezer, Kenneth F., Manog Bhinde, Marwan Houalla, Dennis Broderick, Bruce C. Gates, James R. Katzer, and Jon H. Olson, "A Flow Microreactor for Study of High-Pressure Catalytic Hydroprocessing Reactions," Ind. Eng. Chem. Fundamentals 16, 380 (1977).

3. Chiou, M. J., and J. H. Olson, "A Method for Determining Catalytic Kinetics in a Pulse Microreactor System," submitted to Chem. Eng. Sci.

4. Houalla, M., D. Broderick, V. H. J. de Beer, B. C. Gates, and H. Kwart, Preprints, ACS Div. Petrol. Chem., 22 (3), 941 (1977).

5. Shih, S. S., J. R. Katzer, H. Kwart, and A. B. Stiles, Preprints, ACS Div. Petrol. Chem. 22 (3), 919 (1977).

6. Shih, S. S., J. R. Katzer, H. Kwart, and A. B. Stiles, "Quinoline Hydrodenitrogenation: Reaction Network and Kinetics," submitted to J. Catal.

7. Zawadski, R., S. S. Shih, J. R. Katzer, and H. Kwart, "Kinetics and Reaction Network for Acridine Hydrodenitrogenation," submitted to J. Catal.

8. Shih, S. S., E. Reiff, R. Zawadski, J. R. Katzer, and A. B. Stiles, "Effect of Catalyst Composition on Quinoline and Acridine Hydrodenitrogenation," submitted Ind. Eng. Chem. Prod. Res. Devel.

9. "The Sulfided Co-Mo/γ-Al_2O_3 Catalyst: Evidence of Structural Changes During Hydrodesulfurization of Dibenzothiophene," D. H. Broderick, G. C. A. Schuit, and B. C. Gates, J. Catal., accepted for publication.

10. Houalla, M., N. K. Nag, A. V. Sapre, D. H. Broderick and B. C. Gates, "Hydrodesulfurization of Dibenzothiophene Catalyzed by Sulfided CoO-MoO/γ-Al_2O_3: The Reaction Network." Submitted A.I.Ch.E. Journal.

There has been only one addition in personnel during this quarter. Dr. Dan Fraenkel from the Weizmann Institute of Science, Israel has joined as a Post-doctoral fellow in October 1977.